

Aus der Chirurgischen Universitätsklinik  
Heidelberg Klinik für Allgemein-, Viszeral- und  
Transplantationschirurgie  
(Ärztlicher Direktor: Prof. Dr. med. Dr. h.c. Markus W. Büchler)

**Inhibition of pancreatic cancer progression by sulforaphane-  
mediated downregulation of miR30a-3p and sulforaphane  
derivatives**

Inauguraldissertation  
zur Erlangung des Doctor scientiarum  
humanarum (Dr. sc. hum.)  
an der Medizinischen Fakultät Heidelberg  
der  
Ruprecht-Karls-Universität

vorgelegt  
von  
Christina  
Georgikou  
aus  
Athen  
Griechenland  
2019

Dekan: Prof. Dr. med. Hans-Georg Kräusslich

Doktormutter: Prof. Dr. rer. nat. Ingrid Herr

**TO MY BELOVED FAMILY AND FRIENDS**



## Table of Contents

<b>1. List of Tables .....</b>	<b>1</b>
<b>2. List of Figures.....</b>	<b>1</b>
<b>3. Supplement .....</b>	<b>3</b>
<b>4. Abbreviations and Units.....</b>	<b>4</b>
<b>Abbreviations .....</b>	<b>4</b>
<b>Units .....</b>	<b>5</b>
<b>5. Introduction.....</b>	<b>6</b>
<b>5.1 Pancreatic cancer.....</b>	<b>6</b>
5.1.1 Pathophysiology, risk factors and staging .....	6
5.1.2 Current therapeutic options .....	8
5.1.2.1 Gemcitabine: clinical applications and metabolism .....	8
<b>5.2 Sulforaphane.....</b>	<b>10</b>
5.2.1 Chemical structure and bioavailability .....	10
5.2.2.1 Mechanisms of action.....	11
5.2.2.2 Pharmaceutical relevance of sulforaphane .....	12
<b>5.3 Gap junctions.....</b>	<b>13</b>
5.3.1 Structure and functions.....	13
5.3.2 Gap junctions and cancer.....	14
5.3.2.1 Gap junctions and therapeutic potential .....	15
<b>5.4 MicroRNAs .....</b>	<b>16</b>
5.4.1 Biogenesis and regulation.....	17
5.4.2 miRNAs involved in cancer .....	18
5.4.2.1 miRNAs and Cx43 .....	19
<b>5.5 Aim of the study.....</b>	<b>20</b>
<b>6. Materials and Methods.....</b>	<b>21</b>
<b>6.1 Materials.....</b>	<b>21</b>
6.1.1 Equipment and consumables .....	21
6.1.2 Media and supplements for cell culture.....	23
6.1.3 Chemical agents and enzymes.....	23
6.1.4 Kits .....	24
6.1.5 Buffers and solutions.....	25
6.1.6 Antibodies.....	27
6.1.7 Cell culture .....	27
<b>6.2 Methods.....</b>	<b>28</b>
6.2.1 Cell culture maintenance .....	28
6.2.2 Cell viability assay .....	29
6.2.3 Patient tissue .....	30
6.2.4 Double-dye flow cytometry assay .....	30
6.2.5 Microinjection of Lucifer Yellow.....	32
6.2.6 Flow cytometry detection of gemcitabine bystander effect.....	32
6.2.7 miRNA and mRNA microarray analysis.....	33
6.2.7.1 RNA and miRNA isolation and concentration measurement.....	33
6.2.7.2 mRNA and miRNA expression profiling .....	33
6.2.7.3 mRNA and miRNA data interpretation .....	33
6.2.7.4 Transfection with miRNA inhibitors.....	36
6.2.7.5 Reverse transcription of mRNA to cDNA.....	37
6.2.7.6 Reverse transcription of miRNA to cDNA.....	37
6.2.7.7 Real-time quantitative PCR.....	38

6.2.8 Preparation of chicken eggs and transplantation of established PDA cell lines .....	39
6.2.9 Dual-luciferase reporter assay .....	40
6.2.10 Immunohistochemistry .....	41
6.2.11 Apoptosis assay .....	41
6.2.12 <i>In situ</i> hybridization.....	41
6.2.13 Colony formation assay.....	42
6.2.14 Life span assay .....	42
6.2.15 Chemical synthesis of sulforaphane derivatives.....	43
6.2.16 Statistical analysis .....	43
<b>7. Results .....</b>	<b>45</b>
<b>7.1 Sulforaphane-mediated inhibition of miR30a-3p enhances gap junctional intercellular communication, thereby increasing gemcitabine cytotoxicity in pancreatic cancer.....</b>	<b>45</b>
7.1.1 Sulforaphane induces GJIC .....	45
7.1.2 Sulforaphane potentiates the gemcitabine bystander effect through GJIC .....	47
7.1.3 Sulforaphane inhibits miR30a-3p and enhances Cx43 expression.....	49
7.1.4 miR30a-3p inhibits Cx43 expression by binding to its 3'-UTR .....	51
7.1.5 Inhibition of miR-30a-3p induces GJIC and gemcitabine bystander effect .....	53
7.1.6 miR30a-3p decreases the tumor xenograft volume .....	55
7.1.7 Correlation of miR30a-3p and Cx43 expression in PDA patient tissue .....	57
<b>7.2 Analysis of the therapeutic potential of sulforaphane derivatives in pancreatic cancer.....</b>	<b>59</b>
7.2.1 Chemical structure of the seven sulforaphane derivatives.....	59
7.2.2 SF102 and SF134 are cytotoxic in all the evaluated tumor cells.....	60
7.2.3 SF102 and SF134 induce apoptosis.....	62
7.2.4 SF102 and SF134 diminish colony-forming capacity .....	63
7.2.5 SF102 and SF134 inhibit the growth of tumor xenografts in vivo .....	64
7.2.6 SF102 and SF134 had no adverse side effects on the lifespan of chicken embryos and <i>C. elegans</i> .....	66
7.2.7 Sulforaphane, SF102 and SF134 exhibit similarities and differences regarding microRNA signaling and target gene induction .....	67
<b>8. Discussion.....</b>	<b>72</b>
<b>8.1 Sulforaphane induces gemcitabine cytotoxicity in PDA by the downregulation of miR30a-3p .....</b>	<b>72</b>
8.1.1 Sulforaphane enhances GJ function and gemcitabine bystander effect.....	72
8.1.2 Sulforaphane augments Cx43 expression by inhibiting miR30a-3p expression .....	73
8.1.3 miR30a-3p inhibits gemcitabine resistance in vitro and in vivo .....	74
8.1.4 miR30a-3p and Cx43 expression in pancreatic cancer tissue.....	75
<b>8.2 Sulforaphane derivatives are proposed as new therapeutic agents for PDA .....</b>	<b>76</b>
8.2.1 SF102 and SF134 induce cytotoxicity in cancer cells .....	76
8.2.2 SF102 and SF134 did not cause significant side effects.....	77
8.2.3 Similarities and differences of SF102 and SF134 regarding microRNA signaling and target gene induction .....	77
8.2.4 Clinical relevance of sulforaphane derivatives synthesis .....	78
<b>8.3 Conclusion.....</b>	<b>79</b>
<b>9. Summary.....</b>	<b>80</b>
<b>10. References .....</b>	<b>84</b>
<b>11. Publications .....</b>	<b>97</b>
<b>12. Supplement .....</b>	<b>98</b>
<b>13. Curriculum Vitae.....</b>	<b>108</b>

<b>14. Acknowledgments .....</b>	<b>109</b>
<b>15. Eidesstattliche Versicherung.....</b>	<b>111</b>

## **1. List of Tables**

Table 1: AJCC staging for pancreatic cancer

Table 2: miRNA candidates for Cx43 regulation in cancer

Table 3: Fluorescent dyes for GJIC assay

Table 4: Transfection reactions of miRNA inhibitors

Table 5: Components of Reverse Transcription reaction mix (mRNA to cDNA)

Table 6: Components of Reverse Transcription reaction mix (miRNA to cDNA)

Table 7: Reaction mix of Real-Time PCR

Table 8: Cycling conditions for real-time PCR

## **2. List of Figures**

Figure 1: Progression of pancreatic cancer lesions in humans

Figure 2: Molecular structure of gemcitabine

Figure 3: Gemcitabine metabolism pathway

Figure 4: Main chemopreventive mechanisms of sulforaphane

Figure 5: Life cycle and therapeutic strategies on connexins and gap junctions

Figure 6: Canonical pathway of miRNA biogenesis

Figure 7: Schematic representation of the double-dye flow cytometry analysis

Figure 8: Volcano plots showing the miRNA and gene distribution after SF treatment

Figure 9: IPA filtering tool to confidently identify mRNA targets of miRNAs

Figure 10: Gap junction KEGG pathway map

Figure 11: Experimental procedure of xenograft treatment on fertilized chicken eggs

Figure 12: Sulforaphane increases GJIC

Figure 13: Sulforaphane enhances the gemcitabine bystander effect through GJs

Figure 14: Sulforaphane inhibits miR30a-3p expression

Figure 15: Sulforaphane induces GJA1 expression and upregulation of Cx43 protein.

Figure 16: miR30a-3p inhibits Cx43 expression by binding to its 3'-UTR



Figure 17: Downregulation of miR30a-3p increased the GJIC and gemcitabine bystander effect

Figure 18: miR30a-3p decreases the volume of xenograft tumors

Figure 19: Low Cx43 and high miR30a-3p expression correlate with malignancy

Figure 20: D,L Sulforaphane and sulforaphane derivatives

Figure 21: SF102 and SF134 repress viability of PDA cells

Figure 22: SF102 and SF 134 repress viability in various cancer entities

Figure 23: SF102 and SF134 enhance apoptosis

Figure 24: SF102 and SF134 inhibit the colony forming ability of PDA cells

Figure 25: SF102 and SF134 reduce the volume of tumor xenografts

Figure 26: Effect of SF102 and SF134 on *C.elegans* lifespan and chick embryos

Figure 27: miRNA expression profiling and bioinformatic analysis detects common and different expression patterns induced by sulforaphane, SF102 and SF134

Figure 28: Identification of NF- $\kappa$ B related miRNA-target genes

### **3. Supplement**

Figure S1: Bystander effect flow cytometry plots for PDA cells

Figure S2: Sulforaphane-regulated gap junction pathway map

Figure S3: Description of the pancreas tissue array

Table S1: List of the 36 most significantly SF-regulated miRNAs

Table S2: List of miRNA candidates shown in the heatmaps of Figure 24B

Table S3: List of differently expressed miRNAs shown in Venn diagrams of Figure 24D.

Table S4: Bioinformatics analysis of target genes of the identified miRNA candidates miR2278, miR27b-5p and miR29b-1-5p regarding their involvement in the NF- $\kappa$ B signaling pathway

## 4. Abbreviations and Units

### Abbreviations

AJCC	American Joint Committee on Cancer
BE	Bystander effect
BSA	Bovine Serum Albumin
CAM	Chorioallantoic membrane
Cx	Connexin
DMEM	Dulbecco's Modified Eagle Medium
DMSO	Dimethyl Sulfoxide
DNA	Deoxyribonucleic Acid
FACS	Fluorescence Activated Cell Sorting
GEM	Gemcitabine
GJ	Gap junctions
GJIC	Gap junctional intercellular communication
HEPES	4-(2-Hydroxyethyl)-1-piperazineethanesulfonic Acid
HCl	Hydrochloric Acid
IHC	Immunohistochemistry
IgG	Immunoglobulin G
IPMN	Intraductal Papillary Mucinous Neoplasm
LY	Lucifer Yellow
miRNA	MicroRNA
mRNA	Messenger RNA
MTT	3-(4,5-dimethylthiazol-2-yl)-2,5-diphenyltetrazoliumbromide
PanIN	Pancreatic Intraepithelial Neoplasia
PBS	Phosphate Buffer Solution
PCR	Polymerase Chain Reaction
PDA	Pancreatic adenocarcinoma
PFA	Paraformaldehyde
PH	Potential of Hydrogen
Ol	Oleamide
RNA	Ribonucleic Acid
RNAi	RNA Interference
RT	Room temperature

RT-PCR	Reverse Transcription Polymerase Chain Reaction
SDS	Sodium Dodecyl Sulfate
TEMED	Tetramethylethylenediamine
TNM	Tumor Node Metastasis
UTR	Untranslated Region
7-AAD	7-aminoactinomycin D

### **Units**

°C	degree Celsius
g	gravitational acceleration (9.81m/s <sup>2</sup> )
kDa	kilo Dalton
h	hours
min	minutes
L	liter
ml	milliliter
μl	microliter
A	ampere
mA	milliampere
M	molar (moles/liter)
mM	millimolar
μM	micromolar
nM	nanomolar
cm	centimeter
mm	millimeter
μm	micrometer
mm <sup>3</sup>	Cubic millimeter
g	gram
μg	microgram
ng	nanogram
rpm	revolutions per minute
v/v	volume per volume
w/v	weight per volume

## **5. Introduction**

### **5.1 Pancreatic cancer**

Pancreatic cancer is one of the most aggressive human malignancies due to its late diagnosis and limited response to treatments. The most common malignancy of the pancreas, accounting for almost 80% of the pancreatic cancer incidences (Kleeff et al. 2016), is pancreatic ductal adenocarcinoma (PDA). In 2018, 458.000 new pancreatic cancer cases were estimated worldwide with a high death toll of 432.000 (Bray et al. 2018). In the United States the year 2019, pancreatic cancer is expected to remain the fourth leading cause of cancer-related death, with a very low 5-year survival rate of 9% (Siegel et al. 2019). In order to manage this deadly cancer, understanding of the molecular mechanisms of pancreatic tumor progression as well as development of new therapeutic strategies are urgently needed.

#### **5.1.1 Pathophysiology, risk factors and staging**

Pancreatic cancer mainly originates from ductal epithelial cells and evolves from pre-malignant lesions such as intraductal papillary mucinous neoplasms (IPMN), mucinous cystic neoplasms and the most histologically characterized precursor lesion called pancreatic intraepithelial neoplasia (PanIN) (Iacobuzio-Donahue et al. 2012). PanIN microscopic lesions progress from low to high dysplasia in three different grades, PanIN-1, PanIN-2, and PanIN-3 (Hruban et al. 2001) (Figure 1). The transformation is a result of the accumulation of genetic mutations that include inactivation of the KRAS and CDKN2A (in almost 95% of pancreatic cancer cases) or activation of the TP53 and SMAD4 (in 75% and 55% of pancreatic cancer cases, respectively) (Hidalgo 2010). The causes of the accumulation of these mutations leading to invasive pancreatic cancer are largely unknown, however there are some important risk factors including smoking, heavy alcohol consumption, obesity, chronic pancreatitis, type 2 diabetes mellitus and several inherited genetic syndromes (Wolfgang et al. 2013).

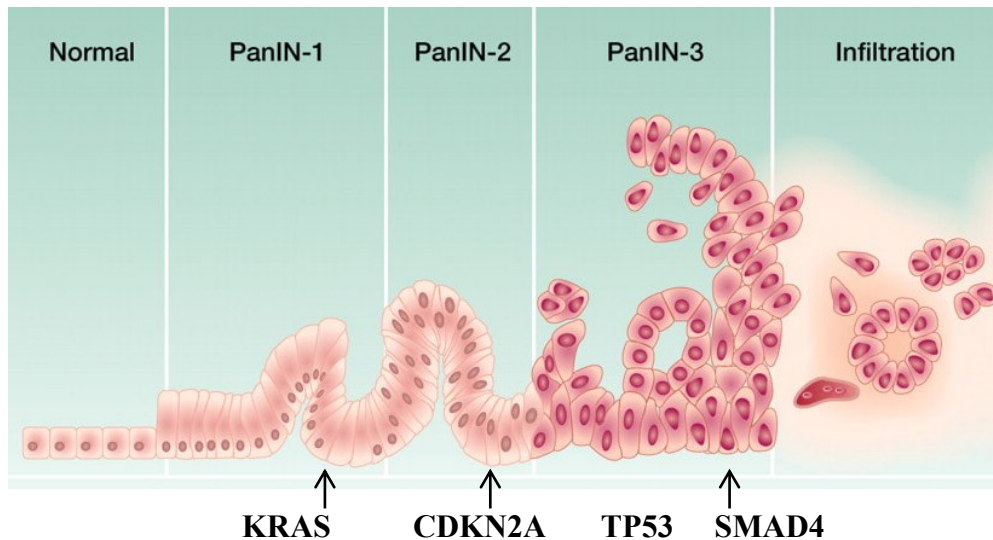


**Figure 1. Progression of pancreatic cancer lesions in humans.** Schematic representation of normal exocrine pancreas cells transforming from PanIN (left) to invasive tumor (right) (Modified from (Iacobuzio-Donahue et al. 2012)).

The majority of malignant neoplasms in the pancreas in terms of percentage of incidence include adenocarcinomas, followed by neuroendocrine tumors, solid-pseudopapillary tumors and acinar cell carcinomas (Kleeff et al. 2016). After the diagnosis of pancreatic cancer, the next step in order to define the treatment is the staging. Tumor-node-metastasis (TNM) classification of pancreatic cancer is widely established by the American Joint Committee on Cancer (AJCC) (Table 1). The information that is taken into account to define the stage includes the location and size of tumor, the association of lymph nodes and distant metastasis (Longo 2012). Patients with advanced stages III and IV cannot undergo putative curative surgery and the median survival time for these patients ranges between 4 and 6 months.

**Table 1: AJCC staging for pancreatic cancer**

AJCC stage	Anatomic stage			Characteristics
	T	N	M	
Stage IA	T1	N0	M0	Tumor limited to pancreas
Stage IB	T2	N0	M0	Tumor limited to pancreas
Stage IIA	T3	N0	M0	Tumor beyond pancreas without lymph-node metastasis
Stage IIB	T1	N1	M0	Tumor beyond pancreas with Regional lymph-node metastasis
	T2	N1	M0	
	T3	N1	M0	
Stage III	T4	Any N	M0	Tumor involved celiac axis or superior mesenteric artery
Stage IV	Any T	Any N	M1	Distant metastases

**Primary Tumor (T)**; T1: Tumor 2 cm or less in greatest dimension; T2: Tumor more than 2 cm in greatest dimension; T3: Tumor extends beyond the pancreas but without involvement of the celiac axis or the superior mesenteric artery; T4: Tumor involves the celiac axis or the superior mesenteric artery; **Regional Lymph Nodes (N)**; N0: No regional lymph node metastasis; N1: Regional lymph node metastasis; **Distant Metastasis (M)**; M0: No distant metastasis; M1: Distant metastasis (Adapted from (Hidalgo 2010)).

### 5.1.2 Current therapeutic options

Pancreatic cancer remains a leading cause of cancer mortality, mainly due to late diagnosis and resistance to current therapeutic treatments (Neoptolemos et al. 2018). Depending on the conditions of patients, different therapeutic strategies such as surgery, radiotherapy, chemotherapy or combinations thereof are used. Surgical resection remains a critical procedure in the pancreatic cancer management, despite the fact that only a small number of patients (10%) receive standard resection in the time of diagnosis (Strobel et al. 2019). For patients with early stage (I and II) resectable pancreatic cancer, curative surgery remains the best option (Shaib et al. 2007), followed by gemcitabine (GEM) plus capecitabine (CAP) adjuvant chemotherapy. The recent ESPAC-4 trial established GEM-CAP adjuvant therapy over GEM monotherapy for patients with resected pancreatic cancer and the 5-year overall survival rate was around 30% (Neoptolemos et al. 2017), (Khorana et al. 2017). For borderline resectable or locally advanced pancreatic cancer, neoadjuvant chemotherapy is proposed, although more evidence from randomized phase III trials are needed (Gillen et al. 2010). The ongoing four-arm randomized ESPAC-5F trial compares immediate surgery with GEM-CAP, FOLFIRINOX and chemoradiotherapy (ISRCTNregistry 2014). For patients with metastatic pancreatic cancer, palliative chemotherapy with FOLFIRINOX and gemcitabine + nab-paclitaxel is the mainstay treatment option (Mohammed et al. 2014), (Ryan et al. 2014).

#### 5.1.2.1 Gemcitabine: clinical applications and metabolism

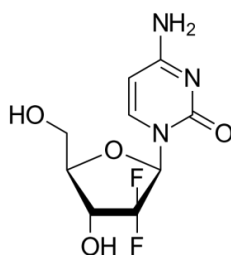


**Figure 2. Molecular structure of gemcitabine.**

4-amino-1-(2-deoxy-2, 2-difluoro-β-D-erythro-entofuranosyl) pyrimidin-2(1H)-on. Fluorine atoms replace the hydrogen atoms on the 2' carbon of deoxycytidine.

Even though the response rate to current chemotherapeutic treatment options is low, chemotherapy is used for PDA patients in any stage, especially in advanced stages when patients have lost the chance of operation (Vincent et al. 2011). Gemcitabine (2',2'-Difluoro-2'-deoxycytidine, dFdC) is a chemotherapeutic drug that has been approved by the Food and Drug Administration (FDA) for the treatment of unresectable pancreatic cancer in 1996 (Network 2019). In 1997, a randomized phase II trial proved the superiority of gemcitabine over fluorouracil (5-FU) as the clinical benefit response of GEM-treated patients (23.8%) was higher compared to the 5-FU-treated patients (4.8%) as well as the median survival time (5.6 months and 4.4 months, respectively) (Burris et al. 1997). Another phase II trial for advanced and metastatic pancreatic cancer has shown that the addition of capecitabine to the gemcitabine monotherapy improved the overall response rate and survival (Cunningham et al. 2009). Until now, gemcitabine has been the mainstay neo-adjuvant, adjuvant and palliative therapy for PDA and has been used for the treatment of various solid tumors including breast, lung and ovarian, however, a big obstacle is that resistance to gemcitabine occurs within the first weeks of treatment (Binenbaum et al. 2015).

Regarding the chemical structure, GEM is a nucleoside analog in which the hydrogen atoms on the 2' carbon of deoxycytidine are replaced by fluorine atoms (Figure 2). The major uptake of gemcitabine takes place via the equilibrative and concentrative type of the nucleoside transporters (ENTs and CNTs, respectively). Once in the cell, the GEM prodrug (dFdC) is activated by an intracellular phosphorylation cascade initiated by the production of dFdCMP by deoxycytidine kinase (dCK). In turn, dFdCMP is converted by other pyrimidine kinases to its active diphosphate and triphosphate derivatives, dFdCDP and dFdCTP, respectively (Figure 3). The final metabolite, dFdCTP, is incorporated into the growing DNA chain as a normal nucleotide and leads to the inhibition of DNA synthesis (Binenbaum et al. 2015). Interestingly, levels of dFdCTP must comprise a sufficient proportion of the cellular pool of deoxyribonucleotides (dNTPs) in order to be efficiently incorporated into DNA and the NTPs pool is maintained by the enzyme ribonucleotide reductase (Liang et al. 2017). An additional self-potential mechanism of gemcitabine includes the binding of dFdCDP to the active site of ribonucleotide reductase leading to a decreased activity and synthesis of the dNTPs, which will further enhance the incorporation of dFdCTP into the DNA and the inhibition of DNA replication (Gesto et al. 2012).



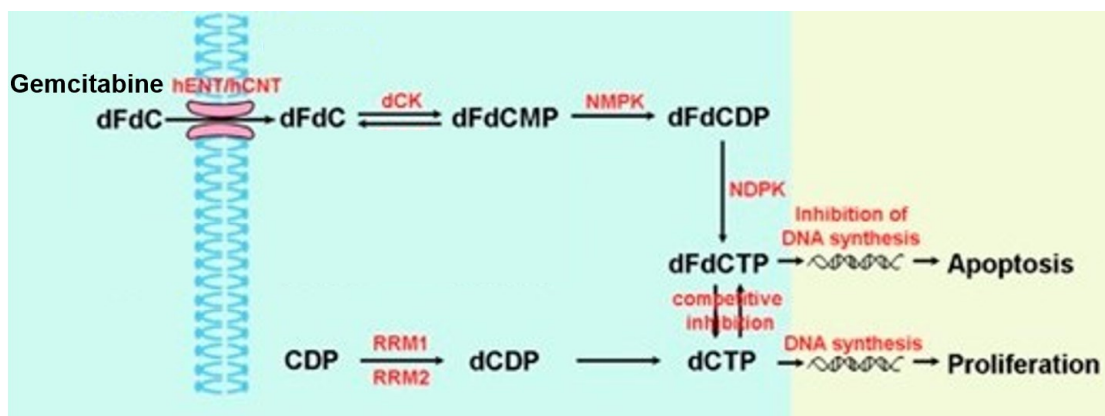


**Figure 3. Gemcitabine metabolism pathway (adapted and modified from (Liang et al. 2017)).** After uptake of gemcitabine (dFdC) by the nucleoside transporters (hENT/hCNT), the GEM prodrug is converted to the dFdC monophosphate (dFdCMP) by deoxycytidine kinase (dCK). Afterwards, dFdCMP is converted to diphosphate (dFdCDP) and triphosphate (dFdCTP) metabolites by nucleoside monophosphate /diphosphate kinase (NMPK/NDPK). dFdCTP incorporates in the DNA causing inhibition of DNA synthesis and induction of apoptosis. dCTP is an endogenous competitor of dFdCTP or DNA-incorporation, and is produced by ribonucleoside reductases (RR).

## 5.2 Sulforaphane

### 5.2.1 Chemical structure and bioavailability

Epidemiological studies indicate that higher consumption of broccoli and other cruciferous vegetables of the *Brassicaceae* family are correlated with a lower cancer risk including PDA and cancer of the breast, lung, kidney, colon, rectum and prostate (Herr et al. 2013), (Kim and Park 2009). *Brassicaceae* are unique compared to other plants in their high content of glucosinolates ( $\beta$ -thioglucoside N-hydroxysulfates), which is a class of sulfur-rich metabolites with more than 120 unique amino acid side chains (Herr and Buchler 2010), (Bayat Mokhtari et al. 2018). A focus has been placed on the glucosinolate glucoraphanin [4-(methylsulfinyl) butyl glucosinolate], which is found in high concentration in broccoli and its sprouts. 60-80% of glucoraphanin is converted upon plant tissue damage (e.g. chewing) to its active form, the isothiocyanate sulforaphane [1-isothiocyanato-(4*R*)-(methylsulfinyl)-butane], by hydrolysis mediated by the  $\beta$ -thioglucosidase enzyme myrosinase or by the microbiota of the human colon. After being absorbed by the cells of the intestinal epithelium, sulforaphane is metabolised through the mercapturic acid pathway. This process involves its initial conjugation with glutathione, while the N-acetylation is important for the subsequent excretion of sulforaphane from the body through the urine, already few hours after consumption (Tortorella et al. 2015), (Atwell et al. 2015).

## 5.2.2 Sulforaphane and cancer

### 5.2.2.1 Mechanisms of action

Sulforaphane is one of the best studied bioactive agents with chemopreventive properties and is proven to induce detoxifying of carcinogens, anti-oxidation, cell cycle arrest, apoptosis and epigenetic regulation, while inhibiting angiogenetic and metastatic progression (de Melo et al. 2018), (Bayat Mokhtari et al. 2018), (Tortorella et al. 2015).

**Inhibition of NF- $\kappa$ B signaling:** Initiation of inflammatory response is related to the nuclear factor kappa B (NF- $\kappa$ B) pathway. NF- $\kappa$ B is an important transcription factor ubiquitously found in all cell types and present in the cytoplasm in resting condition (Jost and Ruland 2007). In PDA, sulforaphane was shown to normalize increased NF- $\kappa$ B signaling by inhibiting transactivation-potent NF- $\kappa$ B subunit c-Rel (Figure 4), which led to repression tumor stem cell features and increase of the sensitivity to cytotoxic drugs (Kallifatidis et al. 2009), (Rausch et al. 2010), (Kallifatidis et al. 2011).

**Induction of apoptosis:** Sulforaphane was demonstrated to enhance apoptosis in glioblastoma cell lines via upregulation of Bax, Bad, Bax/Bcl-2 ratio, cytochrome C and downregulation of Bcl-2 (Figure 4) (Zhang et al. 2016). In prostate cancer, sulforaphane was shown to induce apoptosis by upregulation of Bax, activation of caspases-3, -9 and -8 and downregulation of Bcl-2 (Singh et al. 2004).

**Epigenetic regulation:** Inhibition of tumor progression by sulforaphane also involves the modulation of epigenetic mechanisms such as DNA methylation, histone acetylation and miRNAs (de Melo et al. 2018). Sulforaphane inhibits the activity of DNA methyltransferases (DNMTs) in prostate and breast cancer cell lines (Wong et al. 2014), (Lubecka-Pietruszewska et al. 2015), while the inhibition of histone deacetylases (HDAC) is linked to the sulforaphane-induced apoptosis (Bayat Mokhtari et al. 2018). Recent findings demonstrate that sulforaphane induces microRNA (miRNA) signaling to inhibit NF- $\kappa$ B signaling via binding to the 3'-UTR of the transactivation-potent NF- $\kappa$ B subunit c-Rel (Yin et al. 2019).

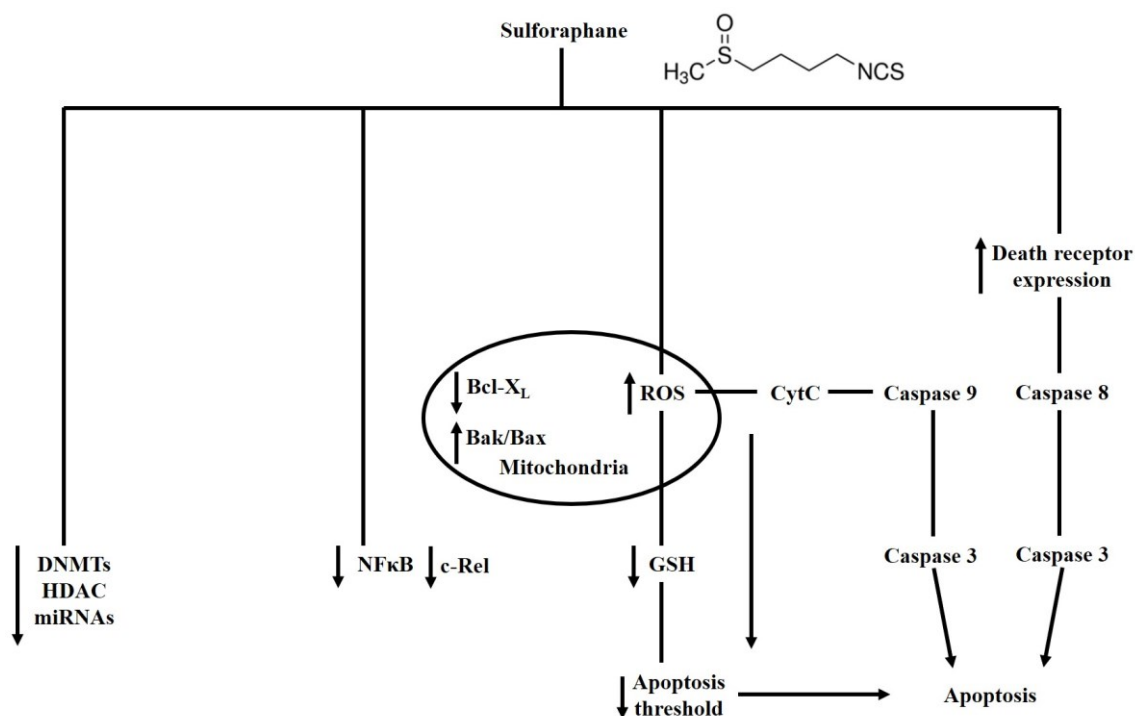


**Figure 4. Main chemopreventive mechanisms of sulforaphane (adapted and modified from (Tortorella et al. 2015)).** Induction of apoptosis is mediated by the increased expression of Bax and Bak as well as caspase 3, 8 and 9 and decreased expression of Bcl-2. Upregulation of Cytochrome C (CytC) enhances apoptosis by inducing Reactive Oxygen Species (ROS) and the anti-inflammatory effect of sulforaphane is displayed through the suppressed activity of NF-κB signaling. Sulforaphane inhibits the activity of DNA methyltransferases, histone acetylases (HDAC) and miRNAs.

### 5.2.2.2 Pharmaceutical relevance of sulforaphane

Sulforaphane is cancer preventive and possesses therapeutic efficacy in treatment of cancer and has shown promising results in both pre-clinical and clinical studies. Pre-clinical *in vivo* studies showed that intraperitoneal injection of sulforaphane (4.4 mg/kg on day 4, 5 and 6) in nude mice carrying PDA xenografts inhibited the tumor growth (Kallifatidis et al. 2009). A pilot study with pulverized broccoli sprouts was performed in the surgery department of the Heidelberg University Clinic with 40 patients involved, suffering from advanced, non-resectable pancreatic cancer. The results indicated that the patients in the broccoli sprout group survived longer compared to the placebo group, although the results were not significant due to the small number of patients (Lozanovski et al. 2019). With regard to other types of cancer, a randomized phase II clinical trial in women with early diagnosed breast intraductal carcinoma (DCIS) proved a decreased proliferative rate in the broccoli sprout extract group compared to the placebo (ClinicalTrials.gov 2018).

A phase II study of sulforaphane-rich broccoli sprout extracts in men with recurrent prostate cancer there was a significant lengthening of the prostate-specific antigen doubling time in the sulforaphane treatment group (Alumkal et al. 2015).

### **5.3 Gap junctions**

Gap junctions are intercellular channels, found in the plasma membrane, that allow the direct communication between the cytoplasm of adjacent cells. These membrane structures contain cluster of channels and enable an intimate way of cell communication symmetrically in both directions (Alberts 2008). Gap junctions allow the exchange of ions, electrical signals, fluorescent dyes, secondary messengers and small metabolites with a mass less than 1 kDa (Evans and Martin 2002), such as  $Ca^{2+}$ , cyclic adenosine monophosphate (cAMP) and inositol 1,4,5-triphosphate (IP3) through a process called gap junctional intercellular communication (GJIC).

#### **5.3.1 Structure and functions**

Gap junctions are formed by a family of proteins called connexins. Connexins are transmembrane proteins and six of them can form a hemichannel or connexon. Two connexons are aligned in the plasma membranes of the two cells forming an intercellular junction and also maintain a distance between the two plasma membranes via separation gap of 2-3 nm (Laird 2006), (Alberts 2008). There are 21 different proteins in the connexin family. Each connexin has four transmembrane (TM) domains, which are connected via the intramolecular disulfide bonds of the two extracellular loops. Connexins also have cytoplasmic N- and C- termini and an extra intracellular loop that links the transmembrane domain 2 and 3. Even though the transmembrane domains, extracellular loops and N- terminus are relatively conserved among the different connexins, the cytoplasmic loop and C-terminus show a great variance in the sequence and length (Mese et al. 2007). The gene structure and the divergence of the cytoplasmic loop leads to subdivision of connexins to five groups ( $\alpha$ ,  $\beta$ ,  $\gamma$ ,  $\delta$  and  $\epsilon$ ). A common abbreviation for connexins includes the 'GJ' from gap junction, the group symbol and the order to discovery of the protein (e.g. Cx32 was the first connexin of  $\beta$ -group, GJB1). However, the widely used nomenclature for connexins is based on their predicted molecular weight (e.g. Cx26 is 26 kDa in size). Connexins are expressed in nearly every cell type, in a tissue-specific manner, and the same cells can express multiple connexins.

Gap junctions with different combinations of connexins also have different permeability properties. Connexons with different connexin isoforms are called heteromeric, while homomeric connexins express only one connexin isoform. The same principle applies for the gap junctions, as homotypic are junctions with the same connexons and heterotypic are with different ones (Nielsen et al. 2012).

From the connexin family, the most extended studies have been conducted on connexin 43 (Cx43), as it is the most ubiquitously expressed connexin in mammals. It was first identified and sequenced in 1987, as a first connexin from the  $\alpha$ -group and is encoded by the GJA1 gene (Laird and Lampe 2018a). Most connexins including Cx43 are co-translationally integrated into the endoplasmic reticulum (ER). If Cx43 is correctly folded, it traffics to the Golgi apparatus, where it oligomerizes in connexons in the trans-Golgi network. The delivery of connexons to the cell surface is facilitated by microtubules via transport vehicles. Connexons could be permeable to small molecules exchange with the extracellular matrix until their docking on the gap junction plaque. Prior to their lysosomal degradation, gap junctions are internalized into connexosomes (Figure 5) (Musil and Goodenough 1993), (Naus and Laird 2010). GJIC can be regulated by various stimuli including gap junction assembly and turnover and posttranslational connexin phosphorylation (Lampe and Lau 2004). In the case of Cx43, the 17 kDa C-terminus is extensively phosphorylated at 21 different phosphorylation sites containing serine or tyrosine residues mainly by protein kinase C (PKC), casein kinase 1 (CK1) and mitogen-activated protein kinase (MAPK) (Axelsen et al. 2013).

### **5.3.2 Gap junctions and cancer**

The first link between gap junctions and tumorigenesis was established in 1966 where the electrical coupling and metabolic cooperation was found to be defect in liver tumor cells compared to healthy hepatocytes (Loewenstein and Kanno 1966). Further studies revealed the loss of GJIC in several tumors (McNutt and Weinstein 1969), (Johnson and Sheridan 1971). After the discovery and characterization of connexins in the late 1980s, there were extended studies about the role of connexin expression in tumor progression. In most of the solid tissue human cancers, connexin expression is lost in the early stages suggesting a tumor suppressive role, while their role in the late stages is more complex as cancer cells seem to restore connexin expression levels in order to achieve tumor progression and metastasis (Naus and Laird 2010), (Aasen et al. 2016).

The tumor suppressive mechanism of connexins is mainly GJIC-dependent and involves the molecules exchange between normal cells and cancer cells, but can also be GJIC-independent.

In a normal tissue condition, the presence of connexins is necessary for the formation of gap junctions, the establishment of GJIC and exchange of specific metabolites. In a cancer tissue, connexins act as tumor suppressors and therefore inhibit the proper formation of gap junctions and the exchange of metabolites. This leads to an autonomous cell behavior and tumor progression (Naus and Laird 2010). In the case of Cx43, it was proven to act as tumor suppressor in colorectal, melanoma and breast cancer cells (Sirnes et al. 2012), (Tittarelli et al. 2015), (Banerjee 2016). Several studies correlated low Cx43 expression with poor prognosis in patients with pancreatic, prostate, colorectal and breast cancer (Benko et al. 2011), (Liang et al. 2010), (Teleki et al. 2014).

### **5.3.2.1 Gap junctions and therapeutic potential**

The lack of intercellular communication lead to autonomous behavior of cancer cells, which results in failure to respond to cellular regulation mechanisms and chemotherapy resistance. Chemotherapeutic drugs and their metabolites can diffuse from cell-to-cell through the gap junctions enabling better therapeutic efficacy through bystander effect (Aasen et al. 2016). Bystander effect refers to the observation that chemotherapeutic drugs and their metabolites can diffuse from treated tumor cells to surrounding non-treated tumor cells amplifying the cytotoxicity of the drugs. It was originally described in the ganciclovir (GCV) suicide gene therapy (Pitts 1994) and has also been documented with other drugs including gemcitabine (Cottin et al. 2010), (Garcia-Rodriguez et al. 2011). Enhancing the GJIC is a therapeutic strategy that can increase the bystander effect and therefore the chemotherapy efficacy (Figure 5). In pancreatic cancer the bioactive agent sulforaphane has been shown to restore GJIC and gemcitabine sensitivity via the upregulation of Cx43 (Forster et al. 2014).

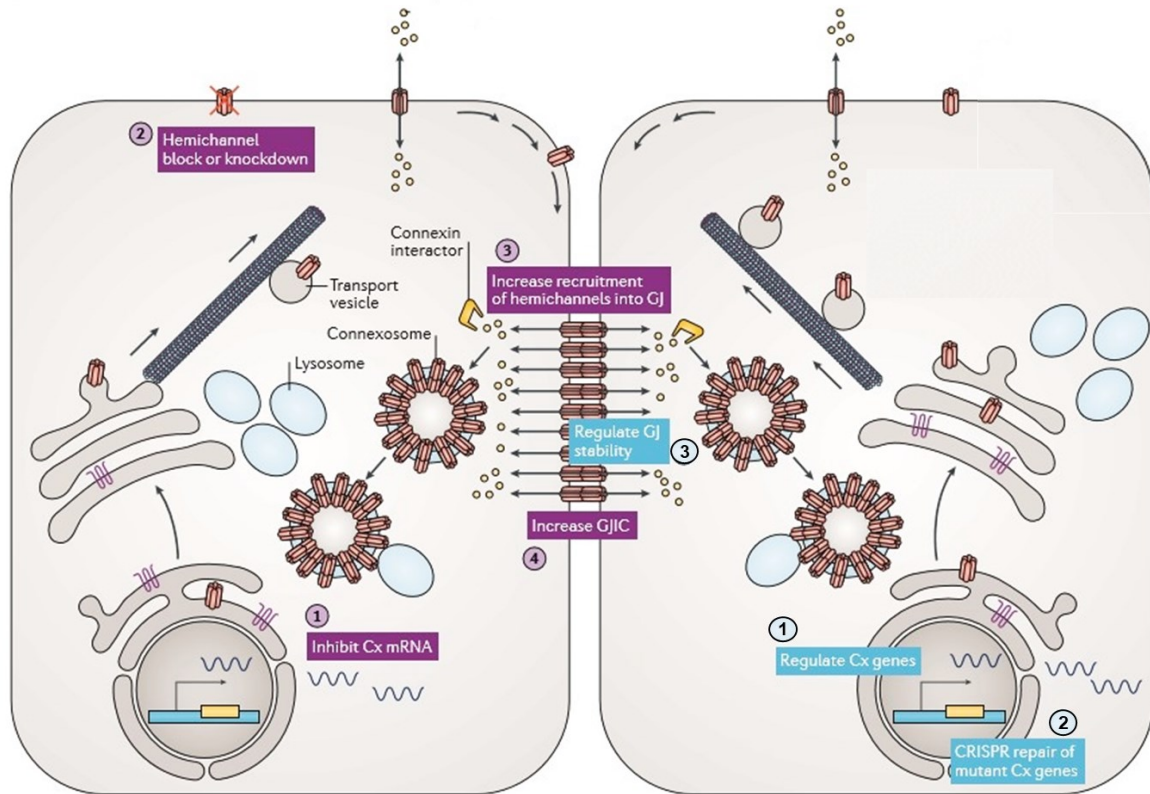


**Figure 5. Life cycle and therapeutic strategies on connexins and gap junctions (Adapted and modified from (Laird and Lampe 2018b)).** Connexins (Cxs) are integrated in the endoplasmic reticulum and, if corrected folded, they enter the secretory pathway and reaching the plasma membrane where they can form the gap junction channels. Cxs oligomerize into connexons either in the endoplasmic reticulum or at more distal sites including the trans-Golgi network. The transfer of connexons to the plasma membrane is conducted via transport vehicles and the transport is mediated by microtubules. Purple boxes refer to the therapeutic strategies with Cxs and gap junctional intercellular communication (GJIC) that are already mentioned such as increasing GJIC (4) or inhibition of connexin (Cx) expression levels. Blue boxes refer to future developments that can lead to better therapeutic results. For example, not only inhibition but also upregulation of Cx genes can be beneficial for cancer treatment (1) as well as the maintenance of the stability of GJs (Burriss et al. 1997).

## 5.4 MicroRNAs

MicroRNAs (miRNAs) are small (19-25 nucleotides) evolutionary conserved, noncoding RNA molecules whose main function is to regulate gene expression through translational repression, mRNA decay or direct mRNA degradation by targeting its 3'-untranslated region (3'-UTR) (Bartel 2009), (Slotwinski et al. 2018). miRNAs were first identified in *C.elegans* where the miRNA *lin-4* inhibited the expression level of LIN-14 protein (Lee et al. 1993) and the miRNA *let-7* inhibited the expression of the LIN-41 protein (Reinhart et al. 2000) by the complementary targeting of the 3'-untranslated region (3'-UTR). Based on the last release of the miRBase database, there are 2654 mature miRNA sequences identified in the human genome (Kozomara et al. 2019).

### **5.4.1 Biogenesis and regulation**

In the nucleus, miRNAs are first transcribed either by RNA polymerase II or by RNA polymerase III into pri-miRNAs (Lee et al. 2004). Pri-miRNAs are long transcripts that consist of hairpin-like miRNA precursors. Pri-miRNAs are cleaved to pre-miRNAs by Drosha endonuclease and its binding partner DGCR8, which form the microprocessor complex (Lee et al. 2003). The 60-70 nucleotides precursor product (pre-miRNA) is then exported to the cytoplasm from the nucleus processed by Exportin-5 and Ran-GTP (Winter et al. 2009). The loop structure of the pre-miRNAs is further cleaved to a miRNA duplex by the RNase III enzyme Dicer, which is interacting with the double-stranded RNA binding protein TRBP (Tar RNA binding protein), PACT (protein kinase R-activating protein) and Argonaute family proteins (Ago1/2) (Gregory et al. 2005). From the miRNA duplex, the single guide strand is incorporated into the RNA-induced silencing complex (RISC) and is used to identify target mRNAs. Based on the complementarity of the guide miRNA strand with the mRNA transcript, there will be either mRNA degradation or translational repression (Slotwinski et al. 2018) (Figure 6).



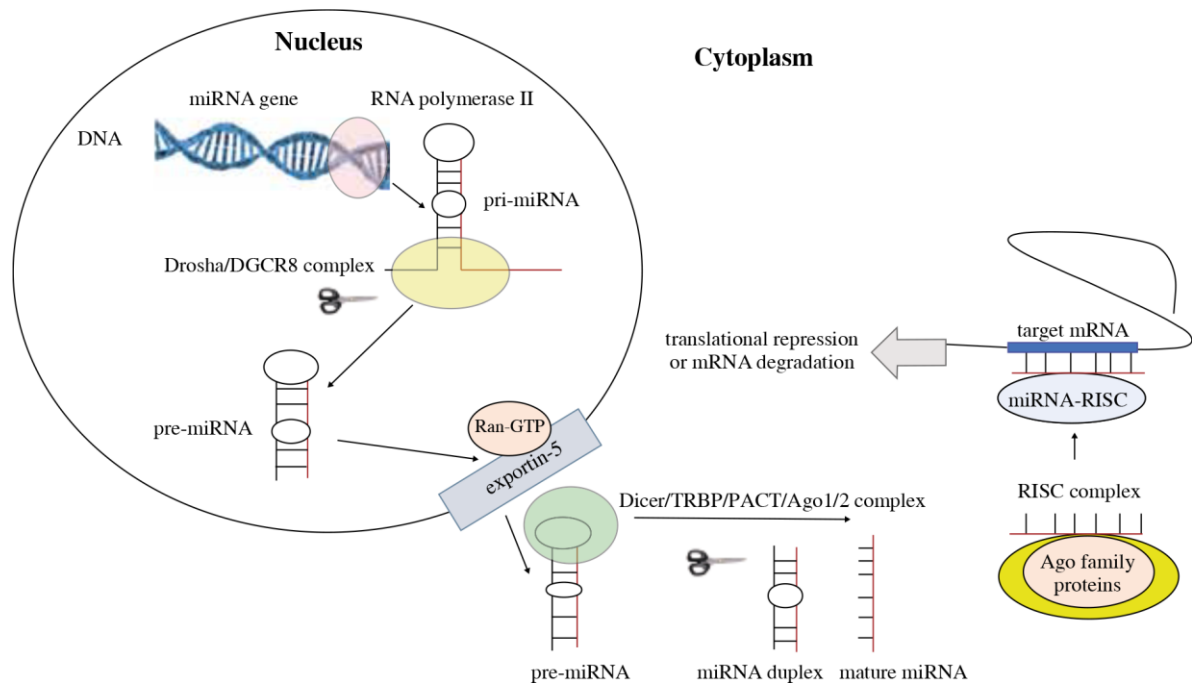


**Figure 6. Canonical pathway of miRNA biogenesis (Slotwinski et al. 2018).**

#### 5.4.2 miRNAs involved in cancer

miRNAs influence numerous cancer-related processes in a tissue-specific manner, such as proliferation, apoptosis, migration, invasion, and drug resistance (Acunzo et al. 2015). The first documentation of miRNA abnormality in cancer was in 2002 where the miR-15 and -16 were observed to be absent or downregulated in most of the chronic lymphocytic leukemia (CLL) patients due to the chromosomal loss of the 13q14 (Calin et al. 2002). Further studies showed that these 2 miRNAs regulate the BCL-2 expression in CLL and, as a result of the chromosomal depletion, the upregulation of BCL-2 leads to increased cell survival and tumorigenesis (Cimmino et al. 2005). Based on their regulation of tumor suppressors or oncogenes, miRNAs can be classified as oncogenic miRNAs (their overexpression leads to the inhibition of tumor-suppressor mRNA) or tumor-suppressing miRNAs (their downregulation leads to the induction of oncogene mRNA) (Kong et al. 2012). The study from Takamizawa et al. suggested *let-7* as tumor-suppressing miRNA, as its reduced expression correlated with shorter survival in lung cancer patients (Takamizawa et al. 2004). MiR-21 has been identified as oncogenic miRNA, as inhibition of miR-21 expression led to increased cell death in glioblastoma cells (Chan et al. 2005). In pancreatic cancer, many different miRNAs are involved in the genetic alterations observed in the 12 core signaling pathways (Jones et al. 2008).

The function of miRNAs as tumor suppressors or oncogenes in PDA can vary even among the signaling pathways and the genes involved. For instance, the expression of miR-181b and miR-21 in PDA, which both regulate the expression of BCL-2, is different as miR-181b is documented to be downregulated, while miR-21 is upregulated (Sun et al. 2015). In the case of *let-7* and miR-96, they both act as tumor-suppressing miRNAs by regulating the KRAS oncogene (Watanabe et al. 2009), (Yu et al. 2010).

#### 5.4.2.1 miRNAs and Cx43

Regulation of connexin expression involves, except post-translational phosphorylation, additional modulating factors such as peptides, antibodies and miRNAs (Aasen et al. 2016). Several studies have detected the inhibition of Cx43 expression at a post-transcriptional level by miRNAs in different types of cancer as summarized in Table 2.

**Table 2. miRNA candidates for Cx43 regulation in cancer**

miRNA Symbol	Cancer Type	References
miR-20a	Prostate cancer	(Li et al. 2012)
miR-221/222	Glioblastoma	(Hao et al. 2012)
miR-125b	Glioma	(Jin et al. 2013)
miR-200a	Breast cancer	(Ming et al. 2015)
miR-206	Breast cancer	(Fu et al. 2015)

## 5.5 Aim of the study

Previous studies in our group showed that sulforaphane enhanced Cx43 expression and restored the defective gap junctional intercellular communication in highly malignant and gemcitabine resistant pancreatic cancer cells (Forster et al. 2014). The first part of my thesis focuses on identifying the underlying mechanism of action of sulforaphane, which leads to gap junction activation and thereby increases gemcitabine sensitivity. **The hypothesis of this project is** that miRNA regulation is involved in the induction of gap junctional intercellular communication and Cx43 expression and this regulation increases gemcitabine cytotoxicity in pancreatic cancer. **The major aim of this project is** to identify a sulforaphane-regulated miRNA candidate and validate its function in gap junctional intercellular communication, Cx43 expression and tumor progression *in vitro*, *in vivo* and *ex vivo*.

The second part of my thesis involves the biological evaluation of seven unprecedented derivatives of sulforaphane in pancreatic cancer and other tumor entities. **The hypothesis of this project is** that chemical modifications of sulforaphane could increase its therapeutic potential against pancreatic cancer. **The major aim of this project is** to evaluate the anti-cancer potential of these new sulforaphane derivatives with the least side effects *in vitro* and *in vivo* and, subsequently, compare the activity and underlying molecular mechanisms of the most effective derivatives to the original sulforaphane.

## 6. Materials and Methods

### 6.1 Materials

#### 6.1.1 Equipment and consumables

6 well plates (Cell Star <sup>®</sup> )	Greiner bio-one, Austria
24 well plates (Cell Star <sup>®</sup> )	Greiner bio-one, Austria
96 well plates (Cell Star <sup>®</sup> )	Greiner bio-one, Austria
Analytical balance (Mettler P220)	Mettler Toledo, Switzerland
Blotting chamber	Starlab, Belgium
Thermal Cycler	Bioer Technology, China
BMG FLUO star OPTIMA Microplate Reader	BMG LABTECH GmbH Germany
Cell counter–Z <sup>TM</sup> Series	Beckman Coulter, USA
Cell counter tubes	Beckman Coulter, USA
Centrifuges	
-Biofuge 15 R	Heraeus, Hanau
-Capsulefuge PMC-060	TOMY, Fremont, USA
-Cytospin 4	Thermo Scientific, USA
-Varifuge 3.0 R	Heraeus, Hanau
Centrifuge tubes (15 ml and 50 ml)	TPP, Switzerland
Cell scraper	Greiner Bio-one, Austria
Cell culture plates	TPP, Switzerland
Cell culture dishes	TPP, Switzerland
CO <sub>2</sub> incubator	MS Laborgeräte, Germany
Cryotubes	Nunc, Denmark
Digital motor breeder	Poultry Farm Hockenberger, Eppingen, Germany
Electrophoresis power supply	Biotec Fisher, Germany
Electrophoresis Semi-Dry Blotters	Starlab, Belgium
Electrophoresis unit	Bio-Rad, USA
Eppendorf Thermomixer comfort	Eppendorf, Germany
BD FACSCanto II flow cytometer	BD Biosciences, Germany

Filter tips	Starlab, Belgium
Fluorescent microscope	Leica, Germany
Freezing container	Nalgene, USA
Gloves latex powder free	Technomed, France
Ice machine (AF80)	Scotsman, USA
Incubator-Digital motor breeders	Siepmann, Germany
Immobilon®-P Transfer membrane (Pore size 0.45 µm)	Millipore, USA
Lab freezers (-20°C, -80°C)	Liebherr, Germany
Laminar Flow Hood, HERA safe	Heraeus Instruments, Germany
Leukosilk® tape	BSN medical, Germany
Light microscope	Leica, Germany
Mr. Frosty Freezing Container	Thermo Fisher, USA
NanoDrop® Spectrophotometer	NanoDrop Tech, USA
Needles Gr20, grey, 27G, 0.4 x 22 mm	BD, USA
Needles yellow, 20G, 0.9 x 40 mm	BD, USA
Odyssey® CLx imager	Li-COR®, USA
Pasteur pipettes	WTW, Germany
pH-meter (pH 538)	WTW, USA
Pipette controller, comfort	IBS Integra, Switzerland
Polystyrene Round-bottom Tube with Cell-Strainer Cap	Neolab, Germany
Repeat pipettor, multistep	Eppendorf, Germany
Shaker–Unimax 2010	Heidolph, Germany
Surgical forceps	Bio-Rad, USA
Surgical syringes	Bio-Rad, USA
Step One™ Real Time PCR system	Applied Biosystems, USA
Thermanox plastic coverslips	Thermo Scientific, USA
Thermo mixer	Eppendorf, Germany
Tissue culture dishes,	Greiner bio-one, Austria
Tissue culture flasks, T-75, T-150	TPP, Switzerland
Vortexer (REAX2000)	Heidolph, Germany
Water bath	Kottermann, Germany

### 6.1.2 Media and supplements for cell culture

DMEM High Glucose (4.5 g/l)	Sigma-Aldrich, USA
DNase/RNase free water	Sigma-Aldrich, USA
Dimethylsulfoxide (DMSO, >99%)	AppliChem, Germany
Dulbecco's Phosphate Buffer Solution (PBS)	Invitrogen, USA
FBS (Fetal Bovine Serum)	Sigma-Aldrich, USA
HEPES Buffer Solution (1M)	PAA Laboratories, Austria
Lipofectamine 2000	Invitrogen, USA
Opti-MEM™ I Reduced Serum Medium	Thermo Fisher, USA
RPMI-1640 without Phenol Red and L-glutamine	C.c.pro, Germany
StemPro™ Accutase™ Cell Dissociation Reagent	Thermo Fisher, USA
Trypsin-EDTA (0.25%)	Sigma-Aldrich, USA
Water–Aqua ad injectabilia	Braun, Germany

### 6.1.3 Chemical agents and enzymes

7-AAD (7-aminoactinomycin D)	Thermo Fisher, USA
2-Propanol	Sigma-Aldrich, USA
Acetone	Sigma-Aldrich, USA
Acrylamide stock solution	Sigma-Aldrich, USA
Ammonium persulfate (APS)	Carl Roth, Switzerland
Bovine Serum Albumin (BSA)	New England Biolabs, USA
Calcein AM Viability Dye	Thermo Fisher, USA
CellTracker™ Red CMTPX Dye	Thermo Fisher, USA
Chloroform	Sigma-Aldrich, USA
DAPI (4,6-diamidino-2-phenylindole)	Sigma-Aldrich, USA
Dimethylsulphoxide (DMSO)	Carl Roth, Switzerland
Dithiothreitol (DTT)	Sigma-Aldrich, USA
D,L-Sulforaphane	Sigma-Aldrich, USA
EDTA-Disodium	Sigma-Aldrich, USA
Ethanol	Sigma-Aldrich, USA
Formalin	Carl Roth, Switzerland

Gemcitabine	Pharmacy, Heidelberg University Hospital
Glycerol	Appli Chem, Germany
Glycine	Appli Chem, Germany
Goat serum	Alexis, Germany
Hydrochloric acid (HCl)	J.T.Baker, Deventer, Netherlands
Hematoxylin solution, Mayers	Sigma-Aldrich, USA
Ketanest 25 mg/ml	Pfizer, New York, USA
Lämmli sample buffer 4x	Bio-Rad, USA
Lucifer Yellow CH dilithium salt	Sigma-Aldrich, USA
Magnesium Chloride (MgCl <sub>2</sub> )	Carl Roth, Switzerland
Methanol	Carl Roth, Switzerland
<i>mirVana</i> <sup>TM</sup> miRNA Inhibitor	Thermo Fisher, USA
<i>mirVana</i> <sup>TM</sup> miRNA Inhibitor, Negative Control	Thermo Fisher, USA
MTT	Sigma-Aldrich, USA
Paraformaldehyde (37%)	Merck, Germany
Potassium chloride (KCl)	Merck, Germany
Potassium dihydrogen phosphate (KH <sub>2</sub> PO <sub>4</sub> )	Merck, Germany
Protease inhibitor cocktail tablets	Carl Roth, Switzerland
Proteinase K	Qiagen, Germany
Protein ladder-Page Ruler <sup>TM</sup>	Fermentas, USA
SDS pellets	Carl Roth, Switzerland
Sheep serum	Jackson ImmunoResearch, USA
Sodium chloride (NaCl)	Carl Roth, Switzerland
Sodium citrate (Na <sub>3</sub> C <sub>6</sub> H <sub>5</sub> O <sub>7</sub> )	Carl Roth, Switzerland
Sodium hydroxide (NaOH)	Carl Roth, Switzerland
TEMED	Merck, Germany
Tris	Merck, Germany
Tween-20	Sigma-Aldrich, USA

#### 6.1.4 Kits

Avidin-Biotin Blocking Kit	Linaris, Germany
----------------------------	------------------

BCA <sup>TM</sup> protein Assay Kit	Thermo Fisher, USA
BCIP/NBT Alkaline Phosphatase (AP) Substrate Kit	VECTOR Laboratories, USA
Clariom D Assay	Thermo Fisher, USA
Dual-Luciferase Reporter Assay System	Promega, Germany
GeneChip <sup>TM</sup> miRNA 4.0 Array	Thermo Fisher, USA
High-Capacity cDNA Reverse Transcription Kit	Thermo Fisher, USA
Lipofectamine <sup>TM</sup> 2000 Transfection Reagent	Thermo Fisher, USA
miRNeasy Mini Kit	Qiagen, Germany
miRCURY LNA <sup>TM</sup> microRNA ISH Optimization Kit (FFPE)	EXIQON, Denmark
PE Annexin V Apoptosis Detection Kit I	BD Biosciences, Germany
PMirTarget_GJA1_3UTR_firefly	OriGene, USA
Pgl4.73[hRluc/SV40]	Promega Germany
RNeasy Mini Kit	Qiagen, Germany
TaqMan <sup>®</sup> MicroRNA Assay	Thermo Fisher, USA
TaqMan <sup>®</sup> MicroRNA Reverse Transcription Kit	Thermo Fisher, USA
TaqMan <sup>®</sup> Universal Master Mix	Thermo Fisher, USA
Pancreas cancer tissue array PA961c	US Biomax INC., USA
Lipofectamine <sup>®</sup> 2000 Reagent	Thermo Fisher, USA
VECTASTAIN Elite ABC HRP Kit	Vector Laboratories, Inc, USA
ZytoChem-Plus HRP polymer kit with AEC	Zytomed Systems, Germany

### 6.1.5 Buffers and solutions

All buffers were prepared in distilled water unless otherwise specified.

FACS Buffer	500 ml PBS 2% FCS 2 mM EDTA
10% APS	1 g Ammonium persulfate Adding ddH <sub>2</sub> O up to 10 ml
1 M Tris-HCl	24.2 g Tris 200 ml ddH <sub>2</sub> O pH 6.8



1.5 M Tris-HCl	36.32 g Tris 200 ml ddH <sub>2</sub> O pH 8.8
10× PBS	2 g KCl 2 g KH <sub>2</sub> PO <sub>4</sub> 14.41g Na <sub>2</sub> HPO <sub>4</sub> ·2H <sub>2</sub> O 80 g NaCl Adding ddH <sub>2</sub> O up to 1L
10% SDS	10 g SDS Adding ddH <sub>2</sub> O up to 100 ml
MTT stock solution	0.5 g Thiazozyl Blue Tetrazolium-Bromide
Transfer Buffer	100 ml 1× PBS 2.930 g Glycine (39 mM) 5.810 g Tris (48 mM) 0.375 g SDS (0.0375% w/v) 200 ml Methanol (20%) Adding ddH <sub>2</sub> O up to 1 L
Chicken PBS	7.2 g NaCl 0.37 g KCl 0.23 g CaCl <sub>2</sub> Made up to 1 L with ddH <sub>2</sub> O
10 × Triethanolamine Buffered Saline (TBS) solution	87.6 g NaCl (1.5 M) 12.1 g Tris (100 mM) 1 g NaN <sub>3</sub> Adjust volume with ddH <sub>2</sub> O up to 1L and pH to 7.5
Proteinase K Buffer	5 ml of 1M Tris-HCl 2 ml of 0.5 M EDTA 0.2 ml of 5M NaCl Adjust volume with ddH <sub>2</sub> O up to 1 L and pH to 7.4, autoclaving
20 x SSC Buffer	175.3 g NaCl 88.2 g Sodium Citrate Adding ddH <sub>2</sub> O up to 1 L and autoclaving
10 x AP Buffer	1 M Tris 1 M NaCl 50 mM MgCl <sub>2</sub>

Adjust volume with ddH<sub>2</sub>O up to 1 L and pH to 9.5 and autoclave (prepare 1 MgCl<sub>2</sub> buffer first and add to the Tris-NaCl buffer after autoclaving)

### 6.1.6 Antibodies

#### Antibodies for flow cytometry

Annexin V, FITC-conjugated	Thermo Fisher, USA
Human Connexin43/GJA1 APC-Conjugated	R&D Systems, Germany
Mouse IgG2A APC-conjugated (Isotype Control)	R&D Systems, Germany

#### Antibodies for immunohistochemistry or immunofluorescence

Anti-Cx43 rabbit polyclonal, 1:100	Cell Signaling, USA
Anti-pan cytokeratin monoclonal, 1:400	Sigma-Aldrich, USA
Anti-Ki67, rabbit, monoclonal, 1:200	Abcam, Cambridge, UK
Anti-Caspase-3, mouse, monoclonal, 1:200	Novus, USA
Anti-mouse-IgG, AlexaFluor 488-conjugated (Goat, polyclonal, immunofluorescence (IF), dilution 1:400)	BD Pharmingen, Heidelberg, Germany
Anti-rabbit-IgG, AlexaFluor 488-conjugated (Goat, polyclonal, IF, dilution 1:400)	BD Pharmingen, Heidelberg, Germany
Anti-mouse-IgG, AlexaFluor 594-conjugated (Goat, polyclonal, for IF, dilution 1:400)	BD Pharmingen, Heidelberg, Germany
Anti-rabbit-IgG, AlexaFluor 594-conjugated (Goat, polyclonal, for IF, dilution 1:400)	BD Pharmingen, Heidelberg, Germany
Alkaline phosphatase-conjugated digoxigenin antibody (sheep polyclonal, for <i>in situ</i> hybridization (ISH), dilution 1:500)	Sigma-Aldrich, USA

### 6.1.7 Cell culture

All the established cancer cell lines and the immortalized non-malignant pancreatic ductal cell line CRL-4023 were purchased from the American Type Culture Collection (ATCC, Manassas, VA, USA).

The gemcitabine-resistant cell line BxGEM was selected from parental BxPC3 cells as previously described (Fan et al. 2016). The cells were cultured in DMEM/high glucose (Sigma-Aldrich, Missouri, USA) supplemented with 10% heat-inactivated FCS (Sigma-Aldrich) and 25 mmol/L HEPES (PAA Laboratories GmbH, Pasching, Austria). Jurkat cells were cultured in RPMI-1640 medium (Sigma-Aldrich) supplemented with 10% heat-inactivated FCS (Sigma-Aldrich) and 25 mmol/L HEPES (PAA). Mycoplasma detection tests were performed for the cultured cells monthly (PlasmoTest, InvivoGen, San Diego, USA). All cell lines were authenticated from a commercial institution (Multiplexion, Heidelberg, Germany).

### **6.1.8 Preparation of stock solutions**

D,L-Sulforaphane and the GJ inhibitor Oleamide (Sigma Aldrich) and the sulforaphane derivatives were dissolved in DMSO to a stock concentration of 100 mM. Gemcitabine solution (126 mM, Lilly Deutschland, Bad Homburg, Germany) was freshly diluted in DMEM medium to a 100  $\mu$ M stock. The fluorescent dyes CellTracker Red (CTR) CMTPX (Thermo Fisher Scientific, Dreieich, Germany) and Calcein-AM (Thermo Fisher Scientific) were dissolved in DMSO to a stock concentration of 10 mM. DMSO was used as a vehicle control for all experiments. Each stock aliquote was used only once immediately after thawing.

## **6.2 Methods**

### **6.2.1 Cell culture maintenance**

#### **Thawing cells**

A vial of cells was taken from the  $-150^{\circ}\text{C}$  freezer and placed in the  $37^{\circ}\text{C}$  water bath for 1 to 2 minutes until cells were thawed. After sterilizing the vial with 70% ethanol, cells were pipetted into a 15 ml tube containing 9 ml pre-warmed complete DMEM medium. The cells were centrifuged at 1500 rpm for 5 min. After centrifugation, the supernatant was discarded, the cell pellet was resuspended with 10 ml of complete DMEM medium, placed into a T-75 flask and incubated at  $37^{\circ}\text{C}$  with 5%  $\text{CO}_2$ .

#### **Passaging cells**

When cells reached 80 to 90% confluence in flasks, they were passaged. After discarding the culture medium, 5 ml of PBS were added to wash the cell monolayer.

One ml trypsin/EDTA was pipetted into the T-75 flask and was put back into the incubator for 5 to 10 minutes. Afterwards, adding complete DMEM medium terminated the digestion, the cells were resuspended with medium for 4-5 times, to avoid the creation of cell clumps. Then the cells were put into a 15 ml tube and centrifuged at 1500 rpm for 5 min. In between, the number of cells was calculated using the Z2™ Coulter Counter® System. The cell pellet was thoroughly resuspended with 10 ml complete medium containing 10% FCS.

### **Freezing cells**

Long-term culturing is prone to genetic drift for immortalized cell lines, or mycoplasma contamination. Therefore, it is very important to freeze cells as a stock to preserve them for long-term usage. The principle of freezing cultured cells is to make stock at a high concentration and at as low passage number as possible. For that reason, cells were washed once with 5 ml 1× PBS and trypsinized. Afterwards, cells were resuspended in medium, centrifuged at 1500 rpm for 5 min and supernatant was discarded. Aliquots of  $3 \times 10^6$  to  $1 \times 10^7$  cells were well resuspended in 900  $\mu$ l FCS and 100  $\mu$ l sterile DMSO, transferred into labeled cryotubes and immediately put in the Mr. Frosty freezing container in order to get a constant decrease in the temperature at a rate of 1°C/min. Subsequently, cryotubes were transferred to the -80°C freezer. Twenty-four hours later, cryotubes were transported to the -150°C freezer.

### **6.2.2 Cell viability assay**

Measurement of cell viability and proliferation was performed by the MTT assay. The MTT (3-(4,5-dimethylthiazol-2-yl)-2,5-diphenyltetrazolium bromide) substrate was prepared in a physiologically balanced solution, added to cells in culture, usually at a final concentration of 0.5 mg/ml (stock 5 mg/ml), and incubated for 1 to 4 hours. Viable cells with active metabolism convert MTT into a purple colored formazan product with an absorbance maximum near 570 nm. Dead cells cannot convert MTT into formazan and therefore purple color appearance in the well indicates viable cells. Twenty-four hours prior to treatment, PDA cells were seeded at a density of  $4 \times 10^4$  to  $6 \times 10^4$ /ml in 96-well plates. After corresponding transfection or treatment, 10  $\mu$ l MTT stock was added to each well. Subsequently, the 96-well plates were incubated for 4h in an incubator at 37°C and 5% CO<sub>2</sub>.

After completely removing media, 200 µl pre-warmed DMSO were added. The plate was shaken until all the blue crystals were completely solubilized. The optical density of each well was detected at 560 nm with an ELISA reader.

### **6.2.3 Patient tissue**

A paraffin-embedded pancreatic cancer tissue array including TNM, clinical stages and pathology grade was obtained from BioCat GmbH-Assay ID: PA961c (Heidelberg, Germany/US Biomax, Inc., Rockville, Maryland, USA).

### **6.2.4 Double-dye flow cytometry assay**

The degree of intercellular communication via GJs was examined by a double-dye flow cytometry assay as previously described (Cottin et al. 2010; Czyz et al. 2000). Briefly, the cells were seeded at a density of  $8 \times 10^4$  cells/well in 6-well cell culture plates and were left untreated or treated with sulforaphane, oleamide or both for 24h. Donor and recipient cell populations were differently labeled with calcein-AM (a GJ-permeable dye) and CellTracker Red (a GJ-impermeable dye) in serum- and phenol red-free RPMI medium (C.c.pro, Oberdorla, Germany), respectively (Table 3). After 30 min at 37°C, the cells were washed with PBS, donor cells were harvested, added to the top of the recipient cells and co-incubated at a ratio of 1:10 (donor: recipient) for 1-2h (Figure 7). The calcein transfer to CellTracker Red-labeled cells through GJs was evaluated by analyzing the fluorescence intensity of the cells with a BD FACSCanto II flow cytometer (BD Biosciences, Heidelberg, Germany) and FlowJo software (BD Biosciences). Similar experiments were also conducted after transfection of the cells with *mirVana*<sup>TM</sup> inhibitor of hsa-miR30a-3p and *mirVana*<sup>TM</sup> Negative Control inhibitor served as a control.

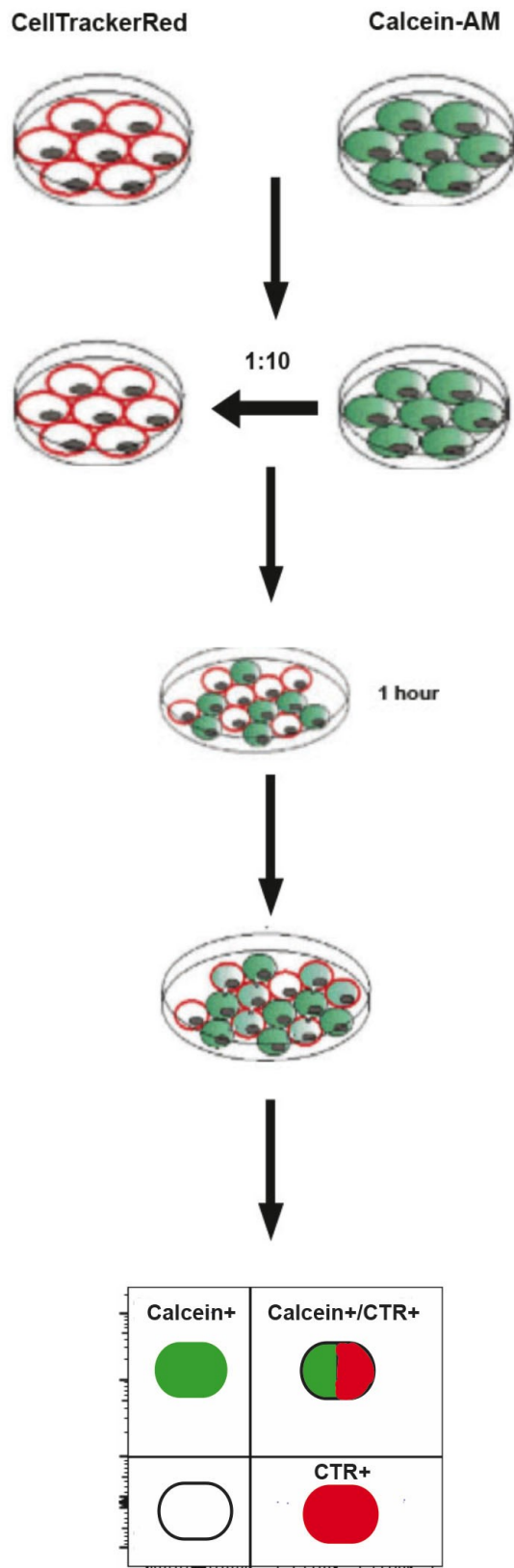


**Figure 7. Schematic representation of the double-dye flow cytometry assay.** Adapted from (Fonseca et al. 2006).

**Table 3. Fluorescent dyes for double-dye flow cytometry assay**

Reagent and Company	Solvent	Stock solution
Calcein-AM, cell-permeant dye Thermo Fisher	5.02 $\mu$ l DMSO	10 mM
Cell-Tracker Red CMTPX dye Thermo Fisher	7.28 $\mu$ l DMSO	10 mM

### 6.2.5 Microinjection of Lucifer Yellow

The microinjection assay is a widely used method, which is allowing the introduction of compounds into the cells via iontophoresis. These compounds allow us to trace the degree and pattern of cell communication through GJ. The GJ-permeable fluorescent dye Lucifer Yellow (Sigma Aldrich) is easily injected by iontophoresis, highly fluorescent and diffuses through the cell rapidly. To investigate GJ communication,  $8 \times 10^4$  BxGEM cells were seeded on 35-mm dishes and after 24h treated with 10  $\mu$ M sulforaphane and 50  $\mu$ M oleamide or both. Before the measurement, the samples containing Oleamide were treated once again to maintain the gap junction blockage. The 2.5% stock solution of Lucifer Yellow was diluted 1:5 with ddH<sub>2</sub>O. The tip of a homemade ultrathin glass pipette was positioned in the intracellular space of a single cell after microscopic observation. Measuring the membrane potential via a wire in the pipette and a ground electrode in the culture medium controlled the position of the pipette. Lucifer Yellow was injected with customized iontophoresis software for 90 s at a constant current of 10 nA. Fluorescence microscopy and video recording documented the distribution of Lucifer yellow to the surrounding cells. The mean gray values of the fluorescent intensity of the injected and direct neighboring cells were evaluated using customized image data processing software (Histo 3.0, University Hospital Heidelberg, Germany).

### 6.2.6 Flow cytometry detection of gemcitabine bystander effect

For the gemcitabine bystander effect experiments, cells were seeded at a density of  $2 \times 10^4$  cells/well in 24-well cell culture plates. Subsequently, the cells were left untreated or treated separately with gemcitabine, sulforaphane, oleamide or a combination of the reagents for 24h. Next, the untreated cells were stained with the red fluorescent dye CellTracker Red, as described in the double-dye flow cytometry assay paragraph.

The treated cells were detached and seeded in 96-round well cell culture plates together with the CellTracker Red-labeled untreated cells at a ratio of 1:1. After 48h co-incubation, the cells were stained with the 7-aminoactinomycin D (7-AAD, BD Biosciences) dye to investigate cell viability and analyzed with a BD FACSCanto II flow cytometer (BD Biosciences) and FlowJo software (BD Biosciences). Similar experiments were also conducted after transfection of the cells with *mirVana*<sup>TM</sup> inhibitor of hsa-miR30a-3p and *mirVana*<sup>TM</sup> Negative Control inhibitor served as a control.

### **6.2.7 miRNA and mRNA microarray analysis**

All products and procedures strictly referred to the manufacturer's instructions according to the protocol of TaqMan<sup>®</sup> Small RNA Assays and TaqMan<sup>®</sup> Gene Expression Assays. Major steps were sequentially performed as explained in the following chapters.

#### **6.2.7.1 RNA and miRNA isolation and concentration measurement**

The miRNeasy Mini Kit and the RNeasy Kit was used for miRNA and mRNA isolation, respectively, according to the manufacturer's instructions (Qiagen, Hilden, Germany). All procedures were performed according to kit manual and the final products were used instantly or were frozen at -80°C for future use. NanoDrop<sup>TM</sup> 2000 Spectrophotometer was used for the concentration measurement.

#### **6.2.7.2 mRNA and miRNA expression profiling**

The microarray analyses were carried out at the Microarray-Analytic Center of the Medical Faculty Mannheim. Briefly, 500 ng mRNA or miRNA was checked by quality control and the concentration was measured again. Human miRNA profiling was analyzed using the Affymetrix GeneChip miRNA 4.0 Array (Thermo Fisher Scientific) and human mRNA profiling was measured by Clariom D Assay (Thermo Fisher Scientific).

#### **6.2.7.3 mRNA and miRNA data interpretation**

The raw fluorescence intensity values were normalized applying quantile normalization and RMA background correction. One-Way ANOVA was performed to identify differential expressed miRNAs and genes.



Volcano plots (Figure 8) and heat maps were created using a commercial software package SAS JMP10 Genomics, version 6, from SAS (SAS Institute, Cary, NC, USA). A false positive rate of  $\alpha=0.05$  with FDR correction was taken as the level of significance. The Ingenuity® Pathway Analysis software (Suppipat et al. 2012)(Qiagen) using the microRNA target filters and the online platform mirWalk (<http://zmf.umm.uni-heidelberg.de/apps/zmf/mirwalk2/>) were used for identification of putative miRNA binding sites of genes of interest (Figure 9). The Target Mining Option provided the option of predicting target gene interaction of a list of miRNAs and the different and common gene interactions can be displayed as graph nodes (Sticht et al. 2018).

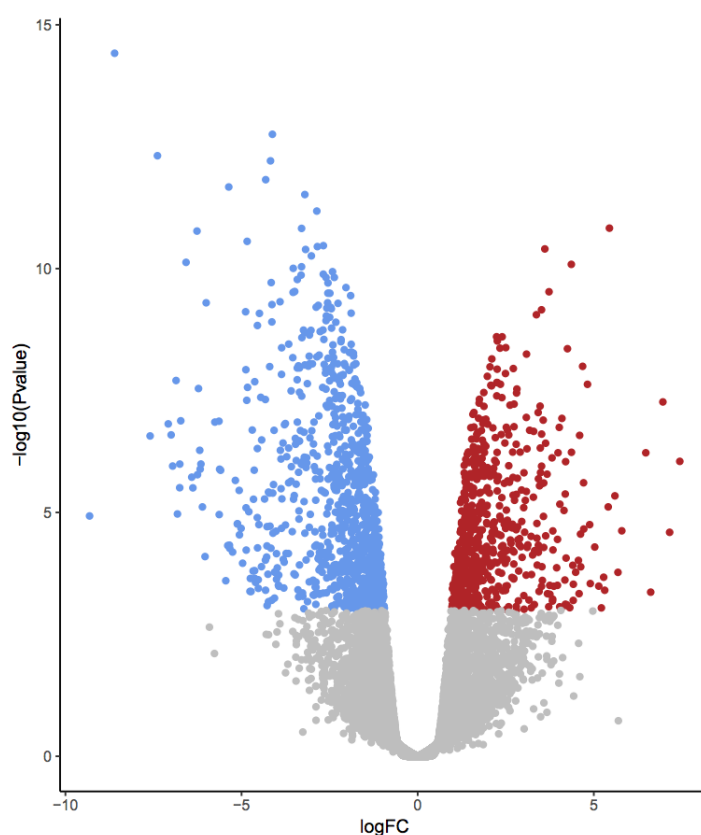


**Figure 8. Volcano plot showing gene distribution (adapted and modified from <https://galaxyproject.github.io/training-material/topics/transcriptomics/tutorials/rna-seq-viz-with-volcanoplot/tutorial.html>). Gene distribution. On the y-axis, the  $P$ -values and significance were plotted. On the x-axis, the fold change is represented.**

**microRNA Target Filter**

50 microRNA have targeting information available.  
Filtered to 50 microRNAs targeting 1339 mRNAs.

ADD/REPLACE MRNA DATASET   EXPRESSION PAIRING

Details \ Summary

ADD TO MY PATHWAY   ADD TO MY LIST   CREATE DATASET

Rows: 1 - 1000 (p1 of 5)   More Info

Use ▾ to filter a column. Add data or more columns using 'Add column(s) + '.

microRNA dataset: MicroRNA...			Relationship		mRNA dataset: OVCa wit	
ID	Symbol	Fold Ch...	Source	Confidence	Expression Pairi...	Symbol
<input type="checkbox"/>	hsa-mir-10b	miR-10a-5p (and other	TarBase, TargetScan Hu	Experimentally Observed	↕	HOXD10
<input type="checkbox"/>	hsa-mir-10b	miR-10a-5p (and other	TargetScan Human	Moderate (predicted)	↕	IL6R
<input type="checkbox"/>	hsa-mir-10b	miR-10a-5p (and other	TargetScan Human	Moderate (predicted)	↕	ITGA1
<input type="checkbox"/>	hsa-mir-10b	miR-10a-5p (and other	TargetScan Human	Moderate (predicted)	↕	KCNQ3
<input type="checkbox"/>	hsa-mir-10b	miR-10a-5p (and other	TargetScan Human	Moderate (predicted)	↕	KIAA0319
<input type="checkbox"/>	hsa-mir-10b	miR-10a-5p (and other	TargetScan Human	Moderate (predicted)	↕	KIAA0753
<input type="checkbox"/>	hsa-mir-10b	miR-10a-5p (and other	TargetScan Human	High (predicted)	↕	KLF11
<input type="checkbox"/>	hsa-mir-10b	miR-10a-5p (and other	TargetScan Human	Moderate (predicted)	↕	MAN1A2
<input type="checkbox"/>	hsa-mir-10b	miR-10a-5p (and other	TargetScan Human	High (predicted)	↕	MAP4K4
<input type="checkbox"/>	hsa-mir-10b	miR-10a-5p (and other	TargetScan Human	Moderate (predicted)	↕	MDM2
<input type="checkbox"/>	hsa-mir-10b	miR-10a-5p (and other	TargetScan Human	High (predicted)	↕	NCOR2
<input type="checkbox"/>	hsa-mir-10b	miR-10a-5p (and other	Ingenuity Expert Findings	Experimentally Observed	↕	NF1
<input type="checkbox"/>	hsa-mir-10b	miR-10a-5p (and other	TargetScan Human	High (predicted)	↕	NFAT5
<input type="checkbox"/>	hsa-mir-10b	miR-10a-5p (and other	TargetScan Human	High (predicted)	↕	NFX
<input type="checkbox"/>	hsa-mir-10b	miR-10a-5p (and other	TargetScan Human	Moderate (predicted)	↕	NFX1
<input type="checkbox"/>	hsa-mir-10b	miR-10a-5p (and other	TargetScan Human	High (predicted)	↕	NKTR

Selected/Total rows : 0/4511

VIEW FILTER SUMMARY   SAVE   CANCEL

**Figure 9.** IPA filtering tool to confidently identify mRNA targets of miRNAs. Adapted from IPA data sheet.

Gene Set Enrichment Analysis (GSEA) was used to evaluate whether defined lists of genes exhibit a statistically significant bias in their distribution within a ranked gene list using the software GSEA (Subramanian et al. 2005). Pathways of different cell functions were obtained from public external databases (KEGG, <http://www.genome.jp/kegg>) (Figure 10).

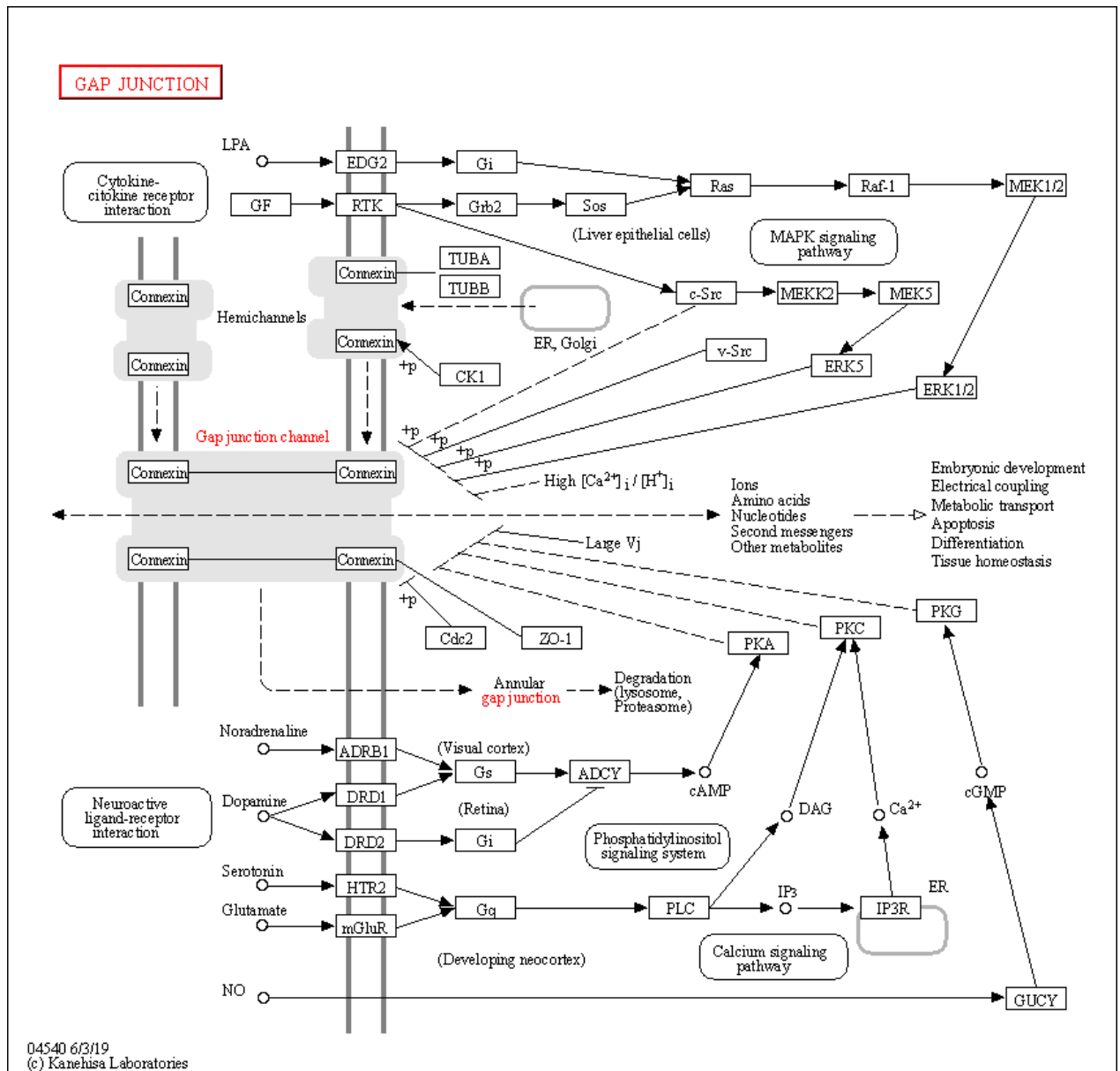


Figure 10. Gap junction KEGG pathway map

#### 6.2.7.4 Transfection with miRNA inhibitors

PDA cells were seeded on 6-well, 24-well or 96-well plates and cultivated until they reach 60 to 70% confluency. Hsa-miR-30a-3p *mirVana*® miRNA inhibitor (Catalog Nr: 4464084) or *mirVana*™ Negative Control inhibitor (Catalog Nr: 4464076) were used for transfection in a concentration of 30 nM (Table 4). Briefly, 30 nM miR30a-3p or negative control inhibitor were diluted in Opti-MEM™ I Reduced Serum Medium. In parallel, Lipofectamine™ 2000 transfection reagent was added to Opti-MEM™ I Reduced Serum Medium (Table 4), mixed well and incubated at RT for 5 min. The diluted inhibitor and lipofectamine transfection complexes were mixed and incubated for 20 min at RT, according to lipofectamine® 2000 reagent manual.

Afterwards, the built-up miRNA-lipofectamine complexes were transferred to corresponding wells and incubated at 37°C in a CO<sub>2</sub> incubator for 24h. After 4 to 6h 10% FCS was added to the serum-free medium in order to maintain the viability of the cells.

**Table 4. Transfection with miRNA inhibitors**

<b>Total volume (V1+V2+V3)</b>	<b>miRNA concentration</b>	<b>miRNA stock</b>	<b>Lipo2000/well</b>
96-well 100 µl (50 µl +25 µl +25 µl)	30 nM	0.15 µl	0.25 µl
24-well 500 µl (400 µl +50 µl +50 µl)	30 nM	0.75 µl	1 µl
6-well 2 ml (1500 µl + 250 µl+ 250 µl)	30 nM	3 µl	5 µl

V1= serum free medium, V2 and V3=Opti-MEM® Medium with diluted miRNA inhibitors and Lipo2000 respectively.

### 6.2.7.5 Reverse transcription of mRNA to cDNA

MRNA was extracted with RNeasy Kit. Hundred ng mRNA were used for reverse transcription with High-Capacity RNA-to-cDNA™ Kit. The reverse transcription reaction mix was prepared on ice according to Table 5.

Consequently, the reverse transcription reaction mix was incubated at 37°C for 60 min, heat-inactivated at 95°C for 5 min and kept at 4°C. The cDNA was used immediately for real-time PCR or stored at -80°C for further use.

**Table 5. Components of Reverse Transcription reaction mix (mRNA to cDNA)**

<b>Component</b>	<b>Volume</b>
2× RT (Reverse Transcription) Buffer	10 µl
20× RT Enzyme Mix	1 µl
Template RNA (100 ng)	9 µl
<b>Total volume</b>	<b>20 µl</b>

### 6.2.7.6 Reverse transcription of miRNA to cDNA

RNA was isolated with the miRNeasy Mini kit and 10 ng were subjected to cDNA synthesis using the TaqMan MicroRNA Reverse Transcription Kit. The reverse transcription reaction mix was prepared on ice according to Table 6. The reverse transcription reaction mix was first denatured at 16°C for 30 min, then annealed at 42°C

for 30 min and elongated at 85°C for 5 min. The cDNA was used immediately for real-time PCR or stored at -80°C for further use.

**Table 6. Components of Reverse Transcription reaction mix (miRNA to cDNA)**

<b>Component</b>	<b>Master mix volume for 15 µl reaction</b>
100mM dNTPs (with dTTP)	0.15 µl
Multiscribe™ Reverse Transcriptase, 50 U/µl	1.00 µl
10x RT Buffer	1.50 µl
RNase Inhibitor, 20 U/µl	0.19 µl
Nuclease-free water	4.16 µl
<b>Total volume</b>	<b>7 µl</b>

### 6.2.7.7 Real-time quantitative PCR

TaqMan® Universal Master mix was used for real-time quantitative PCR. The qPCR reaction mix was pipetted in triplicate according to the protocol and transferred to a 48-well plate (Table 7). After the plate was tightly sealed with film, it was centrifuged for 3 min at 3000 g at room temperature to remove bubbles. Then the real time PCR was set up according to Table 8. The small nuclear RNU6B was used as an endogenous control and GADPH served as a reference gene for normalization.

**Table 7. Reaction compounds of Real-Time PCR**

<b>Component</b>	<b>Volume</b>
20x microRNA or Expression Primer	1 µl
2× TaqMAN Gene Expression Master Mix	10 µl
Nuclease-free water	5 µl
Template cDNA	4 µl
<b>Total volume</b>	<b>20 µl</b>

**Table 8: Cycling conditions for real-time PCR**

<b>Step</b>	<b>Time</b>	<b>Temperature</b>
PCR initial activation step	10 min	95°C
Denaturation	15 s	95°C
Annealing	1 min	60°C
Break	∞	4°C
Cycle number	40 cycles	

### **6.2.8 Preparation of chicken eggs and transplantation of established PDA cell lines**

Fertilized eggs were obtained from a local ecological hatchery (Geflügelzucht Hockenberger, Eppingen, Germany). All eggs were from genetically identical hybrid Lohman Brown (LB) chickens. The delivery day was set as Day 0, the eggs were immediately washed with 70% warm ethanol. Then, the fertilized eggs were incubated in a digital motor breeder at 37.8°C and 45-55% humidity with a rotating mechanism. Four days after incubation, 4 ml albumin were removed with a 21 gauge needle and 5 ml syringe to detach the embryonic structures from the eggshell, then a hole was made over the eggshell in order to observe the embryonic viability and to apply a treatment. The hole was covered with Leukosilk® tape, and the eggs were put back into the incubator for embryonic development without rotation. On day 9 of embryonic development,  $7 \times 10^5$  cells/egg were transplanted at a ratio of 1:1 with Matrigel onto the chorioallantoic membrane (CAM) of fertilized chicken eggs, and five days later, on day 14, 100 nM of gemcitabine or 10  $\mu$ M of sulforaphane and derivatives, diluted in PBS, were injected intravenously (i.v) into the CAM vessels (50  $\mu$ l/egg). The bleeding was stopped with a cotton bud. Control eggs were injected with 50  $\mu$ l PBS alone (Figure 11). Tumor resection and evaluation of tumor growth was conducted at day 18. Tumor volumes were evaluated 3-dimensionally by a USB microscope camera (eScope, Oitez, Hongkong) and digital image editing using a customized mount. The volume was calculated using three main diameters obtained by digital image processing with ImageJ (NIH, Bethesda, MD, USA) and the formula  $V = \frac{4}{3} \times \pi \times r^3$ ;  $r = 0.5 \times \sqrt{(d1 \times d2 \times d3)}$ , d: diameter, r: radius, V: volume.

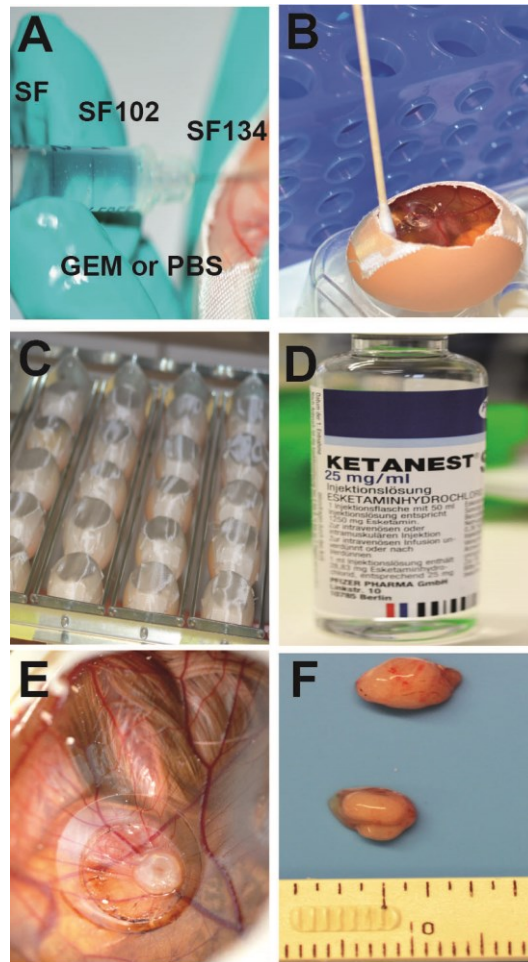


**Figure 11. Experimental procedure of xenograft treatment on fertilized chicken eggs.** (A) Image depicting the intravenous injection into the blood vessels of the CAM depending on the experiment. (B) The bleeding caused by the injection was stopped with a cotton bud. (C) After stopping the bleeding, eggs were sealed again with Leukosilk® tape and turned back to the incubator. (D) The chick is sacrificed after injecting intravenously (i.v) 0.1 ml of Ketanest. (E) Day 18, the last possible point for resection of xenografts before hatching. (F) Egg xenografts after resection.

### 6.2.9 Dual-luciferase reporter assay

Cells were seeded at a density of  $2 \times 10^4$  cells/well in 24-well plates and co-transfected with 30 nM *mirVana*<sup>TM</sup> negative control or miRNA inhibitor, 12.5 ng/well of pRL Renilla luciferase reporter plasmid (Promega, Mannheim, Germany) and 25 ng/well firefly luciferase pMirTarget vector (OriGene, Rockville, USA) either empty (Catalog Nr: PS100062) or expressing Cx43 3'-UTR (Catalog Nr: SC216210). The cells were lysed in 1X Passive Lysis Buffer of the Dual-Luciferase Reporter Assay System (Promega) 24h post-transfection. Firefly and Renilla luciferase activities were measured on a FLUOstar OPTIMA instrument (BMG Labtech, Ortenberg, Germany).

### **6.2.10 Immunohistochemistry**

Immunohistochemistry on 6- $\mu$ m frozen or paraffin-embedded tissue sections was performed using the VECTASTAIN Elite ABC HRP Kit, ZytoChem-Plus HRP polymer kit with AEC according to the manufacturer's instructions. Anti Cx43 (Cell Signaling), pan-cytokeratin (Sigma-Aldrich), Ki67 (Abcam) and Caspase-3 (Novus) were used as primary antibodies. The negative control was prepared without primary antibody. The goat anti-rabbit or anti-mouse biotinylated IgG were used as secondary antibodies for the detection. The signal was amplified with the ABC kit. AEC kit was used as a chromogen. Samples were counterstained with haematoxylin, dehydrated in graded alcohol, rinsed in xylene and mounted in Entellan. The analysis of the stainings was done using a Leica DMRB microscope at a 400x magnification and pictures were taken with the SPOT™ FLEX 15.2 64 Mp shifting pixel digital camera (Diagnostic, Instruments, Inc. USA) and analyzed with the SPOT Basic/Advanced 4.6 Software.

### **6.2.11 Apoptosis assay**

PE Annexin V Apoptosis Detection Kit I was used to analyze cell death with flow cytometry analysis. PE Annexin V staining precedes the loss of membrane integrity, one of the main characteristic events of apoptosis, while 7-AAD is a dye that binds to intracellular DNA when the cells are non-viable. Cells that are only Annexin V positive are considered to be in early apoptotic stage and cells that are Annexin V and 7-AAD positive indicate late apoptosis and necrosis. With refer to the experimental protocol,  $10 \times 10^4$  cells/ml were seeded on 6-well plates and, 24h later, transfected with miRNA inhibitors, according to the experimental design, or treated with sulforaphane derivatives. Afterwards, the cells were transferred in 96-well round bottom plates and stained with Annexin V for 15 min at RT following by 2 washing steps. 7-AAD was added to the samples 10 minutes before the measurement. Proper staining controls were set. Finally, the cells were analyzed with a BD FACSCanto II flow cytometer and FlowJo software.

### **6.2.12 *In situ* hybridization**

Detection of miR30a-3p expression in patient tissue sections was accomplished using the miRCURY LNA™ microRNA Detection Kit, as described in the manufacturer's instructions.



To obtain strong miRNA signal localized in tumor cells, I incubated the tissue with the ISH substrate overnight and sterilize tips and pipettes in order to diminish the RNAses effect. Experiment was performed on a microarray microscopy slide covering 91 human pancreatic cancer and 5 normal tissues. Briefly, the sections were deparaffinized in Roti-Histol and serial dilutions of 100% ethanol, then demasked with proteinase K (20 mg/ml) for 15 min at 37°C, which allows the access of LNA probes to hybridize with the miRNA, following by dehydration of the slides. Hybridization was done for 2h at 54°C using 50 nM of the miR-30a-3p digoxigenin-labeled LNA detection probe (5'CUUUCAGUCGGAUGUUGCAGC3', # 339111) and 0.3 nM of the LNA U6 snRNA as a positive control. After stringent washes the bound LNA-probes were detected with alkaline phosphatase-conjugated digoxigenin antibody and NBT/BCIP as substrate. Sections were mounted using Roti-Mount FluorCare.

#### **6.2.13 Colony formation assay**

Cells were collected and seeded in 6-well plates at a density of  $2-4 \times 10^4$  cells/well, followed by treatment with sulforaphane or sulforaphane derivatives for 24h. Next, cells were centrifuged and re-plated at a low density of 400 cells/well for AsPC-1 and 800 cells/well for BxPC3 in 6-well plates in triplicate. After incubation for two weeks at 37°C without changing medium, cells were fixed with 2 ml 3.7% paraformaldehyde (PFA) for 10 min followed by 2 ml 70% ethanol for another 10 min and one wash with  $1 \times$  PBS. Cells were then washed 3 times with dH<sub>2</sub>O and stained with 0.05% Coomassie blue for 5 min. Subsequently, cells were washed with dH<sub>2</sub>O and dried overnight. A colony was defined as a spot comprising more than 50 cells. The number of colonies was quantified under a dissecting microscope and the percentage of plating efficiency was calculated (plating efficiency of non-treated cultures=1) (Kallifatidis et al. 2009), (Kallifatidis et al. 2011). To investigate the potential for formation of secondary colonies, cells were collected from the colonies above and equal numbers of cells were reseeded. Colonies were calculated in the same manner.

#### **6.2.14 Life span assay**

Life span analysis of the *Caenorhabditis elegans* (*C. elegans*) N2 worms (CGC, Minnesota, USA) was conducted at 20°C.

L4-stage worms (n=100/group) were picked up and transferred into 60 mm medium-sized plates (TPP, Trasadingen, Switzerland) containing S medium and *E. coli* OP50 as a food supply (Stiernagle 2006).

Sulforaphane, SF102, SF134 in a concentration of 400  $\mu$ M or DMSO alone, were added to S Basal medium for 48h. The lifespan was examined by documenting the amount of live and dead worms and they were transferred daily to new *E. coli* plates until they did not lay any more eggs. Worms that died of causes other than aging such as internal hatching or vulva protrusion were excluded from the analysis. Survival curves were created using the Kaplan-Meier analysis.

#### **6.2.15 Chemical synthesis of sulforaphane derivatives**

Seven derivatives of sulforaphane were synthesized and kindly provided by Prof. Carsten Bolm and his co-workers (Institute of Organic Chemistry, RWTH, University of Aachen). The monoaza racemate derivatives of sulforaphane (SF85 and SF101) or its sulfone (SF86, SF102, SF113, SF134, and SF135) were prepared, which differ from the parent compound by formal substitutions of the sulfinyl (S = O) group by either sulfimidoyl (S(NR)) or sulfoximidoyl (S(O)(NR)) moieties. The R substituent at the nitrogen is acetyl (as in SF85 with S(NAc) and SF86 with S(O)(NAc)), pentafluorobenzoyl (as in SF101 with S(NC(O)C<sub>6</sub>F<sub>5</sub>) and SF102 with S(O)(NC(O)C<sub>6</sub>F<sub>5</sub>)), methyl (as in SF113 with S(O)(NMe)), trifluoroacetyl (as in SF134 with S(O)(NCOCF<sub>3</sub>)), and carbamoyl (as in SF135 with S(O)(NCONH<sub>2</sub>)).

#### **6.2.16 Statistical analysis**

The data obtained with established cell lines are presented as the means  $\pm$  SD from at least three separate experiments, which were performed at least in triplicate. The significance of the data was analyzed with Student t-test corrected for multiple comparisons with the Bonferroni-Holm method. The Pearson Product-Moment Correlation was performed to measure the linear correlation between two variables X and Y. For the immunohistochemistry or immunofluorescence experiments, the expression intensity and percentage of positive cells were determined by counting the number of differentiated cells in 10 fields of view for each group.

For evaluation of Kaplan Meyer analysis of *C. elegans* life span, the standard chi-square-based log-rank test was used. For the miRNA microarray data, the JMP software provided by SAS Institute (Heidelberg, Germany) was used.  $P < 0.05$  was considered statistically significant. \* $P < 0.05$ , \*\* $P < 0.01$ .

## 7. Results

### **7.1 Sulforaphane-mediated inhibition of miR30a-3p enhances gap junctional intercellular communication, thereby increasing gemcitabine cytotoxicity in pancreatic cancer**

#### **7.1.1 Sulforaphane induces GJIC**

To address the effect of sulforaphane on gap junction (GJ) formation, a double-dye flow cytometry assay for gap junctional intercellular communication (GJIC) was performed with 2 established PDA cell lines, BxGEM and PANC-1. The rationale for choosing these two cell lines was firstly based on their low or impaired Cx43 expression, which is associated with absent GJ function, and secondly their resistance to chemotherapy. (Forster et al. 2014), (Dovmark et al. 2017). First, donor cells were loaded with calcein, a GJ-permeable green fluorescent dye, and then co-incubated with recipient cells, which were loaded with the GJ-impermeable and membrane-resident red fluorescent dye CellTracker Red (CTR), at a ratio of 1:10. As GJs are permeable to calcein, the transfer of green fluorescence from donor to recipient cells and the appearance of double-positive cells indicate successful GJIC. The percentages of single- and double-stained cells were quantified by flow cytometry (Figure 12A). The flow cytometry assay was conducted with the abovementioned PDA cells, which were left untreated or treated with sulforaphane in the presence or absence of the GJ inhibitor oleamide. After co-incubation, the cells were analyzed, and double-positive cells were present in the right upper quadrant of the dot plot (Figure 12B). A calcein diffusion of approximately 11% was observed in control and oleamide-treated cells. Interestingly, sulforaphane treatment significantly increased calcein diffusion to 25% and 21% in BxGEM and PANC-1 cells, respectively. Sulforaphane and oleamide co-treatment decreased the percentage of double-positive cells (15% in BxGEM and 18% in PANC-1 cells), suggesting that sulforaphane enhances the transfer of calcein by opening the GJs. To further highlight this assumption, I microinjected sulforaphane-treated or untreated BxGEM cells with the GJ-permeable fluorescent dye Lucifer Yellow and measured the distribution to neighboring cells by time-lapse microscopy (Figure 12C). For data analysis, the mean gray values of the fluorescence intensity of the injected and the direct neighboring cells were evaluated using the customized image data processing software, Histo 3.0.

Cells treated with sulforaphane showed a significant increase in Lucifer Yellow distribution up to 20% compared to untreated cells and to cells treated with oleamide alone. Oleamide co-treatment significantly reduced the sulforaphane-mediated Lucifer Yellow transfer to 9%, most likely by the inhibition of the sulforaphane-mediated opening of GJs.

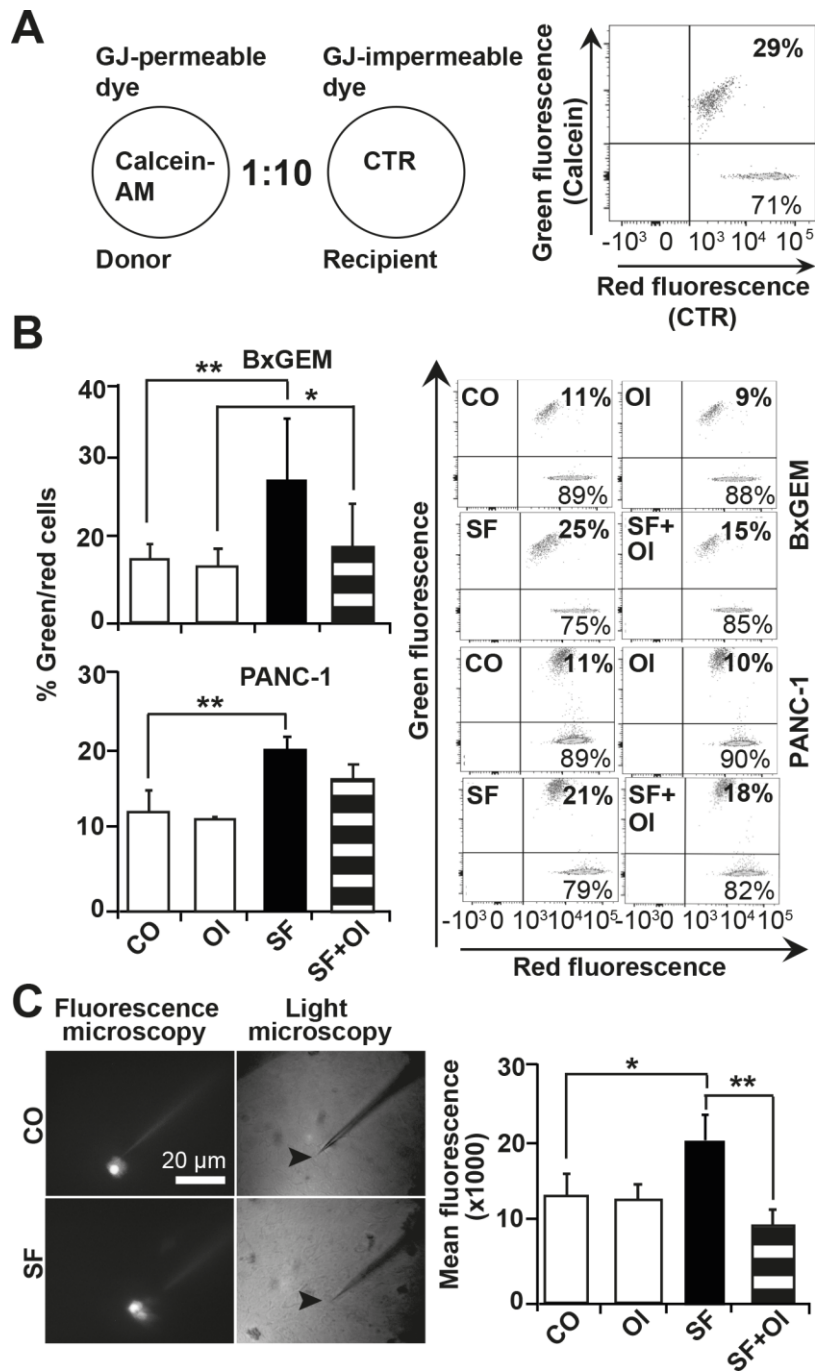


**Figure 12: Sulforaphane increases GJIC.** (A) Experimental design of the double-dye flow cytometry assay. BxGEM and PANC-1 cells were labeled with 1  $\mu$ M calcein-AM or 5  $\mu$ M CellTracker Red. Next, calcein-loaded cells were plated on top of the CTR-stained cells and co-incubated in a donor/target ratio of 1:10. After co-incubation, cells were detached and analyzed by flow cytometry. (B) White bars: Untreated cells (CO), Oleamide-treated cells (OI). Black bar: Sulforaphane-treated cells (SF). Black bar with stripes: co-treatment with sulforaphane and oleamide (SF+OI). In the flow cytometry dot plots, the percentages of double-positive cells (upper right) and single-red labeled cells (down right) are shown. (C) Representative images from fluorescence and light microscopy with Lucifer Yellow-injected cells are displayed. The mean of gray values per group was calculated and shown in the diagram. Scale bar indicates 20  $\mu$ m. The means  $\pm$  SD are shown in the diagrams. \*P<0.05, \*\*P<0.01.

### 7.1.2 Sulforaphane potentiates the gemcitabine bystander effect through GJIC

To gain knowledge about the influence of sulforaphane on gemcitabine cytotoxicity, I performed the well-established method of gemcitabine bystander effect. The aim was to identify whether sulforaphane increases gemcitabine-induced cell death by opening GJs and increasing the uptake of gemcitabine metabolites by neighboring cells. BxGEM and PANC-1 donor cells were treated with gemcitabine, sulforaphane and oleamide alone or in combination. Twenty-four hours later, the cells were co-incubated in a ratio of 1:1 with CTR-labeled but otherwise untreated BxGEM or PANC-1 target cells. After forty-eight hours of co-incubation, the cells were labeled with 7-AAD and cell death was evaluated by flow cytometry. The presence of double-fluorescent target cells (CTR+/7-AAD+) indicates a successful bystander effect (Figure 13A, Figure S1A). The number of double-positive BxGEM target cells was approximately 9% in gemcitabine- and sulforaphane-single-treated cells, and the percentage increased to 11% by co-treatment, whereas co-incubation with oleamide significantly decreased the percentage of double-positive cells to 8%. PANC-1 target cells treated with gemcitabine and sulforaphane together showed a significant increase of 28% compared to untreated target cells with 8% and oleamide co-treatment reduced the percentage of induction to 23% (Figure 13B). Representative microscopy images of cell cultures underline the results obtained by flow cytometry and demonstrate that blocking GJs by oleamide prevents cell death induced by combined treatment with gemcitabine and sulforaphane (Figure 13C).

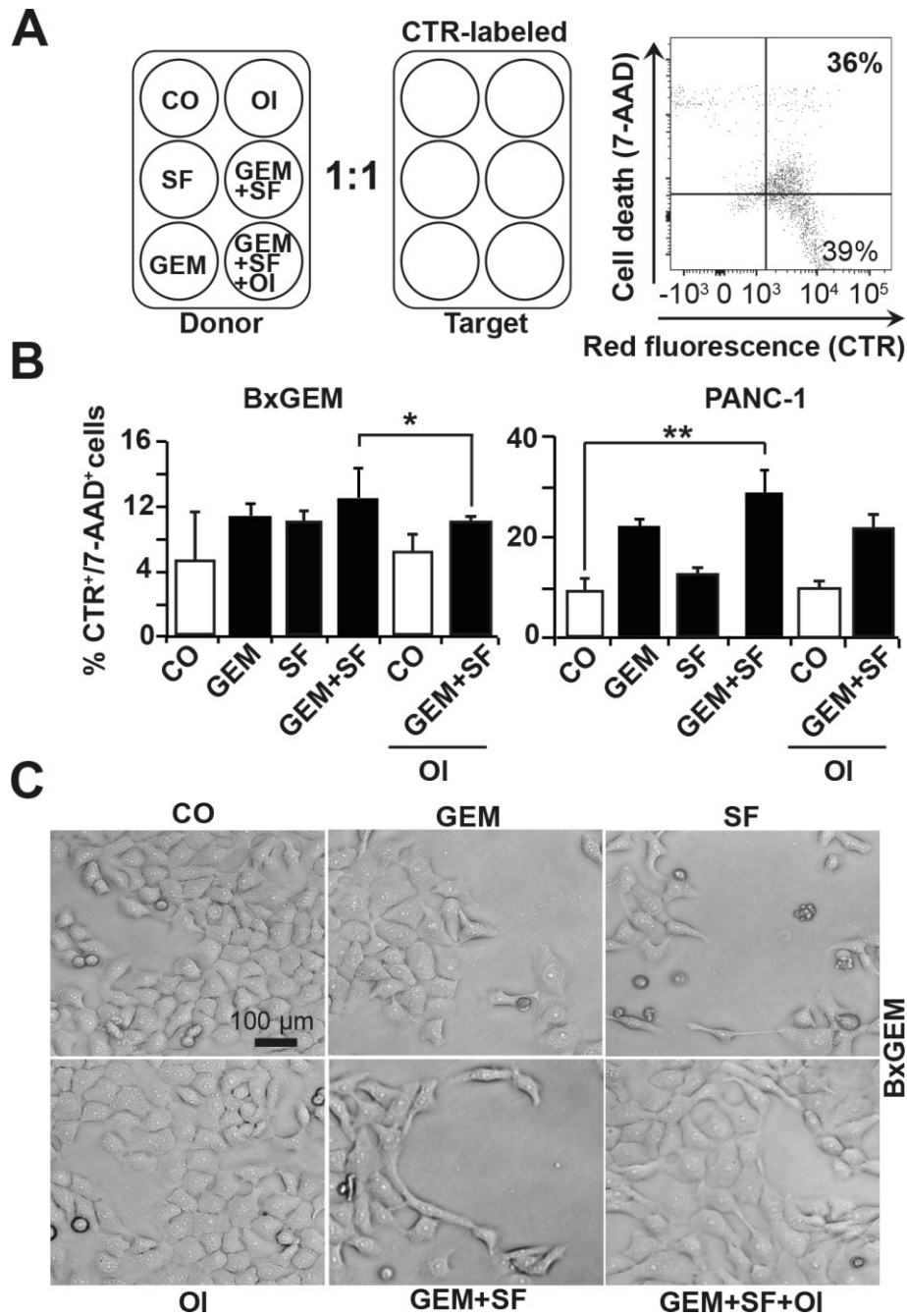


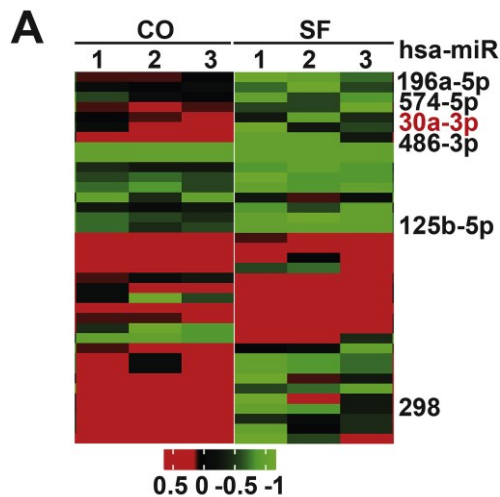
**Figure 13. Sulforaphane enhances the gemcitabine bystander effect through GJs.** Experimental design of the bystander effect assay. BxGEM and PANC-1 donor cells were left untreated (CO) or treated with 3  $\mu\text{M}$  gemcitabine (GEM), 10  $\mu\text{M}$  sulforaphane (SF), 50  $\mu\text{M}$  oleamide (OI) or a combination of the agents for 24h. Next, treated cells were co-incubated with untreated but CellTracker Red (CTR)-stained cells at a ratio of 1:1 (donor: target). After 48h of co-incubation, the cells were detached and stained with 7-aminoactinomycin D (7-AAD), and cell death was evaluated by flow cytometry (**B**). Diagrams interpret the mean percentages of CTR<sup>+</sup>/7-AAD<sup>+</sup> cells from three independent experiments. White bars: Untreated cells (CO), Oleamide-treated cells (OI). Black bars highlight the percentages of GEM, SF, GEM+SF and GEM+SF+OI groups. The means  $\pm$  SD are shown. \* $P < 0.05$ , \*\* $P < 0.01$ . (**C**) The morphology of the cells was observed at 10 $\times$  magnification using a Nikon ECLIPSE Ts100 microscope, and representative images are displayed.

### 7.1.3 Sulforaphane inhibits miR30a-3p and enhances Cx43 expression

To investigate the underlying mechanism of sulforaphane-induced GJIC, I performed miRNA and gene microarray analysis. RNA was isolated from BxGEM cells, which were left untreated or treated with sulforaphane for 24h. Based on bioinformatics evaluation, 36 differentially regulated miRNAs with the highest statistical significance were selected (with  $-\log_{10}$  p-Value of  $\geq 2$ ) and are shown in a heat map (Figure 14A). For further analysis, 6 out of 36 miRNA candidates were selected by *in silico* analysis and a literature search based on two selection criteria: downregulation by sulforaphane and relevance to GJs (Table S1). MiR30a-3p was chosen as the most relevant candidate, because is the only miRNA candidate predicted to regulate the expression of the GJA1 gene that encodes the Cx43 protein (Figure 14B). The qRT-PCR results confirmed that the expression of miR30a-3p in BxGEM and PANC-1 cells was significantly decreased upon sulforaphane treatment (Figure 14C).

To verify the influence of sulforaphane on Cx43 expression, a mRNA profiling array was performed with BxGEM cells treated as described above. From the gene microarray analysis, based on the criteria of significance and upregulation, a heatmap was created with GJA1 and the 10 most significantly upregulated GJ genes (Figure 15A). The expression profile and the interaction of these genes was analyzed by the KEGG search tool (Figure S2). The upregulation of GJA1 mRNA after sulforaphane treatment was confirmed in BxGEM and PANC-1 cells by qRT-PCR (Figure 15B). As the expression of connexins at the cell surface is essential for GJ formation and function, BxGEM cells were left untreated or treated with sulforaphane, and 24h later, these cells were stained with an APC-conjugated Cx43 antibody and analyzed by flow cytometry. Sulforaphane treatment significantly increased the expression of Cx43 at the cell surface (Figure 15C).





**B**

miRNA Symbol	p-value P<0.05	GJ Gene Symbol
125b-5p	0.00159	GJB7
125b-5p	0.00159	GJC1
125b-5p	0.00159	GJC2
125b-5p	0.00159	GJC3
196a-5p	0.000028	GJB2
298	0.00092	GJC2
30a-3p	0.00492	GJA1
30a-3p	0.00492	GJB6
574-5p	0.00158	GJA9
574-5p	0.00158	GJB7
486-3p	0.00354	SGSM3

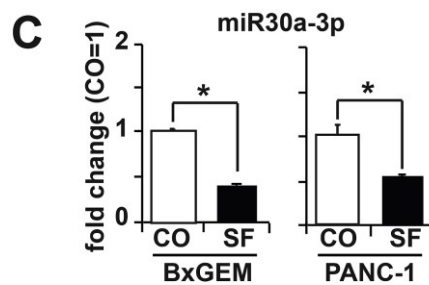


**Figure 14. Sulforaphane inhibits miR30a-3p expression.** (A) BxGEM cells were left untreated (CO) or treated with 10  $\mu$ M sulforaphane (SF). Total RNA was harvested 24h later and used for GeneChip miRNA 4.0 Array in triplicate. The heatmap presents the top 36 significantly regulated miRNAs after sulforaphane treatment and the names of the six most relevant candidates are shown. The red color marks high expression, and the green color marks low expression within a scale from 0.5 to -1, as indicated. (B) *In silico* analysis using IPA software and the keywords gap junctions, pancreatic cancer revealed 6 miRNA candidates with putative target sites in GJ genes. A table summarizes the significance (p-value) of the downregulation of the miRNA candidates after sulforaphane treatment and their GJ target genes. (C) BxGEM and PANC-1 cells were treated as described above, and 24h later, the RNA was harvested, and the fold change in miR30a-3p expression was determined by qRT-PCR and normalized to RNU6B. The mean fold change in the control was set to 1.

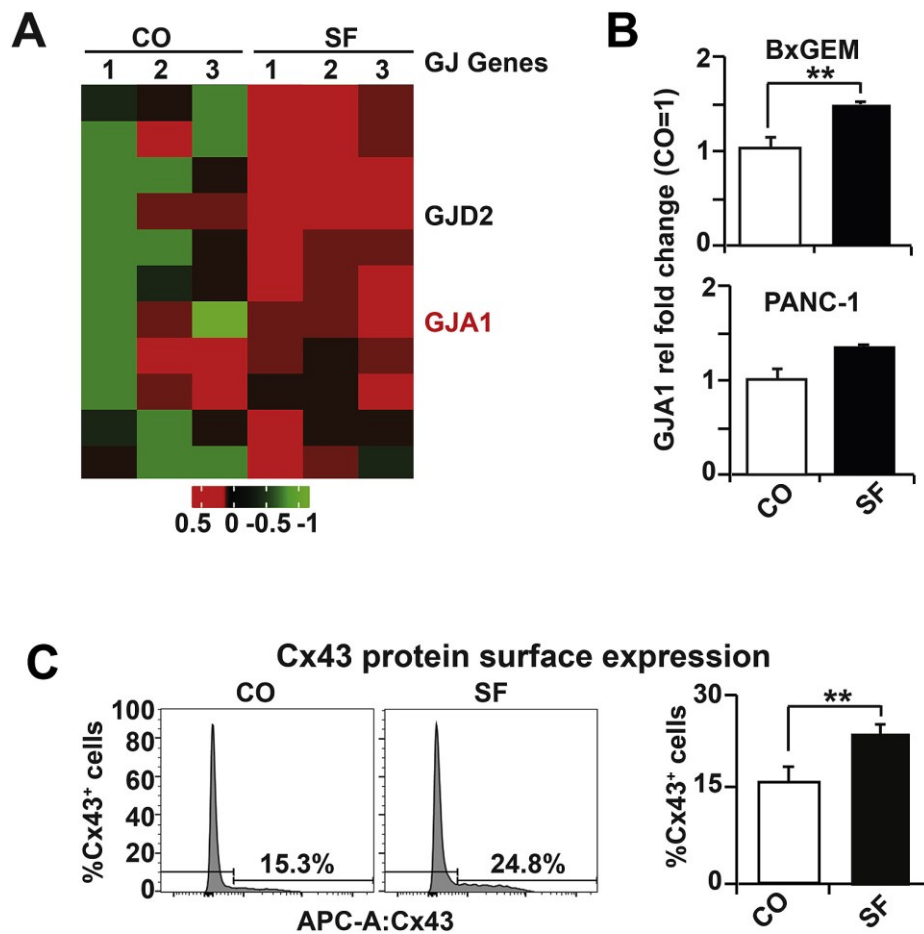


**Figure 15. Sulforaphane induces GJA1 expression and upregulation of Cx43 protein.** (A) BxGEM cells were left untreated (CO) or treated with 10  $\mu$ M sulforaphane (SF). Total RNA was harvested, followed by gene expression profiling in triplicate using the Clariom D Assay. The heatmap presents the top 11 upregulated GJ genes after sulforaphane treatment and the 2 most relevant genes are shown. (B) BxGEM and PANC-1 cells were treated as previously described, and RNA was harvested. The fold change in GJA1 expression was determined by qRT-PCR and normalized to GAPDH. The controls were set to 1 (C) Cx43 surface protein expression levels were evaluated in BxGEM cells by flow cytometry analysis. Right: representative histogram plots. Left: Mean percentage Cx43 surface expression from three independent experiments. The means  $\pm$  SD are shown. \* $P < 0.05$ , \*\* $P < 0.01$ .

#### 7.1.4 miR30a-3p inhibits Cx43 expression by binding to its 3'-UTR

To obtain knowledge about the interaction of miR30a-3p and Cx43, I performed a search in the TargetScan database (Agarwal et al. 2015) to identify the putative binding sites of miR30a-3p on the Cx43 3'-UTR (Figure 16A). The next step was to prove the binding of miR30a-3p to the 3'-UTR of Cx43.

For this purpose, a commercially available luciferase reporter construct expressing the Cx43 3'-UTR was lipotransfected into BxGEM cells, and a firefly reporter construct or a Renilla control plasmid was co-transfected in the presence or absence of miR30a-3p mimic or a negative control mimic. Twenty-four hours after transfection, the luciferase activity was quantified using a luminescence microplate reader. I observed a significantly reduced luciferase activity of the Cx43 reporter upon co-transfection of the construct with miR30a-3p, which was not observed with the controls or miR30a-3p alone (Figure 16B), suggesting that miR30a-3p suppressed Cx43 mRNA expression.

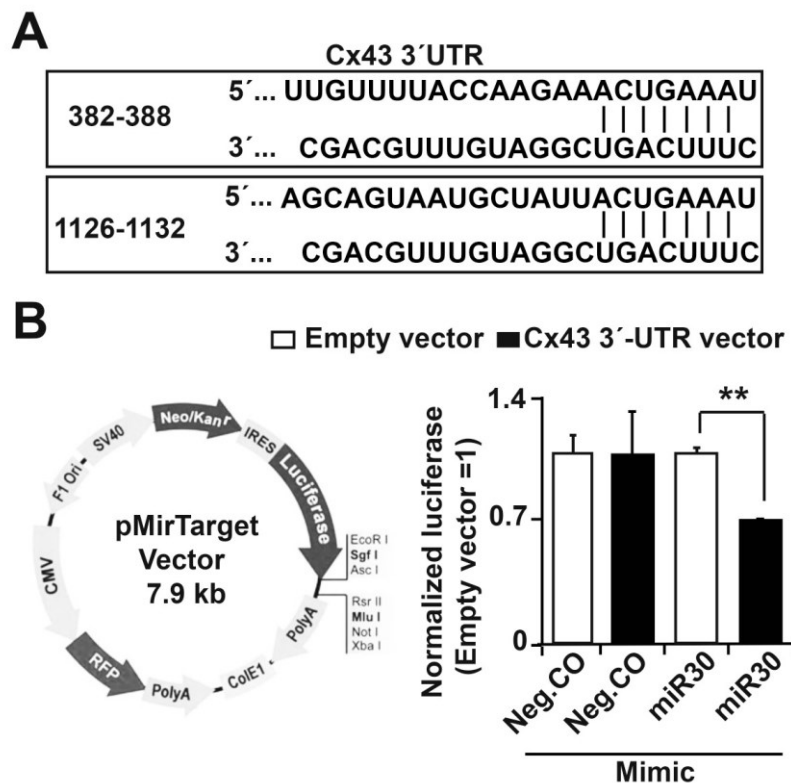


**Figure 16. miR30a-3p inhibits Cx43 expression by binding to its 3'-UTR.** (A) Two putative binding sites of miR30a-3p in the Cx43 3'-UTR are shown. (B) BxGEM cells were co-transfected with a firefly reporter construct of the Cx43 3'-UTR plasmid in the presence or absence of either 30 nM miR30a-3p (miR30) or a negative control (Neg. CO) inhibitor. The co-transfection of a Renilla luciferase (0.25 ng/ $\mu$ l) served as a control for equal conditions. Twenty-four hours after transfection, the expression of Renilla and firefly luciferase was detected. Firefly luciferase activities were normalized to Renilla luciferase activities. The negative control was set to 1. \*\*P<0.01.

### **7.1.5 Inhibition of miR-30a-3p induces GJIC and gemcitabine bystander effect**

To clarify whether sulforaphane enhances GJIC through inhibition of miR30a-3p, a double-dye flow cytometry assay was conducted with BxGEM cells, which were transfected with 30 nM *mirVana*<sup>TM</sup> negative control or miR30a-3p inhibitors for 24h. Then, donor and recipient cells were labeled and co-incubated as described in paragraph 7.1.1., The percentages of single- and double-stained cells were quantified by flow cytometry (Figure 17A). Calcein diffusion of 12% was observed in BxGEM cells after control transfection, whereas miR30a-3p inhibition significantly increased the percentage to 23% in a similar manner to sulforaphane treatment. To identify whether miR30a-3p transfection can influence the gemcitabine bystander effect, BxGEM donor cells were transfected with the negative control or miR30a-3p inhibitor and were additionally treated with gemcitabine, oleamide or a combination of both (Figure 17B). Twenty-four hours later, the cells were co-incubated with CellTracker Red-labeled untreated target cells and evaluated for cell death as mentioned in Figure 13A. The amount of double-positive BxGEM target cells was significantly higher in miR-transfected cells compared to the control (19% and 13%, respectively). Gemcitabine treatment in miR-transfected cells significantly augmented cell death up to 33%, while oleamide treatment adequately decreased the percentage of dead target cells to 19% (Figure 17C and Figure S1B). Therefore, our data suggest that miR30a-3p suppression induces the gemcitabine bystander effect through GJs.

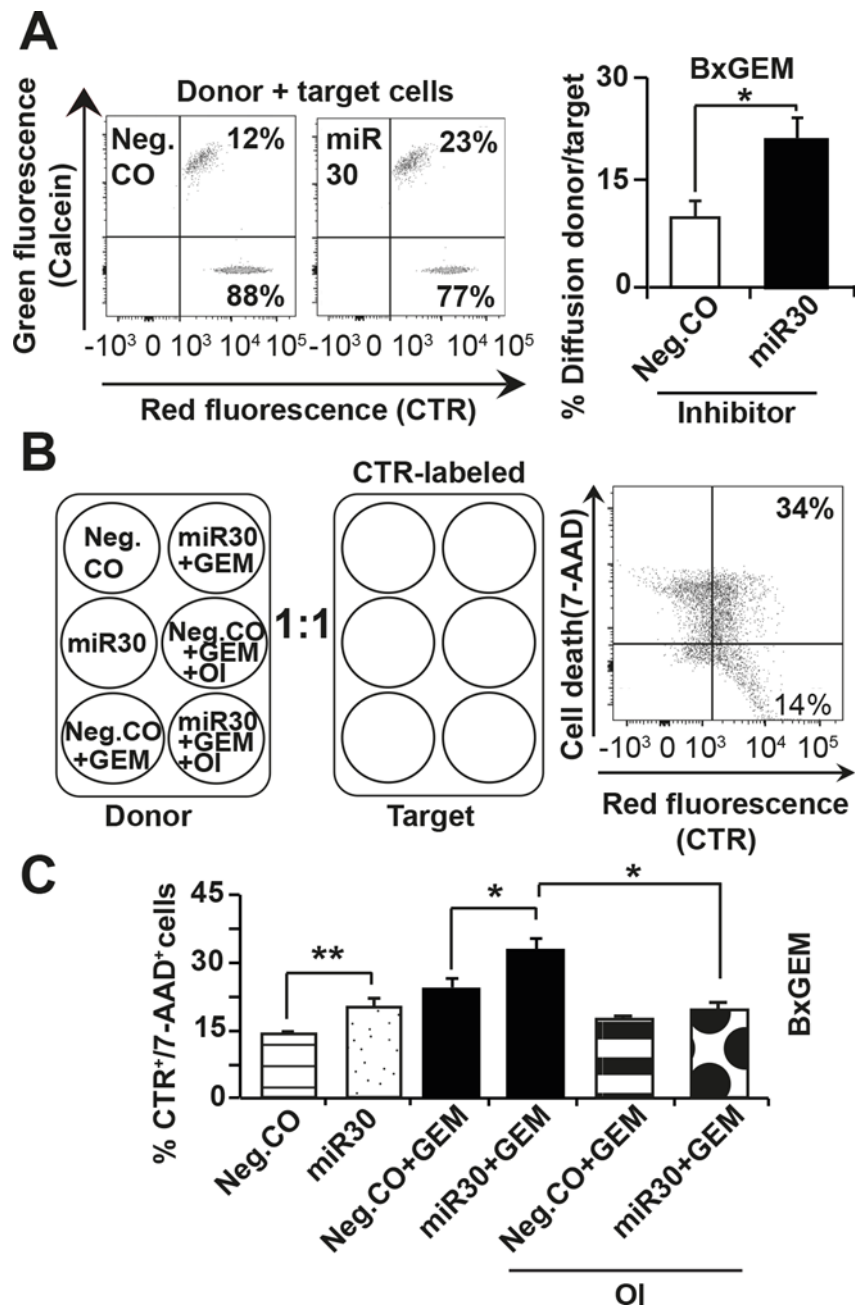


**Figure 17. Downregulation of miR30a-3p increased the GJIC and gemcitabine bystander effect.** BxGEM cells were lipofected with 30 nM miR30a-3p (miR30) or negative control (Neg. CO) inhibitors, followed by fluorescence labeling, co-incubation of the cells and flow cytometry analysis as described in Figure 13A. **(A)** The percentages of double-positive cells (upper right) and single-red labeled cells (down right) are shown. Bar graphs represent the percentage of double-positive cells and correspond to results from at least three independent experiments. **(B)** Experimental design of the bystander effect assay after miR30a-3p transfection. BxGEM donor cells were transfected with miR30a-3p (miR30) or negative control (Neg. CO) inhibitors and treated with 3  $\mu$ M gemcitabine (GEM), 50  $\mu$ M oleamide (OI) or a combination of the agents for 24h. Next, treated cells were co-incubated with untreated but CellTracker Red (CTR)-stained cells in a ratio of 1:1 (donor: target). After 48h of co-incubation, the cells were detached and stained with 7-aminoactinomycin D (7-AAD), and cell death was evaluated by flow cytometry **(C)** Graphs showing the mean percentages of CTR<sup>+</sup>/7-AAD<sup>+</sup> cells from three independent experiments. The means  $\pm$  SD are shown. \* $P < 0.05$ , \*\* $P < 0.01$ .

### 7.1.6 miR30a-3p decreases the tumor xenograft volume

To evaluate the *in vivo* relevance of my findings, I performed xenograft studies using the fertilized chicken egg model, which has been successfully applied in my laboratory for many years (Zhao et al. 2018), (Bauer et al. 2014). BxGEM cells were lipotransfected with 30 nM negative control or miR30a-3p inhibitors, and at 24h post-transfection, the cells were transplanted onto the chorioallantoic membrane on day 9 of embryonic development. Five days later, 100 nM gemcitabine or PBS was injected into the chorioallantoic membrane vessels, and the tumor xenografts were resected on day 18. I measured the xenograft tumor size by calipers, and the mean sizes are displayed in a diagram (Figure 18A). The tumor size was decreased in the xenografts derived from miR30a-3p-transfected cells. Moreover, inhibition of miR30a-3p significantly enhanced gemcitabine cytotoxicity compared to the control or single miR30a-3p-transfected tumors. To evaluate Cx43 expression in xenograft tissues, I performed immunohistochemistry staining and evaluated the fluorescence intensity with ImageJ software (Figure 18B). MiR30a-3p-transfected tumors showed significantly higher Cx43 expression, suggesting that inhibition of miR30a-3p induces chemotherapy competence in PDA xenografts most likely via Cx43. These results suggest that sulforaphane downregulates miR30a-3p expression, which in turn leads to upregulation of Cx43 protein expression, enhanced GJIC and gemcitabine sensitivity (Figure 18C).

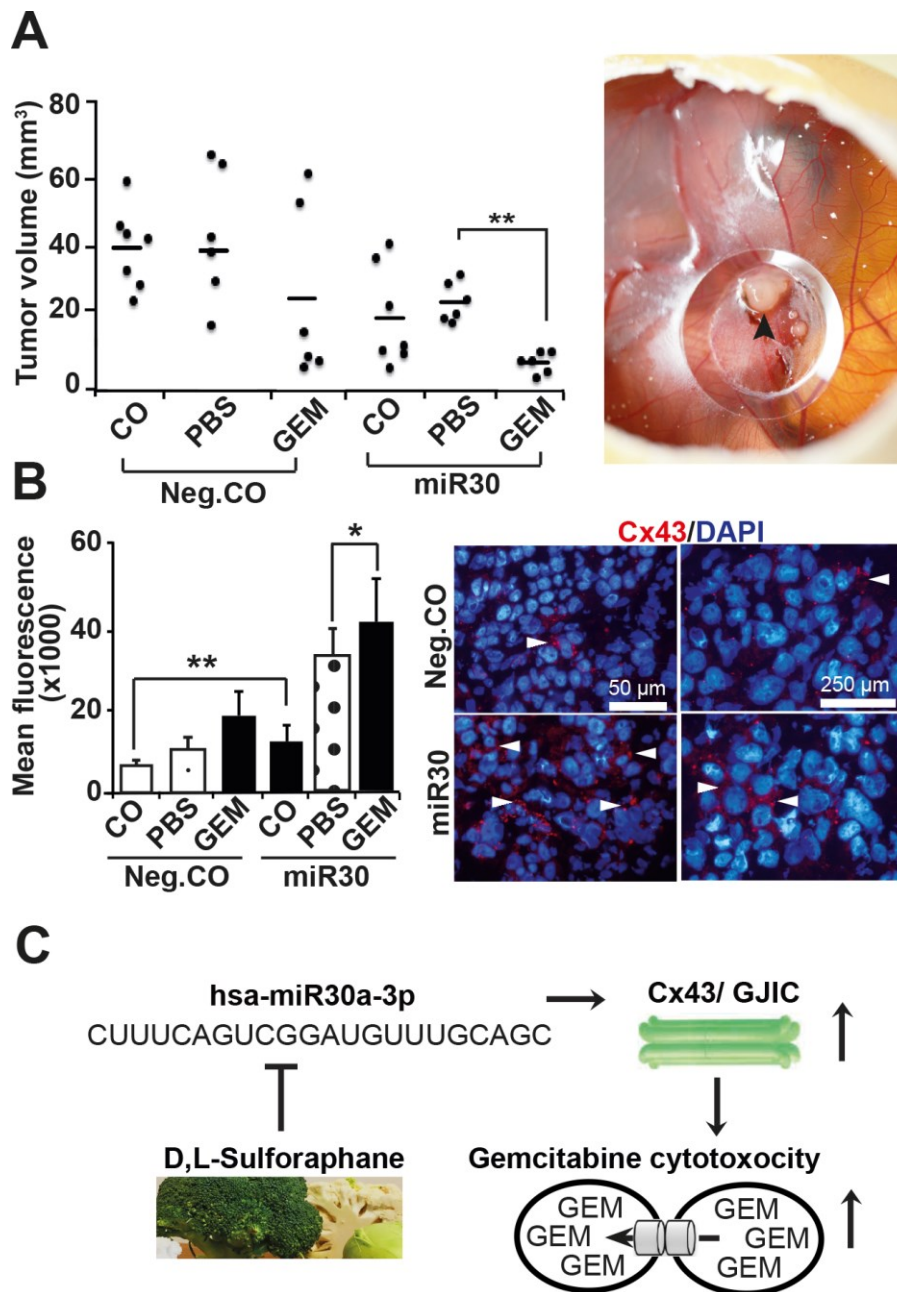


**Figure 18. miR30a-3p decreases the volume of xenograft tumors.** (A) BxGEM cells were lipofected with 30nM miR30a-3p (miR30) or a negative control (Neg. CO) and then seeded onto the CAM of the egg on day 9. Xenografts were treated with gemcitabine (GEM) or PBS on day 14 and were resected and analyzed on day 18. The control (CO) group refers to transfected xenografts that did not receive injection. Tumor volumes are presented as black dots, and the mean tumor volume is presented as black line for each experimental group. A representative image of a tumor xenograft growing on the CAM of a fertilized chicken egg (black arrow) is shown. (B) Frozen tissue sections were examined by immunohistochemistry and staining of Cx43. The cell nuclei were counterstained with DAPI (blue). The intensity of the immunofluorescence signal was quantified in 10 vision fields with ImageJ. The means  $\pm$  SD are shown. \*\*P<0.01. Representative images are shown on the right and positive Cx43 stainings (red) are marked (white arrows). (C) Scheme of sulforaphane-induced inhibition of miR30a-3p expression, which induces Cx43 expression, followed by increased GJIC and gemcitabine cytotoxicity.

### 7.1.7 Correlation of miR30a-3p and Cx43 expression in PDA patient tissue

To verify the clinical relevance of my findings, I detected the expression of miR30a-3p and Cx43 in a pancreatic cancer tissue array with 91 human pancreatic cancer tissues and 5 normal pancreatic tissues by *in situ* hybridization and immunohistochemistry, respectively (Figure S3). The expression patterns were evaluated by scoring the staining intensity and signal localization after microscopic observation, as presented in the scheme of the tissue array (Figure 19A). In PDA tissue, miR30a-3p expression was high, with the most positive signal found in ductal epithelium, whereas the expression in normal pancreatic tissue was low. On the contrary, normal pancreatic tissues expressed higher levels of Cx43 compared to PDA tissues (Figure 19B). The correlation of miR30a-3p and Cx43 expression was analyzed with the Pearson Product-Moment Correlation method and the representative scatter plot revealed a negative correlation with a p value of  $<0.01$ , suggesting that high miR30a-3p correlates with low Cx43 expression in PDA tissue. A negative correlation was also observed for pathological grading and Cx43 expression with a p value of  $<0.01$ , suggesting that Cx43 expression negatively correlates with malignancy in pancreatic cancer (Figure 19C).



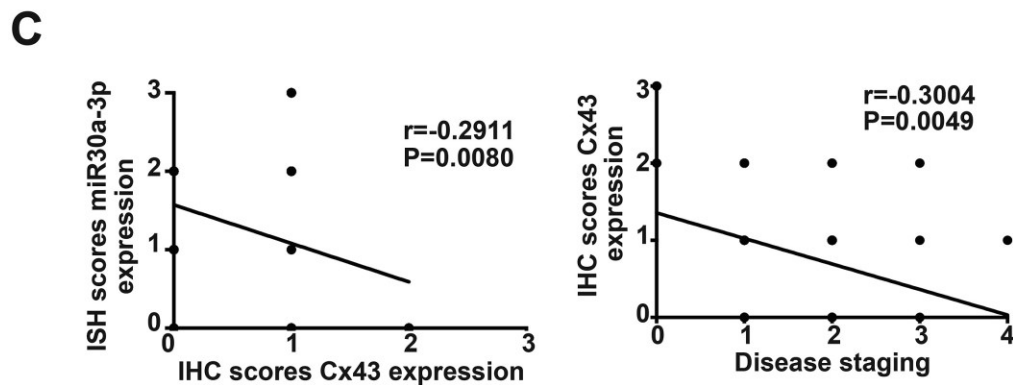
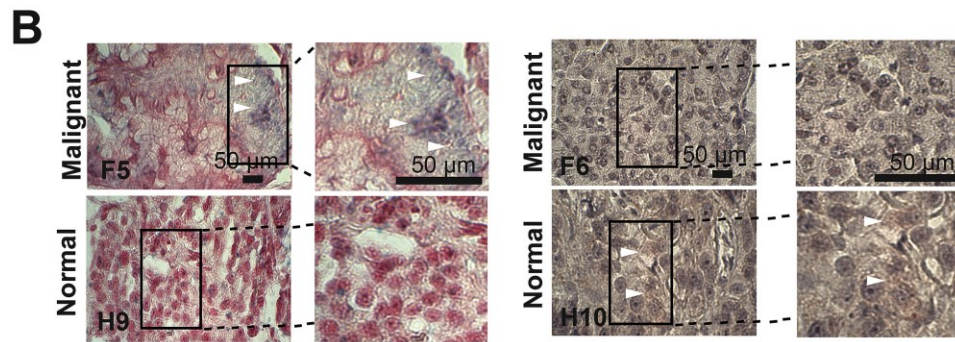
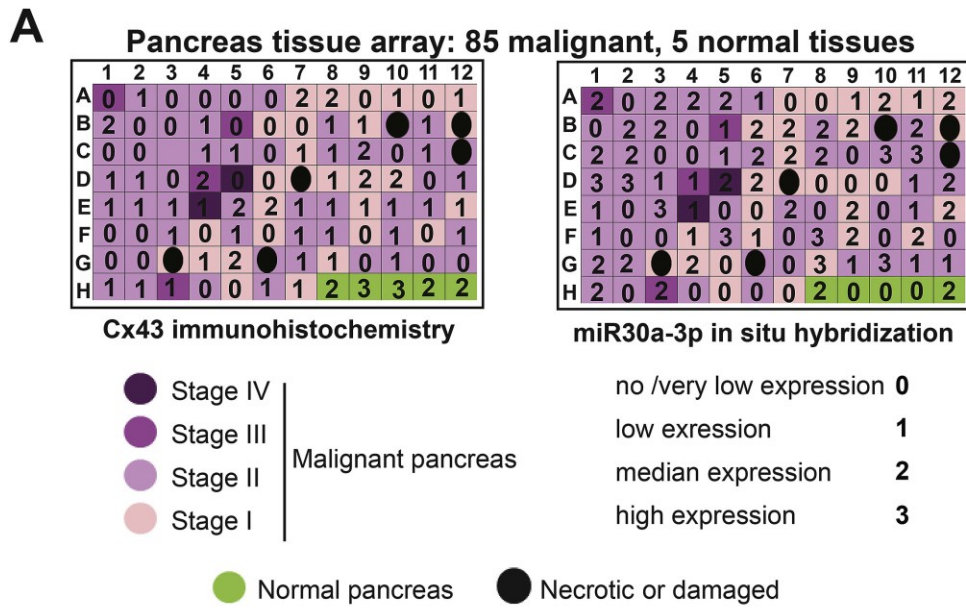


**Figure 19. Low Cx43 and high miR30a-3p expression correlate with malignancy.** A paraffin-embedded tissue microarray slide containing 91 cases of pancreatic cancer and 5 normal pancreatic tissues was used. The expression of miR30a-3p and Cx43 was detected by *in situ* hybridization (ISH) and immunohistochemistry (IHC), respectively. (A) The score of miR30a-3p and Cx43 expression was evaluated by using a semiquantitative scoring system based on the percentage of positive cells: high (3), medium (2), low (1) and absent (0). Six tissues of the microarray were either necrotic or damaged and therefore were excluded from the evaluation (thick black dot). (B) Positive miR30a-3p expression in PDA tissue (malignant) is shown in representative images. Arrows mark the localization of miR30a-3p, which is appeared to be light blue colored. Positive Cx43 expression in normal pancreatic tissue (normal) is shown in representative images. Arrows in the images highlight the localization of Cx43, detected as light red colored. (C) A scatterplot of miR30a-3p ISH and Cx43 IHC scores in the pancreatic tissues is shown. Pearson's correlation coefficient ( $r$ ) = -0.2911,  $p$  value ( $P$ ) = 0.0080. A scatterplot of Cx43 IHC scores and the correlation with pathological grading is depicted. Pearson's correlation coefficient ( $r$ ) = -0.3004,  $p$  value ( $P$ ) = 0.0049. All images were taken at 400x magnification and the scale bar indicates 50  $\mu$ m.

## 7.2 Analysis of the therapeutic potential of sulforaphane derivatives in pancreatic cancer

### 7.2.1 Chemical structure of the seven sulforaphane derivatives

With the aim to produce sulforaphane-based derivatives with higher bioactivity, the group of Professor Bolm synthesized 7 racemate derivatives of sulforaphane, which differ from the parent compound by formal substitutions of the sulfinyl (S = O) group by either sulfimidoyl (S(NR)) or sulfoximidoyl (S(O)(NR)) moieties. (Figure 20).

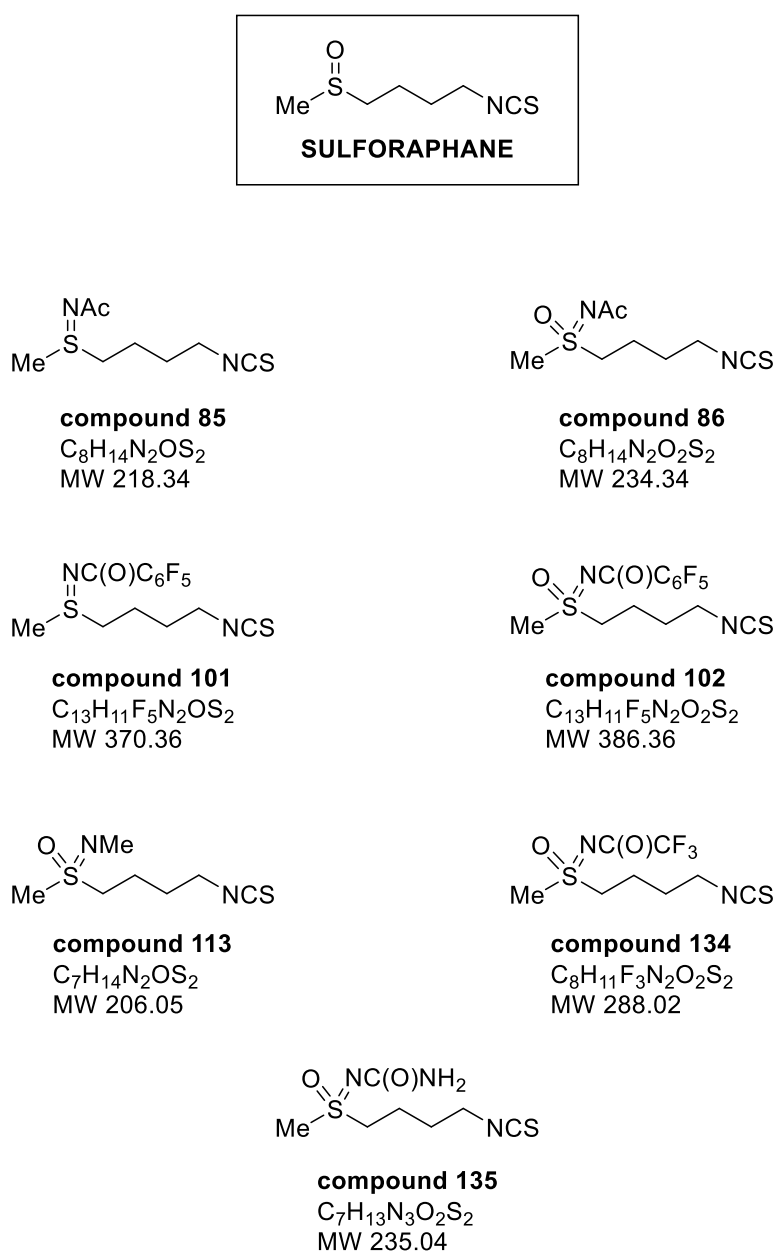
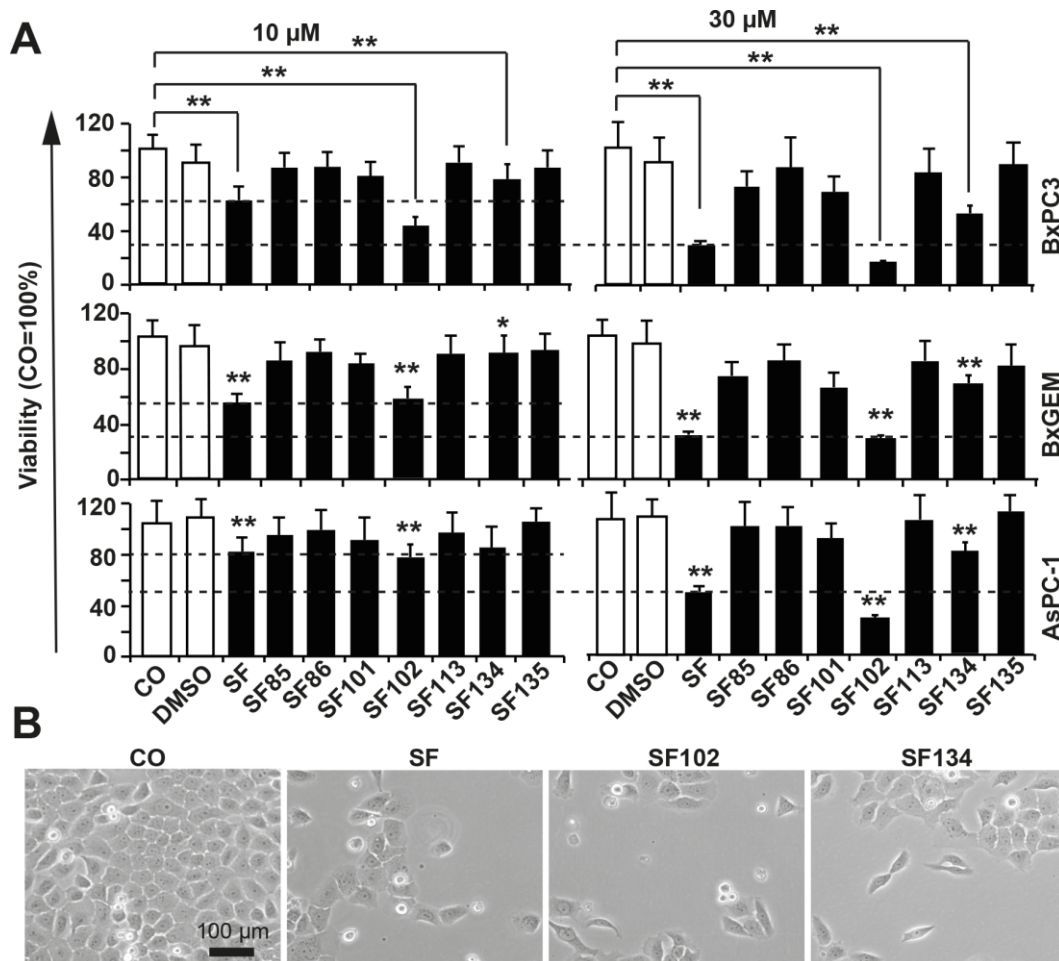


Figure 20. D,L Sulforaphane and seven sulforaphane derivatives

## 7.2.2 SF102 and SF134 are cytotoxic in all the evaluated tumor cells

To investigate whether the 7 sulforaphane derivatives display cytotoxic properties, BxPC3, BxGEM, and AsPC-1 pancreatic cancer cells were left untreated or were treated with 10 or 30  $\mu\text{M}$  sulforaphane or its derivatives SF85, SF86, SF101, SF102, SF113, SF134 and SF135. DMSO alone or untreated cells served as controls. Twenty-four hours after treatment, the cell viability was measured by MTT assay and documented by microscopy. Sulforaphane strongly reduced the viability in all cell lines compared to solvent DMSO controls or untreated cells, as expected (Figure 21A, B). The effects of SF102 were comparable to sulforaphane, whereas SF134 was less potent. All other derivatives had no significant effects, and consequently, they were excluded from further testing.



**Figure 21. SF102 and SF134 repress viability of PDA cells.** (A) BxPC3, BxGEM, and AsPC-1 cells were left untreated (CO) or treated with 10 or 30  $\mu\text{M}$  sulforaphane (SF) and derivatives (85,86,101,102,113,134,135). Twenty-four hours later, viability was measured by MTT assay. DMSO was used as a vehicle control. Data are means  $\pm$  SD of at least three independent experiments. (B) BxGEM cells were treated, as described above, the morphology of the cells was observed and representative images are shown. Scale bar indicates 100  $\mu\text{m}$ . The means  $\pm$  SD are shown. \* $P < 0.05$ , \*\* $P < 0.01$ .

The therapeutic effects of SF102 and SF134 were not restricted to pancreatic cancer cell lines, but also occurred in cancer cells from cervix, ovary, prostate, breast, colorectum, and lung, as well as in hepatocellular, neuroblastoma, T-cell leukemia and glioblastoma cell lines, as detected by MTT assay 24h after treatment (Figure 22).

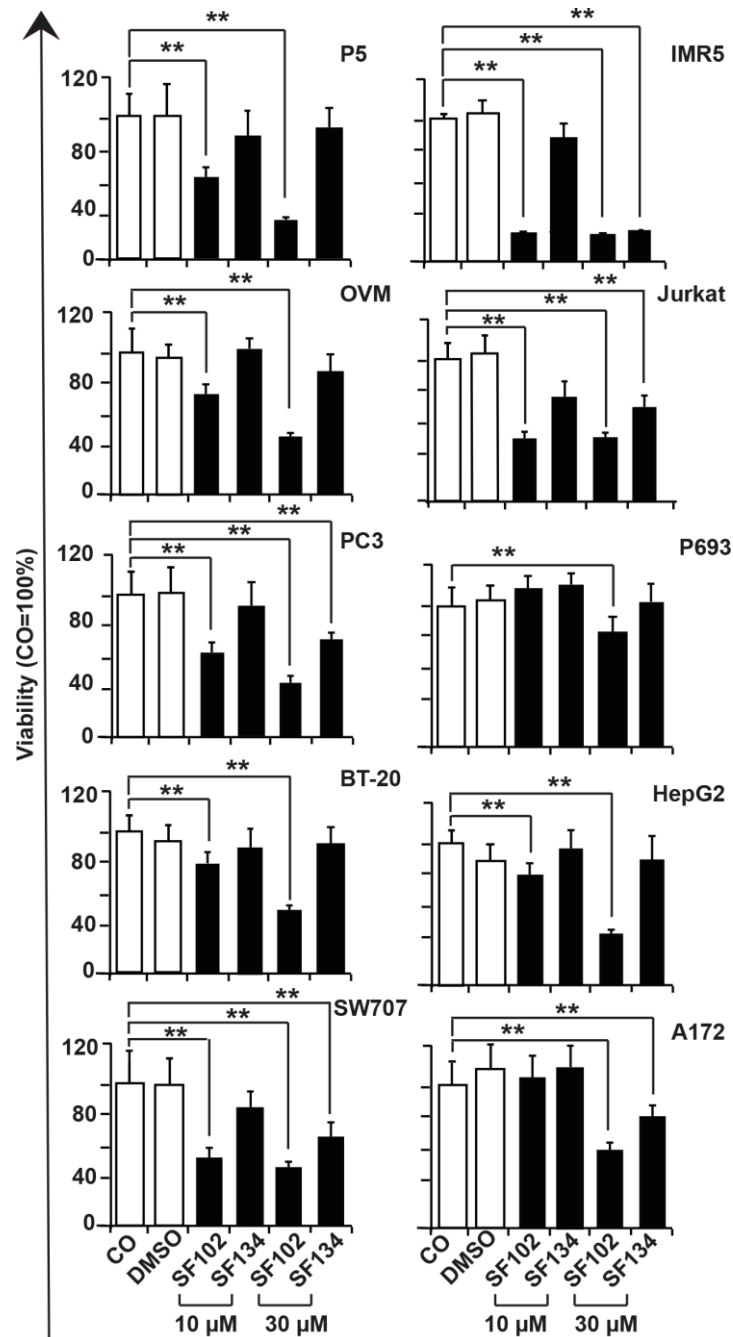


**Figure 22. Sulforaphane derivatives repress viability in various cancer entities.** All the tested cells were left untreated (CO) or treated with 10 or 30 μM sulforaphane 102 or 134 (SF102, SF134). Twenty-four hours later, viability was quantified by MTT assay. DMSO was used as a vehicle control. Diagrams represent means ± SD of at least three independent experiments. \*P<0.05, \*\*P<0.01. P5: cervical cancer, OVM: ovarian cancer, PC3: prostate cancer, BT-20: breast cancer, SW707: rectal adenocarcinoma, IMR5: neuroblastoma, Jurkat: T-cell acute lymphoblastic leukemia, P693: lung carcinoma, HepG2: hepatocellular carcinoma, A172: glioblastoma.

### 7.2.3 SF102 and SF134 induce apoptosis

To further elucidate whether SF102 and SF134 suppress viability via apoptosis, BxPC3, BxGEM, and AsPC-1 cells were left untreated or treated with sulforaphane, SF102 and SF134 for 24h. Next, cells were labeled with the PE-conjugated antibody against Annexin V and the fluorescent dye 7-aminoactinomycin D and analyzed by flow cytometry. The presence of double-fluorescent cells ( $Ann^+/7\text{-AAD}^+$ ) indicates late apoptosis (Figure 23). Sulforaphane in a concentration of 10 or 30  $\mu\text{M}$  induced a percentage of apoptosis around 30% in the most sensitive cell line BxPC3, whereas the effects in the chemoresistant cell lines BxGEM and AsPC-1 were marginal. However, SF102 induced significant apoptosis in these resistant cells of approximately 30% and of around 60% in BxPC3 cells, whereas SF134 was less active than parental sulforaphane

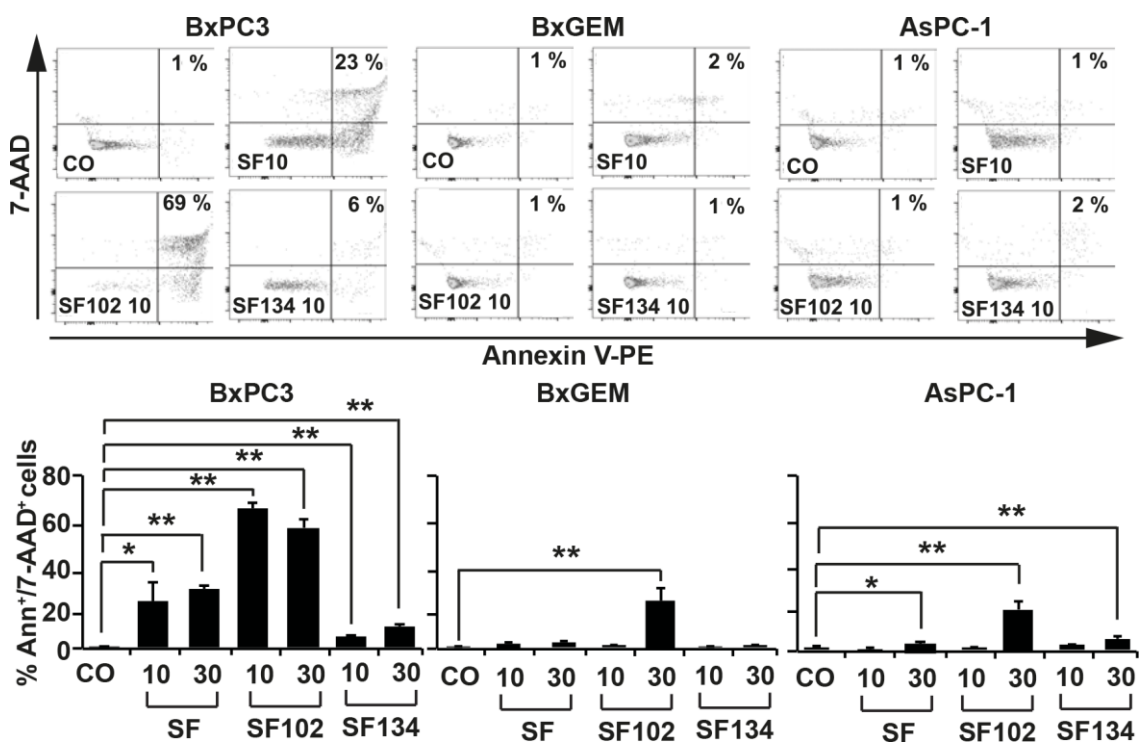


**Figure 23. SF102 and SF134 enhance apoptosis in PDA cells.** BxPC3, BxGEM, and AsPC-1 cells were left untreated (CO) or treated with 10  $\mu\text{M}$  sulforaphane (SF) and sulforaphane derivatives (SF102, SF134). After 24h, the cells were stained with PE-conjugated Annexin V and 7-AAD and then evaluated for cell death by flow cytometry. The percentage of double-stained cells ( $Ann^+/7\text{-AAD}^+$ ) is an indication of late apoptosis. Bar graphs depict the percentage of  $Ann^+/7\text{-AAD}^+$  cells that were analyzed by flow cytometry after treatment with 10 or 30  $\mu\text{M}$  sulforaphane (SF) and sulforaphane 102 and 134 (SF102, SF134). The means  $\pm$  SD are shown. \* $P < 0.05$ , \*\* $P < 0.01$ .

### 7.2.4 SF102 and SF134 diminish colony-forming capacity

To study the ability of sulforaphane derivatives to interfere with clonogenicity, which is a typical tumor stem cell feature, BxPC3 and AsPC-1 cells were left untreated or treated with sulforaphane, SF102 and SF134. After 24h, a colony-forming assay was performed, and the number of surviving cells was evaluated by microscopy (Figure 24A). SF102 and SF134 significantly reduced the number of colonies in chemoresistant AsPC-1 cells, although the effect of the original sulforaphane was more pronounced. In BxPC3 cells, SF102 was most potent in reducing colony formation, followed by sulforaphane or SF134 (Figure 24B). To test if the effect on the clonogenicity is long lasting, I isolated single live cells from the colonies and re-seeded them without additional treatment. In the resulting second generation, the number of colonies was further reduced compared to the first generation suggesting that SF102 and SF134 treatment eliminated the more aggressive, colony-forming, tumor stem-like cancer cells.

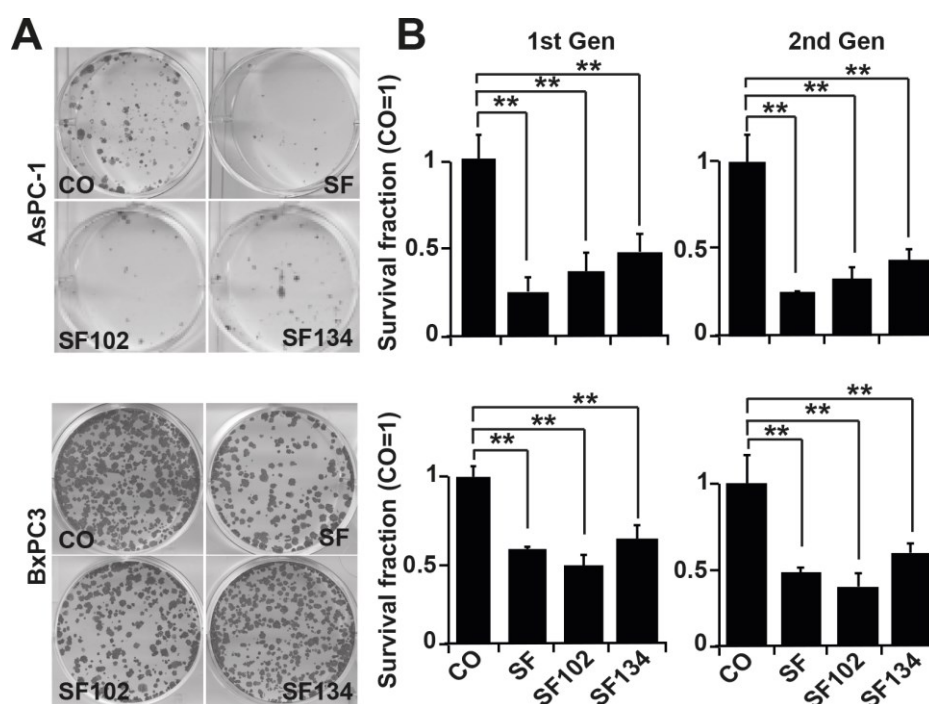


**Figure 24. SF102 and SF134 inhibit the colony forming ability of PDA cells.** BxPC3 and AsPC-1 cells were treated as described above, followed by plating of the cells 24h later at a low density (BxPC-3: 500 cells/well, AsPC-1:1000 cells/well) in 6-well plates. After two weeks, colonies were fixed with 3,7% PFA and Coomassie-stained. Colonies containing more than 50 cells were quantified under a dissecting microscope and photographed. (A) Representative images of fixed colonies are shown. (B) The percentage of plating efficiency was calculated and showed in the bar diagrams (plating efficiency of non-treated cultures was set to 1). Cells were harvested from non-fixed and non-Coomassie-stained duplicate plates of the first generation (1st Gen) of colony formation and re-plated at the same density in 6-well plates. Two weeks later, the clonogenic survival of the second generation (2nd Gen) was evaluated. The means  $\pm$  SD are shown. \*\*P<0.01.

### **7.2.5 SF102 and SF134 inhibit the growth of tumor xenografts in vivo**

To evaluate the *in vivo* relevance of my findings, I performed xenograft studies using BxPC3 or BxGEM cells that were transplanted onto the CAM of fertilized chicken eggs on day 9 of development. Five days later, sulforaphane, SF102, SF134 or a PBS control were injected into the CAM vessels and the tumor xenografts were resected on day 18. The size of each tumor was measured with calipers and the individual, as well as the mean, sizes are displayed in the diagrams (Figure 25A). The size of the BxGEM-derived tumors was significantly lower after treatment with SF102 compared to the control xenografts. The tumor suppressing effect of SF102 on BxPC3-derived xenografts was apparent, although the data were not statistically significant. To examine proliferation, xenograft cryosections were stained with the marker Ki67, followed by immunohistochemistry and evaluation of fluorescence intensity (Figure 25B). The quantification of Ki67 positive cells revealed that proliferation was significantly decreased to about 20% after SF102 treatment. Similarly, the cleaved fragment of activated caspase-3 was significantly upregulated in SF102-treated tumors indicating enhanced apoptosis (Figure 25C).

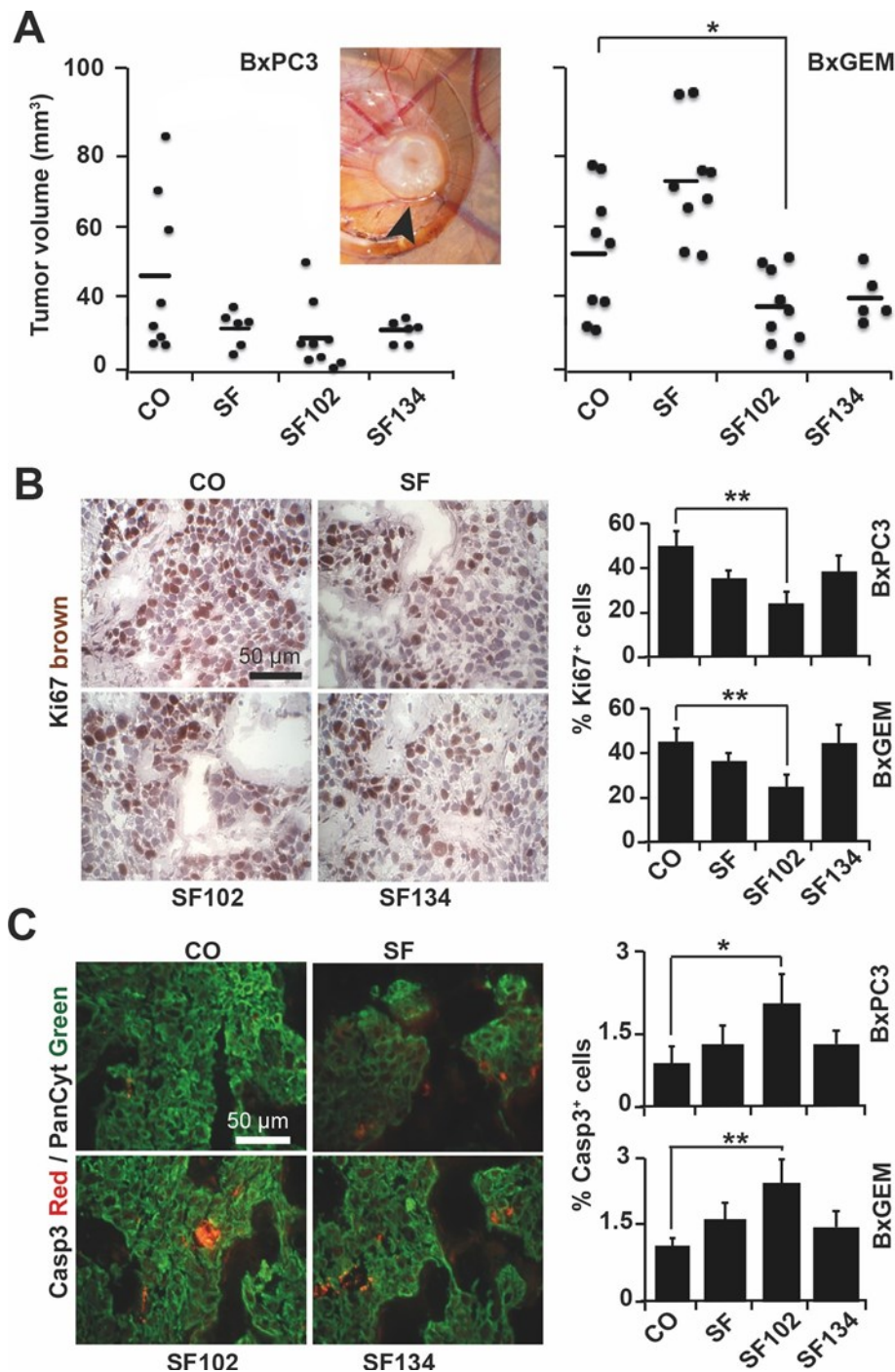


**Figure 25. SF102 and SF134 reduce the volume of tumor xenografts.** BxPC3 or BxGEM cells were seeded onto the CAM of the egg on day 9 of embryonal development. Xenografts were treated with 10  $\mu$ M sulforaphane (SF) and derivatives (SF102, SF134) on day 14. The tumor xenografts were resected on day 18, and the tumor volumes were calculated as described in the methods part. Control (CO) group refers to xenografts that have received an injection with PBS. **(A)** The volumes of individual tumors (black dots) and the mean tumor volume of each experimental group (black lines) are demonstrated in the diagrams. A representative image of a tumor xenograft on the CAM (black arrow) on day 18 is shown. Immunohistochemistry staining of the frozen tissue sections were conducted with **(B)** the proliferation marker Ki67 (brown) **(C)** the apoptosis marker “cleaved fragment of caspase-3” (Casp3, Red) and the epithelial marker pan-cytokeratin (PanCyt, green). All images were taken at 400x magnification and the scale bar indicates 50  $\mu$ m. The intensity of the Ki67 and Casp3 immunofluorescence signal was quantified in 10 randomly chosen vision fields with ImageJ and the means  $\pm$  SD are shown. \* $P < 0.05$ , \*\* $P < 0.01$ .



### 7.2.6 SF102 and SF134 had no adverse side effects on the lifespan of chicken embryos and *C. elegans*

To further investigate whether SF102 and SF134 induce toxic side effects, the liver morphology of the chick embryos and their body weight at the day 18 of development were analyzed. As indicated by hematoxylin staining, no necrotic areas were detected in liver tissue (Figure 26A). Likewise, the body weight of chick embryos was around 12 to 14 g without significant differences between groups (Figure 26B). To further rule out any side effects, I treated wild type *C. elegans* nematodes with sulforaphane, SF102, SF134 or the vehicle DMSO alone for 48h. The survival of the worms was documented over a period of 35 days by Kaplan Meier analysis. I did not observe a shorter survival of worms after treatment with sulforaphane, SF102 and SF134 compared to the control (Figure 26C), which suggests no apparent side effects regarding reproduction and development.

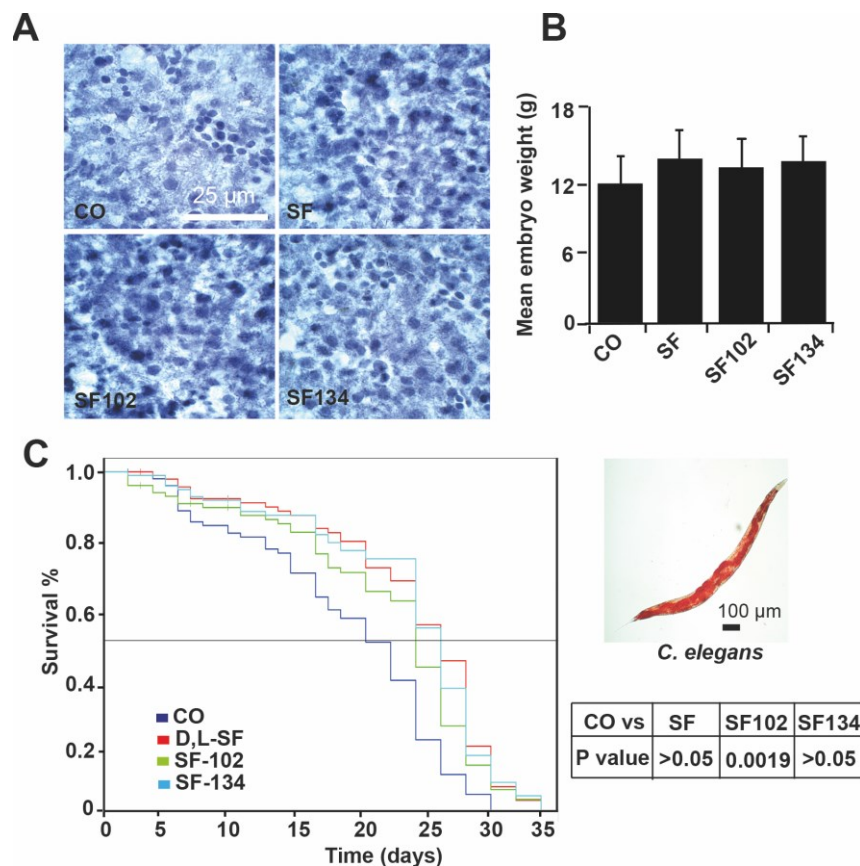


**Figure 26. Effect of SF102 and SF134 on *C. elegans* lifespan and chicken embryos.**

(A) Hematoxylin staining of embryonal liver sections of embryos derived from fertilized chicken eggs, which were treated as described above. The scale bar indicates 25 µm. (B) The mean embryonic weight of the chick embryos was determined by weighting and the means of 15 embryos per group ± SD are shown. (C) Wild type *C. elegans* worms were treated with sulforaphane (SF), SF102, or SF134 for 48h, or were left untreated (CO) and Kaplan Meier analysis was performed. SF102 significantly prolonged the lifespan of the nematodes compared to the control. A representative microscopy image from a *C. elegans* worm is shown on the right. The scale bar indicates 100 µm.

### **7.2.7 Sulforaphane, SF102 and SF134 exhibit similarities and differences regarding microRNA signaling and target gene induction**

To further highlight the underlying signaling pathways responsible for the observed anti-tumor effects of SF102 and SF134, miRNA microarray expression profiling and bioinformatics evaluation of potential target genes was performed. AsPC-1 cells were treated with sulforaphane, SF102 or SF134 or were left untreated and the RNA was isolated 24h later. In cooperation with Dr. Sticht, I identified 500 significant ( $P < 0.05$ ) and differentially regulated miRNAs compared to the control. As presented in the heat map, there were many similar clusters but also obvious differences in miRNA expression following sulforaphane, SF102 and SF134 treatment (Figure 27A). Next, the top 10 most significantly regulated miRNAs were evaluated in three comparison groups: (1) sulforaphane versus control, (2) SF102 versus control (3) SF134 versus control (Figure 27B). Through this analysis, miR2278 was identified as common and most significant downregulated miRNA after sulforaphane, SF102 and SF134 treatment (Table S2). To identify further differences in miRNA expression between sulforaphane, SF102 and SF134, I created Volcano plots from the most significant differentially regulated miRNAs with  $-\log_{10} p$  values  $> 2$  among the comparison groups mentioned above and an extra group, SF102 versus SF134. MiR27b-5p and miR29b-1-5p were identified as the most interesting candidates, as they were downregulated after sulforaphane treatment compared to control, but upregulated by SF102 and SF134 compared to sulforaphane (Figure 27C). Interestingly, the comparison between SF102 and SF134 showed a small number of differentially regulated miRNAs. The miRNAs identified from the volcano plot comparisons were summarized in a Venn diagram and the names of the miRNA candidates were provided in a supplementary table (Figure 27D, Table S3). Altogether, the three miRNA candidates, miR228, miR27b-5p and miR29b-1-5p came out from the bioinformatic analyses as the most important candidates in order to differentiate the pathway regulation between sulforaphane and its derivatives.

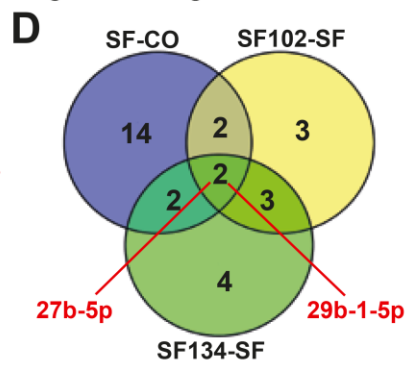
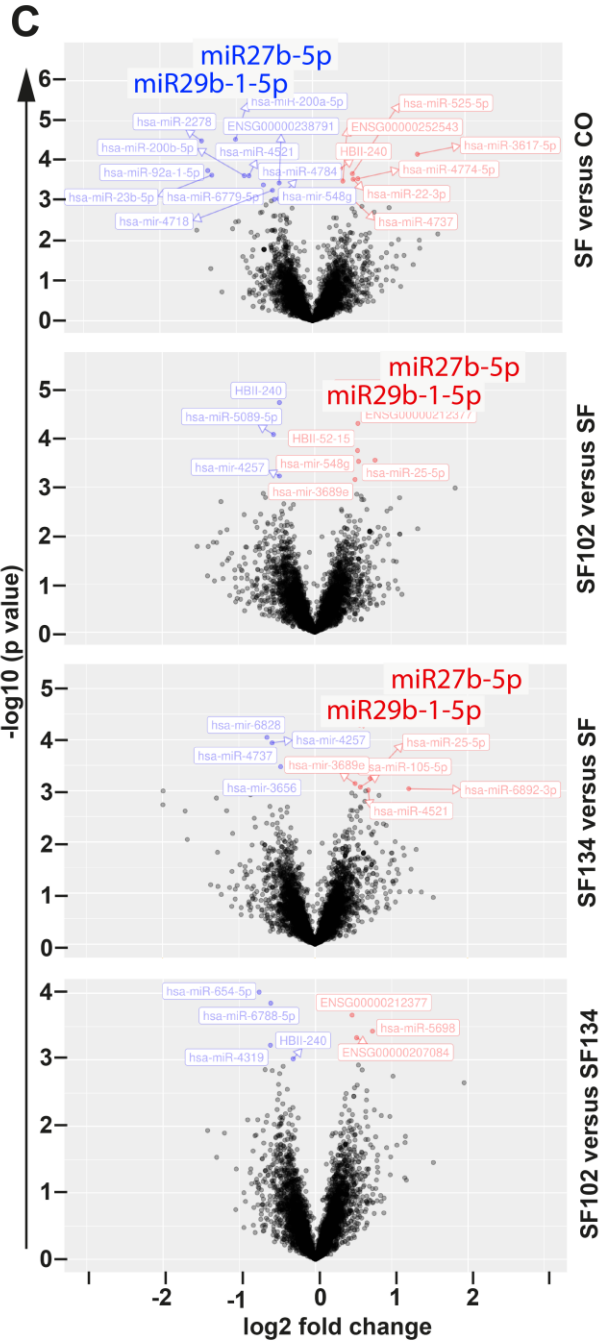
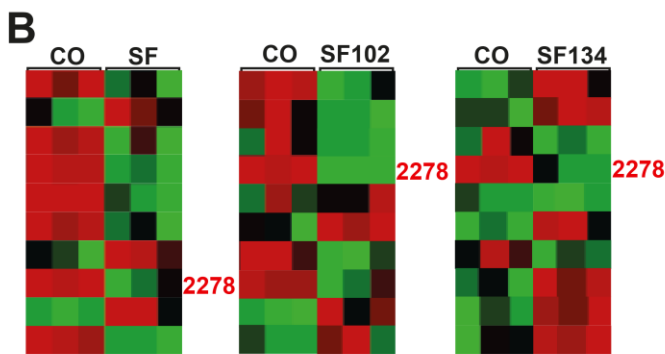
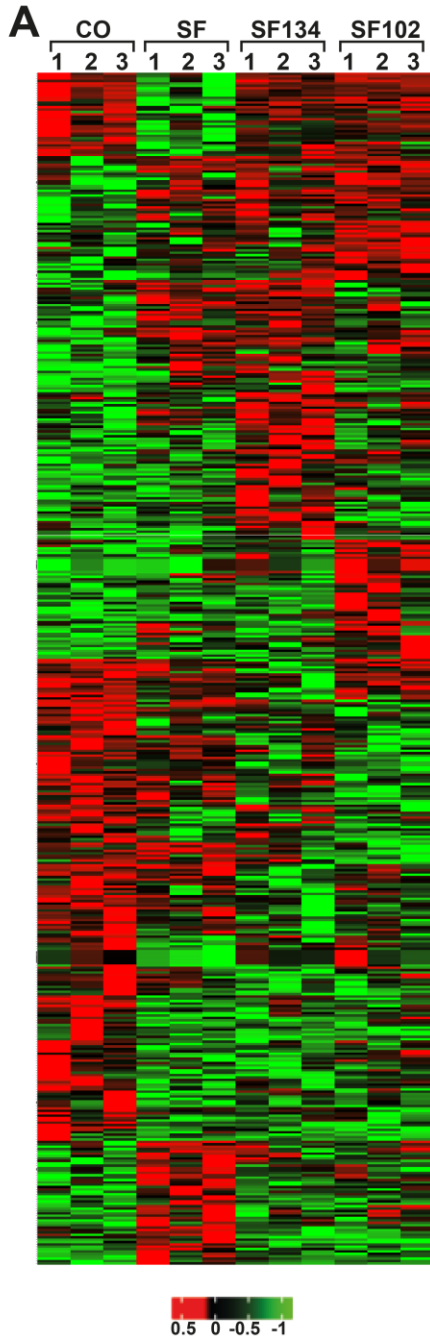


**Figure 27. miRNA expression profiling and bioinformatic analysis detects common and different expression patterns induced by sulforaphane and sulforaphane, SF102 and SF134.** (A) AsPC-1 cells were treated with 10  $\mu$ M sulforaphane (SF), SF102, or SF134, or were left untreated (CO). Twenty-four hours later, RNA was isolated and analyzed by a GeneChip miRNA 4.0 Array in triplicates. The heatmap presents the top significantly regulated miRNAs after sulforaphane and its derivatives treatment. The red color marks high expression, and the green color marks low expression within a scale from 0.5 to -1, as indicated. (B) The 3 heatmaps present the top 10 significantly regulated miRNAs after sulforaphane and its derivatives treatment. MiR2278 is highlighted in red color (C) Volcano plots show the miRNA distribution. On the y-axis, the  $-\log_{10}$  p value is plotted, whereas on the x-axis, the fold change is represented. (D) Venn diagram shows the distribution of differentially expressed miRNAs among three groups compared: SF-CO, SF102-SF and SF134-SF. The overlapping region identified two miRNAs, miR27b-5p and miR29b-1-5p, that are differentially expressed between sulforaphane and the 2 derivatives.

To obtain information about target genes regulated by the three candidate miRNAs, a bioinformatic analysis using the Target Mining tool of mirWalk platform was performed. After providing the list of miRNAs and generating the search output based on the prediction of miRNA-target gene interactions, the data are depicted as a network plot. This search resulted in 309 target genes that are individually or commonly regulated by the 3 miRNA candidates (Figure 28A). To follow up on our previous studies showing that sulforaphane normalizes enhanced NF- $\kappa$ B activity by miRNA signaling (Kallifatidis et al. 2009), (Yin et al. 2019), the abovementioned 309 target genes were filtered for NF- $\kappa$ B signaling and the selected genes were displayed in a separate network plot (Figure 28B). MiR2278 is predicted to regulate the highest number of NF- $\kappa$ B-related target genes, which partially overlap with genes that are regulated by miR27b-5p and miR29b-5p (Table S4).



**Figure 28. Identification of NF- $\kappa$ B related miRNA-target genes.** (A) Using the Target Mining option of the mirWalk online platform, 309 target genes of miR2278, miR27b-5p and miR29b-1-5p were identified and displayed as a network graph. Each orange dot is associated to a target gene. The black lines symbolize e.g. the joint target gene CCDC141 of miR2278 and miR29b-1-5p, the joint target gene CREB5 of miR-29b-1-5p and the joint target genes RPRD1A, CLMN, and LRRC8C of miR-2278 and miR27b-5p. (B) A miRNA-target gene analysis with focus on NF- $\kappa$ B signaling identified the most significantly NF- $\kappa$ B-related target genes of miR29b-1-5p, miR2278 and miR27b-5p. TIRAP and DDX58 are target genes of miR2278 and miR29b-1-5p, CFLAR, ERC1 and PRKCB are target genes of miR2278 and miR27b-5p, and PLCG1 and TRIM25 are target genes of miR29b-1-5p and miR27b-5p.

## **8. Discussion**

### **8.1 Sulforaphane induces gemcitabine cytotoxicity in PDA by the downregulation of miR30a-3p**

In this part of my thesis, I focused to elucidate the mechanism of action of sulforaphane-induced gap junction formation and how the presence of gap junctions could further potentiate gemcitabine activity in PDA. I analyzed the involvement of miRNA signaling in sulforaphane-induced GJIC in PDA cells. MiR30a-3p was identified as a promising GJ-related candidate, whose downregulation either by sulforaphane or by transfection of miR30a-3p inhibitors enhanced gemcitabine sensitivity through GJ-related overexpression of Cx43 *in vitro* in PDA cells and *in vivo* in tumor xenografts derived from PDA cells. Patient tissue analyses revealed that high miR30a-3p expression correlates to low Cx43 expression, which could in turn associate with PDA staging.

#### **8.1.1 Sulforaphane enhances GJ function and gemcitabine bystander effect**

In this work I demonstrated that sulforaphane induced the GJIC in highly malignant PDA cells and this effect was clearly diminished when cells were co-treated with sulforaphane and the gap-junction inhibitor oleamide. This finding was consistent with former studies done in my laboratory (Forster et al. 2014). To prove the effect of sulforaphane on GJIC, I applied the well-established double-dye flow cytometry assay, which was used to study the function of GJs not only in PDA (Garcia-Rodriguez et al. 2011), but also in glioblastoma (Hitomi et al. 2015) and melanoma (Tittarelli et al. 2015).

Sulforaphane has already been shown to induce the gemcitabine cytotoxicity in PDA cells via suppression of the highly aggressive cancer stem cells (Kallifatidis et al. 2011). Herein I presented that sulforaphane re-stored the chemosensitivity of PDA cells to gemcitabine this time through induction of GJIC. The GJ-specificity of the result was confirmed with the presence of the gap-junction inhibitor oleamide. In line with my results, Cottin et al. demonstrated that functional GJs are essential for the induction of gemcitabine bystander effect in glioblastoma and osteosarcoma cell lines (Cottin et al. 2010).

To examine the gemcitabine bystander effect in PDA cells, I combined cell death analysis with double-dye flow cytometry to identify the percentage of dead and non-pretreated target cells. The key advantage of this method compared to e.g., the MTT assay or microscopic observation (Cottin et al. 2010), (Garcia-Rodriguez et al. 2011), (Alexandre et al. 2007), is the specific quantification of dead target cells, which are recognized as double-fluorescent cells from the flow cytometer.

A better combined effect of sulforaphane and gemcitabine combination compared to the single substances was observed in PDA cells. **This was a major achievement** because it did not only show that the cytotoxicity of PDA cells to gemcitabine was higher after sulforaphane treatment but also provided an alternative therapeutic option, in which the cytotoxic molecules can be transferred to PDA cells that do not receive initial treatment (Kandouz and Batist 2010).

### **8.1.2 Sulforaphane augments Cx43 expression by inhibiting miR30a-3p expression**

Hereby I demonstrated that sulforaphane enhanced the Cx43 expression on the surface of PDA cells, an expected result linked to the activated GJs. The tumor suppressive role of Cx43 in PDA and its significance for GJ function and cancer progression was previously documented (Forster et al. 2014), (Dovmark et al. 2017). Concerning chemotherapy bystander effect and Cx43 expression, my results correlated high Cx43 expression with gemcitabine sensitivity in PDA. As a supporting evidence of these findings, high Cx43 expression was found to be important as well for paclitaxel cytotoxicity in ovarian carcinoma (Toler et al. 2006), while in breast cancer PQ1, a Cx43-enhancer, restored defective GJIC and counteracted cisplatin resistance (Ding and Nguyen 2012).

The missing link between sulforaphane-induced restoration of GJIC and Cx43 expression was identified and it involved miR30a-3p in the regulation of Cx43. My study is the first to show the regulation of Cx43 through miR30a-3p. The binding of miR30a-3p to the Cx43 3'-UTR was demonstrated, suggesting that the reduction of miR30a-3p levels is directly involved in the modulation of Cx43 expression. These results explain one crucial mechanism, which has been first mentioned in our former study (Forster et al. 2014).



In this study though, sulforaphane was shown to enhance the expression levels of Cx43 protein, but did not upregulate Cx43 mRNA expression, in contrast to my current findings. This might be due to different experimental conditions regarding time points of sulforaphane treatment (6h in the former study and 24h in the actual study) and the Cx43 primers used. Whereas the former study used self-made PCR primers and conventional qRT-PCR conditions, the actual study used TaqMan ready-to-use primers and TaqMan PCR conditions.

The high miR30a-3p expression in PDA cell lines is in line with the study of Zhang et al., although that study did not evaluate the function of the miRNA (Zhang et al. 2009). On the contrary, studies in hepatocellular carcinoma propose a rather tumor suppressive function of miR30a-3p, as its downregulation promotes invasion and metastasis (Wang et al. 2014). The exact reason for these opposing results is not clear, however it is assumed that the expression of miR30a-3p could be cancer and tissue type-specific.

### **8.1.3 miR30a-3p inhibits gemcitabine resistance in vitro and in vivo**

Transfection with miR30a-3p inhibitors induced both GJIC and gemcitabine bystander effect and this result confirmed our main hypothesis that miR30a-3p is the underlying key regulator of sulforaphane for the induction of GJIC, Cx43 expression and gemcitabine sensitivity in PDA cells. Interestingly, I could observe a much stronger bystander effect after transfection with liposomes, which could possibly be explained by the fact that transfection itself induces background cytotoxicity (Wang et al. 2018).

To confirm that administration of miR30a-3p could be effective *in vivo*, I used the fertilized chicken egg model for tumor xenotransplantation, because this system is an ethical alternative to experiments performed on mammals (Aleksandrowicz and Herr 2015) and has been evaluated in several of our recent studies (Zhao et al. 2018), (Bauer et al. 2014), (Nwaeburu et al. 2017). A major advantage of the chicken egg model is its natural immunodeficiency because immunocompetence in birds develops only after hatching. Xenografts are transplanted to the CAM, usually on day 8 or 9 of development, when the blood vessel network is dense enough to support the growth of a tumor xenograft. Fast tumor growth and potential for drug delivery studies are major advantages to widely establish this model for cancer research (Ribatti 2017).

By the use of this model I confirmed my *in vitro* results and proved that miR30a-3p transfection decreased tumor growth and increased gemcitabine sensitivity of PDA xenografts, which were transfected *in vitro* and treated with gemcitabine *in vivo*.

#### **8.1.4 miR30a-3p and Cx43 expression in pancreatic cancer tissue**

To assess the clinical relevance of my results, a screening of miR30a-3p and Cx43 expression in a pancreatic cancer tissue array with 96 normal or malignant patient tissue sections was performed. My data showed that the expression of miR30a-3p in malignant tissue is higher than in normal tissue on average. These findings are consistent with data from miRNA tissue atlas that detected low miR30a-3p in normal pancreatic tissue (Ludwig et al. 2016). An interesting observation was that higher miR30a-3p expression in the tissue array was observed in the stage II of malignant pancreatic cancer, which is an important stage for the initiation of metastasis (Hidalgo 2010). Furthermore, malignant tissue displayed lower Cx43 expression compared to normal tissue, which underlines the significance of our previous findings on Cx43 expression in malignant pancreatic tissues (Forster et al. 2014). Similar results regarding the Cx43 expression in pancreatic cancer patients were found in the Human Protein Atlas Database, where immunohistochemistry data showed low or medium expression in most patients (<https://www.proteinatlas.org/ENSG00000152661GJA1/pathology/pancreatic+cancer#Location>). The correlation of miR30a-3p and Cx43 expression was statistically significant, however it was poor, based on the Pearson correlation coefficient ( $r = -0.2911$ , a strong correlation is considered when  $r \leq -0.8$ ) (Akoglu 2018). Likewise, Cx43 expression was poor but significantly correlated with pathological staging of pancreatic cancer ( $r = -0.3004$ ). Possible reason for the poor correlation could be the variance in gene expression between ductal adenocarcinomas and different types of pancreatic cancer, that were examined within the tissue array, as well as the small patient cohort. Taken together, in this study I demonstrated that miR30a-3p and Cx43 in PDA tissues followed the expression pattern of my *in vitro* bioinformatic analyses. The correlation of Cx43 with miR30a-3p expression and malignancy of PDA were, to best of my knowledge, demonstrated for the first time.

## **8.2 Sulforaphane derivatives are proposed as new therapeutic agents for PDA**

There are many promising pre-clinical and clinical studies using sulforaphane as an anti-cancer agent, however, a sulforaphane-based drug is not clinically approved until now. In the second part of my thesis, I examined whether a series of unprecedented derivatives of sulforaphane could exhibit better anti-cancer properties compared to the parental sulforaphane. Viability assay led to identification of two promising sulforaphane derivatives, SF102 and SF134. These two derivatives, and more effectively sulforaphane SF102, reduced viability and stem cell features of PDA cells by induction of apoptosis. Treatment with SF102 and SF134 also inhibited the xenograft tumor growth *in vivo* without inducing additional toxicity in chicken embryos and *C.elegans*. By conducting microarray analysis and bioinformatics evaluation, I detected similarities and differences in signal transduction among the treatments. The most striking similarity was that all of them had in common the regulation of NF- $\kappa$ B-related target genes.

### **8.2.1 SF102 and SF134 induce cytotoxicity in cancer cells**

The establishment of sulforaphane analogues by molecular single atom changes in form of oxygen-to-nitrogen substitutions at the central sulfur atom, are unprecedented in the context of sulforaphane chemistry. SF102 and SF134 were the two out of the seven derivatives that could inhibit the viability, via induction of apoptosis, and the colony-forming potential of PDA cells. To the best of my knowledge, this is the first time that the cytotoxicity of synthetic sulforaphane derivatives has been tested and evaluated in PDA cells. Previously, other synthesized sulforaphane derivatives were shown to inhibit proliferation of melanoma cells (Kielbasinski et al. 2014) or to induce cell cycle arrest and apoptosis in hepatocellular carcinoma cells (Hu et al. 2013). Shi et al. demonstrated that sulforaphane heterocyclic derivatives enhanced apoptosis and eliminated the CSC population in breast cancer cells (Shi et al. 2016).

These data are in line with my results, as the most effective derivatives, SF102 and SF134, did not only inhibit the viability of PDA cells but also of breast, hepatocellular and several other cancer types, suggesting a broad range of anti-tumor activity.

### **8.2.2 SF102 and SF134 did not cause significant side effects**

To confirm whether administration of sulforaphane derivatives could be effective *in vivo*, I used the fertilized chicken egg model. These experiments showed that SF102 decreased tumor growth, inhibited proliferation and induced apoptosis by increasing the expression of caspase-3 at a higher rate compared to sulforaphane and SF134. Sulforaphane was previously shown to have no pronounced side effects in non-malignant cells or in mice experiments (Kallifatidis et al. 2011), (Herr et al. 2013). Likewise, SF102 and SF134 caused no severe side effects in chicken embryos, as there were no signs of necrosis in the liver of the embryos or abnormal weight loss. To strengthen this observation, experiments on another animal model, *C. elegans*, demonstrated that sulforaphane derivatives did not disturb the lifespan and reproduction of the worms. Interestingly, SF102 even significantly induced longevity in the worms, a process that has been already proven to be anticarcinogenic (Kyriakakis et al. 2015).

### **8.2.3 Similarities and differences of SF102 and SF134 regarding microRNA signaling and target gene induction**

My results suggest that SF102 and SF134 decrease the viability, clonogenicity, and tumor growth, and induce apoptosis in pancreatic cancer cells as potent or, in the case of SF102, even better than sulforaphane. Sulforaphane exhibits its anti-cancer activity in PDA mainly by normalizing the overactivated NF- $\kappa$ B signaling in tumor stem cells and thereby mediates chemosensitization (Kallifatidis et al. 2009), (Appari et al. 2014). The bioinformatic analysis of miRNA data predict that sulforaphane, SF102 and SF134 affect NF- $\kappa$ B signaling by the induction of miR2278, which is involved in the regulation of many NF- $\kappa$ B target genes. Additionally, while sulforaphane inhibits the expression of miR27b-5p and miR29b-1-5p compared to untreated control cells, SF102 and SF134 rather induce these miRNAs compared to their expression in sulforaphane-treated cells. This finding is of high relevance, because, according to our *in silico* analysis miR27b-5p and miR29b-1-5p are also regulators NF- $\kappa$ B-related target genes. According to the Human Protein Atlas Database, the predicted target genes PLCG1 (<https://www.proteinatlas.org/ENSG00000124181PLCG1/pathology>) and TRIM25 (<https://www.proteinatlas.org/ENSG00000121060-TRIM25/pathology>) are of high relevance in pancreatic cancer, because patients with high PLCG1 (n = 110) or TRIM25 (n = 121) expression survive longer than those with low expression (n = 66, n = 55,

respectively). Interestingly, the miRNA candidates miR2278, miR27b-5p and miR29b-1-5p have never before been documented in pancreatic cancer, as far as I know. The only available information about miR2278 and cancer is that its upregulation is associated with the inhibition of leukemic cell proliferation and enhanced apoptosis (Kaymaz et al. 2015). However, Kim et al. demonstrated both miR27b-5p and miR29b-1-5p as markers for gastric cancer progression (Kim et al. 2018), while miR29b-1-5p overexpression induced epithelial-mesenchymal transition (EMT) in oral squamous cell carcinoma (Kurihara-Shimomura et al. 2019).

Except of these three miRNAs and their regulation of the NF- $\kappa$ B target genes, another interesting question that arises is whether sulforaphane derivatives could have similar or better effect on the miR30a-3p/Cx43 mechanism that was mentioned in the first part of my study. Analysis of the miRNA data revealed that there was no difference in expression of miR30a-3p after SF102 or SF134 treatment compared to the control.

Moreover, preliminary Western Blot results showed no influence on Cx43 expression after SF102 or SF134 treatment. The fact that sulforaphane derivatives could not reproduce the same result on miR30a-3p/Cx43 mechanism point outs that the original sulforaphane and its synthesized derivatives may differ in the mechanisms they induce to tackle PDA progression.

#### **8.2.4 Clinical relevance of sulforaphane derivatives synthesis**

During the last years, several clinical studies have been conducted with sulforaphane as a drug for cancer treatment. The most common method for delivery of sulforaphane to the patients is by sulforaphane rich-broccoli sprout extracts (Alumkal et al. 2015), (Lozanovski et al. 2019), because broccoli sprouts are known to contain a much higher amount of glucoraphanin, precursor of sulforaphane, compared to mature broccoli (Fahey et al. 1997). However, the daily intake of a large number of capsules in order to reach a high concentration of sulforaphane is very unpleasant for the patients and it can lead to high drop-out rates, as it occurred in the pilot study in the surgery department in Heidelberg (Lozanovski et al. 2019). Moreover, patients with terminal stage PDA anyway experience severe side effects from the disease and the high drug intake can lead to worsening of pre-existing conditions.

Therefore, the development of a drug with highly active sulforaphane or a derivative thereof is urgently required to circumvent the unpleasant side effects of broccoli sprouts consumption and increase the intake of a high amount of sulforaphane within a single capsule.

### **8.3 Conclusion**

My study proposes new sulforaphane-based therapeutic approaches in order to inhibit the progression of the highly aggressive PDA.

Firstly, I demonstrated that sulforaphane enhances gemcitabine cytotoxicity *in vitro* and *in vivo* as a result of an increased bystander effect, mediated by inhibition of miR30a-3p and upregulation of GJ-related Cx43 expression. MiR30a-3p and Cx43 expression profile in PDA patients provided promising preliminary data for their significance in PDA progression. Future clinical studies are necessary to address whether a systemic application of sulforaphane or miR-30a-3p inhibitors can improve the efficacy of gemcitabine treatment in pancreatic cancer patients.

Secondly, two derivatives of sulforaphane, SF102 and SF134, have been evaluated as new therapeutic agents. These two derivatives and especially SF102 showed strong inhibition in viability and colony formation in PDA cells and reduced the xenograft growth *in vivo* without profound adverse side effects. Therefore, sulforaphane derivatives can be a basis for the development of new therapeutic drugs with better pharmacokinetic properties in pancreatic cancer patients. However, more extensive studies on animal models and PDAC patients are needed to validate their therapeutic potential.

## 9. Summary

PDA is one of the deadliest cancers with poor prognosis and profound therapy resistance, which is associated with the loss of gap junctional intercellular communication and Cx43 expression. A promising bioactive agent with multiple anti-cancer activities is sulforaphane, an isothiocyanate that is naturally found in cruciferous vegetables. Sulforaphane restored the gap junctional intercellular communication and thereby therapy sensitivity in PDA and I investigated whether microRNA signaling is involved in this mechanism. Established cell lines were evaluated *in vitro* by gap junction and gemcitabine bystander effect assays, microRNA and gene arrays, bioinformatics analysis and luciferase reporter assay, while *in ovo* xenograft studies with miRNA-transfected tumors were performed. miRNA and gene expression were also analyzed in patient tissue by *in situ* hybridization and immunohistochemistry. My results revealed that sulforaphane inhibited the expression of the top candidate miR30a-3p. Transfection with miR30a-3p inhibitors increased the gap junctional intercellular communication, Cx43 expression and gemcitabine bystander effect. *In ovo*, the xenotransplantation of these transfected cells decreased the tumor volume and enhanced the efficacy of gemcitabine. In a pancreatic cancer tissue array, the expression of miR30a-3p was present in malignant tissues but not in normal and the opposite result was observed for Cx43 expression. These findings provide new knowledge on the mechanism of sulforaphane-induced gap junctional intercellular communication and gemcitabine cytotoxicity in pancreatic cancer. With the aim to develop sulforaphane-based drugs for pancreatic cancer, I screened 7 unprecedented sulforaphane derivatives for their bioactivity against PDA and other tumor entities. MTT and colony forming assays, apoptosis analysis with flow cytometry, immunohistochemistry, microRNA studies as well as tumor xenograft and *C. elegans* studies were performed with these analogs. My observations suggest the anti-tumor activity of two out of the 7 derivatives, SF102 and SF134. SF102 was most effective in inhibition of viability, clonogenicity and tumor growth along with induction of apoptosis, followed by SF134, most importantly without obvious side effects. miRNA array profiling revealed differentially expressed candidates between sulforaphane derivatives and parental sulforaphane. My results indicate that sulforaphane-induced downregulation of the miR30a-3p enhances gap junctional intercellular communication and gemcitabine efficacy in pancreatic cancer. Sulforaphane derivatives SF102 and SF134 are shown to suppress the progression of

pancreatic cancer. I expect that the development of new sulforaphane- or sulforaphane analogs-related drugs will forge new therapeutic options for pancreatic cancer.



## 9. Zusammenfassung

Bauchspeicheldrüsenkrebs ist einer der tödlichsten Krebsarten mit schlechter Prognose und tiefgreifender Therapieresistenz, der mit dem Verlust der interzellulären Kommunikation und Cx43 Expression verbunden ist. Ein vielversprechender Pflanzenstoff mit mehreren anti-Krebs-Aktivitäten ist Sulforaphan, ein Isothiocyanat, das in Kreuzblütlern enthalten ist. Sulforaphan stellte die Gap Junction-Kommunikation und damit die Therapieempfindlichkeit der Chemotherapie bei Bauchspeicheldrüsenkrebs wieder her. Ich habe untersucht ob microRNAs an diesem Mechanismus beteiligt sind. Etablierte Zelllinien wurden *in vitro* durch Gap Junction und Gemcitabin Bystander Effekt assays, microRNA – und Gen arrays, Bioinformatische Auswertung getestet, während *in ovo* Xenograft Studien mit miRNA-transfizierten Tumoren durchgeführt wurden. MiRNA und Genexpression wurden auch in Bauchspeicheldrüsenkrebsgeweben durch *in situ* Hybridisierung und Immunhistochemie analysiert. Meine Ergebnisse haben gezeigt, dass Sulforaphan die Expression des Spitzenkandidaten miR30a-3p hemmt. Transfektion mit miR30a-3p Inhibitoren hat die Gap Junction-Kommunikation, Cx43 Expression und Gemcitabin Bystander Effekt verbessert. *In vivo*, die Xenotransplantation dieser transfizierten Zellen verringerte das Tumolvolumen und erhöhte die Wirksamkeit von Gemcitabin. In einem Bauchspeicheldrüsenkrebs-Gewebearray, war die Expression von miR30a-3p im Vergleich zu normalen Bauchspeicheldrüsen-Geweben erhöht und das umgekehrte Ergebnis wurde für die Cx43-Expression beobachtet. Diese Ergebnisse enthüllen den Mechanismus der Sulforaphan-induzierten Gap Junction-Kommunikation und der Gemcitabin-Zytotoxizität in Bauchspeicheldrüsenkrebs. Mit dem Ziel Sulforaphan-bezogene Medikamente für den Bauchspeicheldrüsenkrebs zu entwickeln, habe ich 7 einzigartige Sulforaphan-Derivate auf ihre Bioaktivität gegen den Bauchspeicheldrüsenkrebs und andere Tumorentitäten untersucht. MTT- und koloniebildende Assays, Apoptose Analyse mit Durchflusszytometrie, Immunhistochemie, MikroRNA-Array sowie Tumor Xenograft- und *C.elegans* Studien wurden mit diesen Analoga durchgeführt. Meine Ergebnisse deuten auf die Anti-Tumor-Aktivität von zwei der SF Derivate, SF102 und SF134, hin. SF102 war am effektivsten bei der Hemmung der Lebensfähigkeit, Klonogenität und des Tumorwachstums zusammen mit der Induktion der Apoptose, gefolgt von SF134, vor allem ohne offensichtliche Nebenwirkungen. MiRNA Array Profiling zeigte unterschiedlich

exprimierte Kandidaten zwischen Sulforaphan-Derivaten und ursprüngliches Sulforaphan. Meine Ergebnisse deuten darauf hin, dass die Sulforaphan-induzierte downregulation des miR30a-3p die Gap Junction-Kommunikation und die Gemcitabin-Wirksamkeit bei Bauchspeicheldrüsenkrebs verbessert. Sulforaphan-Derivate SF102 und SF134 unterdrücken nachweislich das Fortschreiten von Bauchspeicheldrüsenkrebs. Ich vermute, dass die Entwicklung neuer Sulforaphan- oder Sulforaphan-Analoga – Medikamente die neuen Therapiemöglichkeiten für Bauchspeicheldrüsenkrebs eröffnen wird.

## 10. References

- Aasen, T., Mesnil, M., Naus, C. C., Lampe, P. D. and Laird, D. W. (2016). **Gap junctions and cancer: communicating for 50 years**. *Nat Rev Cancer* 16, 775-788, doi: 10.1038/nrc.2016.105.
- Acunzo, M., Romano, G., Wernicke, D. and Croce, C. M. (2015). **MicroRNA and cancer--a brief overview**. *Adv Biol Regul* 57, 1-9, doi: 10.1016/j.jbior.2014.09.013.
- Agarwal, V., Bell, G. W., Nam, J. W. and Bartel, D. P. (2015). **Predicting effective microRNA target sites in mammalian mRNAs**. *Elife* 4, doi: 10.7554/eLife.05005.
- Akoglu, H. (2018). **User's guide to correlation coefficients**. *Turk J Emerg Med* 18, 91-93, doi: 10.1016/j.tjem.2018.08.001.
- Alberts, B. (2008). **Molecular biology of the cell, 5th edition**, Garland Science, New York.
- Aleksandrowicz, E. and Herr, I. (2015). **Ethical euthanasia and short-term anesthesia of the chick embryo**. *ALTEX* 32, 143-147, doi: 10.14573/altex.1410031.
- Alexandre, J., Hu, Y., Lu, W., Pelicano, H. and Huang, P. (2007). **Novel action of paclitaxel against cancer cells: bystander effect mediated by reactive oxygen species**. *Cancer Res* 67, 3512-3517, doi: 10.1158/0008-5472.CAN-06-3914.
- Alumkal, J. J., Slotke, R., Schwartzman, J., Cherala, G., Munar, M., Graff, J. N., Beer, T. M., Ryan, C. W., Koop, D. R., Gibbs, A., Gao, L., Flamiatos, J. F., Tucker, E., Kleinschmidt, R. and Mori, M. (2015). **A phase II study of sulforaphane-rich broccoli sprout extracts in men with recurrent prostate cancer**. *Invest New Drugs* 33, 480-489, doi: 10.1007/s10637-014-0189-z.
- Appari, M., Babu, K. R., Kaczorowski, A., Gross, W. and Herr, I. (2014). **Sulforaphane, quercetin and catechins complement each other in elimination of advanced pancreatic cancer by miR-let-7 induction and K-ras inhibition**. *Int J Oncol* 45, 1391-1400, doi: 10.3892/ijo.2014.2539.
- Atwell, L. L., Hsu, A., Wong, C. P., Stevens, J. F., Bella, D., Yu, T. W., Pereira, C. B., Lohr, C. V., Christensen, J. M., Dashwood, R. H., Williams, D. E., Shannon, J. and Ho, E. (2015). **Absorption and chemopreventive targets of sulforaphane in humans following consumption of broccoli sprouts or a myrosinase-treated broccoli sprout extract**. *Mol Nutr Food Res* 59, 424-433, doi: 10.1002/mnfr.201400674.

- Axelsen, L. N., Calloe, K., Holstein-Rathlou, N. H. and Nielsen, M. S. (2013). **Managing the complexity of communication: regulation of gap junctions by post-translational modification.** *Front Pharmacol* 4, 130, doi: 10.3389/fphar.2013.00130.
- Banerjee, D. (2016). **Connexin's Connection in Breast Cancer Growth and Progression.** *Int J Cell Biol* 2016, 9025905, doi: 10.1155/2016/9025905.
- Bartel, D. P. (2009). **MicroRNAs: target recognition and regulatory functions.** *Cell* 136, 215-233, doi: 10.1016/j.cell.2009.01.002.
- Bauer, N., Liu, L., Aleksandrowicz, E. and Herr, I. (2014). **Establishment of hypoxia induction in an in vivo animal replacement model for experimental evaluation of pancreatic cancer.** *Oncol Rep* 32, 153-158, doi: 10.3892/or.2014.3196.
- Bayat Mokhtari, R., Baluch, N., Homayouni, T. S., Morgatskaya, E., Kumar, S., Kazemi, P. and Yeger, H. (2018). **The role of Sulforaphane in cancer chemoprevention and health benefits: a mini-review.** *J Cell Commun Signal* 12, 91-101, doi: 10.1007/s12079-017-0401-y.
- Benko, G., Spajic, B., Demirovic, A., Stimac, G., Kru Sbreve Lin, B. and Tomas, D. (2011). **Prognostic value of connexin43 expression in patients with clinically localized prostate cancer.** *Prostate Cancer Prostatic Dis* 14, 90-95, doi: 10.1038/pcan.2010.51.
- Binenbaum, Y., Na'ara, S. and Gil, Z. (2015). **Gemcitabine resistance in pancreatic ductal adenocarcinoma.** *Drug Resist Updat* 23, 55-68, doi: 10.1016/j.drug.2015.10.002.
- Bray, F., Ferlay, J., Soerjomataram, I., Siegel, R. L., Torre, L. A. and Jemal, A. (2018). **Global cancer statistics 2018: GLOBOCAN estimates of incidence and mortality worldwide for 36 cancers in 185 countries.** *CA Cancer J Clin* 68, 394-424, doi: 10.3322/caac.21492.
- Burris, H. A., 3rd, Moore, M. J., Andersen, J., Green, M. R., Rothenberg, M. L., Modiano, M. R., Cripps, M. C., Portenoy, R. K., Storniolo, A. M., Tarassoff, P., Nelson, R., Dorr, F. A., Stephens, C. D. and Von Hoff, D. D. (1997). **Improvements in survival and clinical benefit with gemcitabine as first-line therapy for patients with advanced pancreas cancer: a randomized trial.** *J Clin Oncol* 15, 2403-2413, doi: 10.1200/JCO.1997.15.6.2403.
- Calin, G. A., Dumitru, C. D., Shimizu, M., Bichi, R., Zupo, S., Noch, E., Aldler, H., Rattan, S., Keating, M., Rai, K., Rassenti, L., Kipps, T., Negrini, M., Bullrich, F. and Croce, C. M. (2002). **Frequent deletions and down-regulation of micro- RNA genes miR15 and miR16 at 13q14 in chronic lymphocytic leukemia.** *Proc Natl Acad Sci U S A* 99, 15524-15529, doi: 10.1073/pnas.242606799.

- Chan, J. A., Krichevsky, A. M. and Kosik, K. S. (2005). **MicroRNA-21 is an antiapoptotic factor in human glioblastoma cells**. *Cancer Res* 65, 6029-6033, doi: 10.1158/0008-5472.CAN-05-0137.
- Cimmino, A., Calin, G. A., Fabbri, M., Iorio, M. V., Ferracin, M., Shimizu, M., Wojcik, S. E., Aqeilan, R. I., Zupo, S., Dono, M., Rassenti, L., Alder, H., Volinia, S., Liu, C. G., Kipps, T. J., Negrini, M. and Croce, C. M. (2005). **miR-15 and miR-16 induce apoptosis by targeting BCL2**. *Proc Natl Acad Sci U S A* 102, 13944-13949, doi: 10.1073/pnas.0506654102.
- ClinicalTrials.gov (2018). **Study to Evaluate the Effect of Sulforaphane in Broccoli Sprout Extract on Breast Tissue**. URL: <https://clinicaltrials.gov/ct2/show/study/NCT00982319?cond=sulforaphane&draw=4&rank=29> [as of].
- Cottin, S., Ghani, K., de Campos-Lima, P. O. and Caruso, M. (2010). **Gemcitabine intercellular diffusion mediated by gap junctions: new implications for cancer therapy**. *Mol Cancer* 9, 141, doi: 10.1186/1476-4598-9-141.
- Cunningham, D., Chau, I., Stocken, D. D., Valle, J. W., Smith, D., Steward, W., Harper, P. G., Dunn, J., Tudur-Smith, C., West, J., Falk, S., Crellin, A., Adab, F., Thompson, J., Leonard, P., Ostrowski, J., Eatock, M., Scheithauer, W., Herrmann, R. and Neoptolemos, J. P. (2009). **Phase III randomized comparison of gemcitabine versus gemcitabine plus capecitabine in patients with advanced pancreatic cancer**. *J Clin Oncol* 27, 5513-5518, doi: 10.1200/JCO.2009.24.2446.
- Czyz, J., Irmer, U., Schulz, G., Mindermann, A. and Hulser, D. F. (2000). **Gap-junctional coupling measured by flow cytometry**. *Exp Cell Res* 255, 40-46, doi: 10.1006/excr.1999.4760.
- de Melo, F. H. M., Oliveira, J. S., Sartorelli, V. O. B. and Montor, W. R. (2018). **Cancer Chemoprevention: Classic and Epigenetic Mechanisms Inhibiting Tumorigenesis. What Have We Learned So Far?** *Front Oncol* 8, 644, doi: 10.3389/fonc.2018.00644.
- Ding, Y. and Nguyen, T. A. (2012). **Gap Junction Enhancer Potentiates Cytotoxicity of Cisplatin in Breast Cancer Cells**. *J Cancer Sci Ther* 4, 371-378, doi: 10.4172/1948-5956.1000170.
- Dovmark, T. H., Saccomano, M., Hulikova, A., Alves, F. and Swietach, P. (2017). **Connexin-43 channels are a pathway for discharging lactate from glycolytic pancreatic ductal adenocarcinoma cells**. *Oncogene* 36, 4538-4550, doi: 10.1038/onc.2017.71.
- Evans, W. H. and Martin, P. E. (2002). **Gap junctions: structure and function (Review)**. *Mol Membr Biol* 19, 121-136, doi: 10.1080/09687680210139839.

- Fahey, J. W., Zhang, Y. and Talalay, P. (1997). **Broccoli sprouts: an exceptionally rich source of inducers of enzymes that protect against chemical carcinogens**. *Proc Natl Acad Sci U S A* 94, 10367-10372, doi: 10.1073/pnas.94.19.10367.
- Fan, P., Liu, L., Yin, Y., Zhao, Z., Zhang, Y., Amponsah, P. S., Xiao, X., Bauer, N., Abukiwan, A., Nwaeburu, C. C., Gladkich, J., Gao, C., Schemmer, P., Gross, W. and Herr, I. (2016). **MicroRNA-101-3p reverses gemcitabine resistance by inhibition of ribonucleotide reductase M1 in pancreatic cancer**. *Cancer Lett* 373, 130-137, doi: 10.1016/j.canlet.2016.01.038.
- Fonseca, P. C., Nihei, O. K., Savino, W., Spray, D. C. and Alves, L. A. (2006). **Flow cytometry analysis of gap junction-mediated cell-cell communication: advantages and pitfalls**. *Cytometry A* 69, 487-493, doi: 10.1002/cyto.a.20255.
- Forster, T., Rausch, V., Zhang, Y., Isayev, O., Heilmann, K., Schoensiegel, F., Liu, L., Nessling, M., Richter, K., Labsch, S., Nwaeburu, C. C., Mattern, J., Gladkich, J., Giese, N., Werner, J., Schemmer, P., Gross, W., Gebhard, M. M., Gerhauser, C., Schaefer, M. and Herr, I. (2014). **Sulforaphane counteracts aggressiveness of pancreatic cancer driven by dysregulated Cx43-mediated gap junctional intercellular communication**. *Oncotarget* 5, 1621-1634, doi: 10.18632/oncotarget.1764.
- Garcia-Rodriguez, L., Perez-Torras, S., Carrio, M., Cascante, A., Garcia-Ribas, I., Mazo, A. and Fillat, C. (2011). **Connexin-26 is a key factor mediating gemcitabine bystander effect**. *Mol Cancer Ther* 10, 505-517, doi: 10.1158/1535-7163.MCT-10-0693.
- Gesto, D. S., Cerqueira, N. M., Fernandes, P. A. and Ramos, M. J. (2012). **Gemcitabine: a critical nucleoside for cancer therapy**. *Curr Med Chem* 19, 1076-1087, doi: 10.2174/092986712799320682.
- Gillen, S., Schuster, T., Meyer Zum Buschenfelde, C., Friess, H. and Kleeff, J. (2010). **Preoperative/neoadjuvant therapy in pancreatic cancer: a systematic review and meta-analysis of response and resection percentages**. *PLoS Med* 7, e1000267, doi: 10.1371/journal.pmed.1000267.
- Gregory, R. I., Chendrimada, T. P., Cooch, N. and Shiekhattar, R. (2005). **Human RISC couples microRNA biogenesis and posttranscriptional gene silencing**. *Cell* 123, 631-640, doi: 10.1016/j.cell.2005.10.022.
- Herr, I. and Buchler, M. W. (2010). **Dietary constituents of broccoli and other cruciferous vegetables: implications for prevention and**

- therapy of cancer.** *Cancer Treat Rev* 36, 377-383, doi: 10.1016/j.ctrv.2010.01.002.
- Herr, I., Lozanovski, V., Houben, P., Schemmer, P. and Buchler, M. W. (2013). **Sulforaphane and related mustard oils in focus of cancer prevention and therapy.** *Wien Med Wochenschr* 163, 80-88, doi: 10.1007/s10354-012-0163-3.
- Hidalgo, M. (2010). **Pancreatic cancer.** *N Engl J Med* 362, 1605-1617, doi: 10.1056/NEJMra0901557.
- Hitomi, M., Deleyrolle, L. P., Mulkearns-Hubert, E. E., Jarrar, A., Li, M., Sinyuk, M., Otvos, B., Brunet, S., Flavahan, W. A., Hubert, C. G., Goan, W., Hale, J. S., Alvarado, A. G., Zhang, A., Rohaus, M., Oli, M., Vedam-Mai, V., Fortin, J. M., Futch, H. S., Griffith, B., Wu, Q., Xia, C. H., Gong, X., Ahluwalia, M. S., Rich, J. N., Reynolds, B. A. and Lathia, J. D. (2015). **Differential connexin function enhances self-renewal in glioblastoma.** *Cell Rep* 11, 1031-1042, doi: 10.1016/j.celrep.2015.04.021.
- Hruban, R. H., Adsay, N. V., Albores-Saavedra, J., Compton, C., Garrett, E. S., Goodman, S. N., Kern, S. E., Klimstra, D. S., Kloppel, G., Longnecker, D. S., Luttges, J. and Offerhaus, G. J. (2001). **Pancreatic intraepithelial neoplasia: a new nomenclature and classification system for pancreatic duct lesions.** *Am J Surg Pathol* 25, 579-586, doi: 10.1097/00000478-200105000-00003.
- Hu, K., Qi, Y. J., Zhao, J., Jiang, H. F., Chen, X. and Ren, J. (2013). **Synthesis and biological evaluation of sulforaphane derivatives as potential antitumor agents.** *Eur J Med Chem* 64, 529-539, doi: 10.1016/j.ejmech.2013.03.045.
- Iacobuzio-Donahue, C. A., Velculescu, V. E., Wolfgang, C. L. and Hruban, R. H. (2012). **Genetic basis of pancreas cancer development and progression: insights from whole-exome and whole-genome sequencing.** *Clin Cancer Res* 18, 4257-4265, doi: 10.1158/1078-0432.CCR-12-0315.
- ISRCTNregistry (2014). **Espac-5f: European study group for pancreatic cancer - trial 5f.** URL: <http://www.isrctn.com/ISRCTN89500674> [as of].
- Johnson, R. G. and Sheridan, J. D. (1971). **Junctions between cancer cells in culture: ultrastructure and permeability.** *Science* 174, 717-719, doi: 10.1126/science.174.4010.717.
- Jones, S., Zhang, X., Parsons, D. W., Lin, J. C., Leary, R. J., Angenendt, P., Mankoo, P., Carter, H., Kamiyama, H., Jimeno, A., Hong, S. M., Fu, B., Lin, M. T., Calhoun, E. S., Kamiyama, M., Walter, K., Nikolskaya, T., Nikolsky, Y., Hartigan, J., Smith, D. R., Hidalgo, M., Leach, S. D., Klein, A. P., Jaffee, E. M., Goggins, M., Maitra, A., Iacobuzio-Donahue, C.,

- Eshleman, J. R., Kern, S. E., Hruban, R. H., Karchin, R., Papadopoulos, N., Parmigiani, G., Vogelstein, B., Velculescu, V. E. and Kinzler, K. W. (2008). **Core signaling pathways in human pancreatic cancers revealed by global genomic analyses**. *Science* 321, 1801-1806, doi: 10.1126/science.1164368.
- Jost, P. J. and Ruland, J. (2007). **Aberrant NF-kappaB signaling in lymphoma: mechanisms, consequences, and therapeutic implications**. *Blood* 109, 2700-2707, doi: 10.1182/blood-2006-07-025809.
- Kallifatidis, G., Labsch, S., Rausch, V., Mattern, J., Gladkich, J., Moldenhauer, G., Buchler, M. W., Salnikov, A. V. and Herr, I. (2011). **Sulforaphane increases drug-mediated cytotoxicity toward cancer stem-like cells of pancreas and prostate**. *Mol Ther* 19, 188-195, doi: 10.1038/mt.2010.216.
- Kallifatidis, G., Rausch, V., Baumann, B., Apel, A., Beckermann, B. M., Groth, A., Mattern, J., Li, Z., Kolb, A., Moldenhauer, G., Altevogt, P., Wirth, T., Werner, J., Schemmer, P., Buchler, M. W., Salnikov, A. V. and Herr, I. (2009). **Sulforaphane targets pancreatic tumour-initiating cells by NF-kappaB-induced antiapoptotic signalling**. *Gut* 58, 949-963, doi: 10.1136/gut.2008.149039.
- Kandouz, M. and Batist, G. (2010). **Gap junctions and connexins as therapeutic targets in cancer**. *Expert Opin Ther Targets* 14, 681-692, doi: 10.1517/14728222.2010.487866.
- Kaymaz, B. T., Gunel, N. S., Ceyhan, M., Cetintas, V. B., Ozel, B., Yandim, M. K., Kipcak, S., Aktan, C., Gokbulut, A. A., Baran, Y. and Can, B. K. (2015). **Revealing genome-wide mRNA and microRNA expression patterns in leukemic cells highlighted "hsa-miR-2278" as a tumor suppressor for regain of chemotherapeutic imatinib response due to targeting STAT5A**. *Tumour Biol* 36, 7915-7927, doi: 10.1007/s13277-015-3509-9.
- Khorana, A. A., Mangu, P. B., Berlin, J., Engebretson, A., Hong, T. S., Maitra, A., Mohile, S. G., Mumber, M., Schulick, R., Shapiro, M., Urba, S., Zeh, H. J. and Katz, M. H. G. (2017). **Potentially Curable Pancreatic Cancer: American Society of Clinical Oncology Clinical Practice Guideline Update**. *J Clin Oncol* 35, 2324-2328, doi: 10.1200/JCO.2017.72.4948.
- Kielbasinski, P., Luczak, J., Cierpial, T., Blaszczyk, J., Sieron, L., Wiktorska, K., Lubelska, K., Milczarek, M. and Chilmonczyk, Z. (2014). **New enantiomeric fluorine-containing derivatives of sulforaphane: synthesis, absolute configurations and biological activity**. *Eur J Med Chem* 76, 332-342, doi: 10.1016/j.ejmech.2014.02.036.



- Kim, M. K. and Park, J. H. (2009). **Conference on "Multidisciplinary approaches to nutritional problems". Symposium on "Nutrition and health". Cruciferous vegetable intake and the risk of human cancer: epidemiological evidence.** Proc Nutr Soc 68, 103-110, doi: 10.1017/S0029665108008884.
- Kim, Y. J., Hwang, K. C., Kim, S. W. and Lee, Y. C. (2018). **Potential miRNA-target interactions for the screening of gastric carcinoma development in gastric adenoma/dysplasia.** Int J Med Sci 15, 610-616, doi: 10.7150/ijms.24061.
- Kleeff, J., Korc, M., Apte, M., La Vecchia, C., Johnson, C. D., Biankin, A. V., Neale, R. E., Tempero, M., Tuveson, D. A., Hruban, R. H. and Neoptolemos, J. P. (2016). **Pancreatic cancer.** Nat Rev Dis Primers 2, 16022, doi: 10.1038/nrdp.2016.22.
- Kong, Y. W., Ferland-McCollough, D., Jackson, T. J. and Bushell, M. (2012). **microRNAs in cancer management.** Lancet Oncol 13, e249-258, doi: 10.1016/S1470-2045(12)70073-6.
- Kozomara, A., Birgaoanu, M. and Griffiths-Jones, S. (2019). **miRBase: from microRNA sequences to function.** Nucleic Acids Res 47, D155-D162, doi: 10.1093/nar/gky1141.
- Kurihara-Shimomura, M., Sasahira, T., Shimomura, H., Nakashima, C. and Kirita, T. (2019). **The Oncogenic Activity of miR-29b-1-5p Induces the Epithelial-Mesenchymal Transition in Oral Squamous Cell Carcinoma.** J Clin Med 8, doi: 10.3390/jcm8020273.
- Kyriakakis, E., Markaki, M. and Tavernarakis, N. (2015). **Caenorhabditis elegans as a model for cancer research.** Mol Cell Oncol 2, e975027, doi: 10.4161/23723556.2014.975027.
- Laird, D. W. (2006). **Life cycle of connexins in health and disease.** Biochem J 394, 527-543, doi: 10.1042/BJ20051922.
- Laird, D. W. and Lampe, P. D. (2018a). **Therapeutic strategies targeting connexins.** Nat Rev Drug Discov 17, 905-921, doi: 10.1038/nrd.2018.138.
- Laird, D. W. and Lampe, P. D. (2018b). **Therapeutic strategies targeting connexins.** Nat Rev Drug Discov, doi: 10.1038/nrd.2018.138.
- Lampe, P. D. and Lau, A. F. (2004). **The effects of connexin phosphorylation on gap junctional communication.** Int J Biochem Cell Biol 36, 1171-1186, doi: 10.1016/S1357-2725(03)00264-4.
- Lee, R. C., Feinbaum, R. L. and Ambros, V. (1993). **The C. elegans heterochronic gene lin-4 encodes small RNAs with antisense**

**complementarity to lin-14.** *Cell* 75, 843-854, doi: 10.1016/0092-8674(93)90529-y.

Lee, Y., Ahn, C., Han, J., Choi, H., Kim, J., Yim, J., Lee, J., Provost, P., Radmark, O., Kim, S. and Kim, V. N. (2003). **The nuclear RNase III Drosha initiates microRNA processing.** *Nature* 425, 415-419, doi: 10.1038/nature01957.

Lee, Y., Kim, M., Han, J., Yeom, K. H., Lee, S., Baek, S. H. and Kim, V. N. (2004). **MicroRNA genes are transcribed by RNA polymerase II.** *EMBO J* 23, 4051-4060, doi: 10.1038/sj.emboj.7600385.

Liang, C., Shi, S., Meng, Q., Liang, D., Ji, S., Zhang, B., Qin, Y., Xu, J., Ni, Q. and Yu, X. (2017). **Complex roles of the stroma in the intrinsic resistance to gemcitabine in pancreatic cancer: where we are and where we are going.** *Exp Mol Med* 49, e406, doi: 10.1038/emm.2017.255.

Liang, Q. L., Wang, B. R., Chen, G. Q., Li, G. H. and Xu, Y. Y. (2010). **Clinical significance of vascular endothelial growth factor and connexin43 for predicting pancreatic cancer clinicopathologic parameters.** *Med Oncol* 27, 1164-1170, doi: 10.1007/s12032-009-9354-1.

Loewenstein, W. R. and Kanno, Y. (1966). **Intercellular communication and the control of tissue growth: lack of communication between cancer cells.** *Nature* 209, 1248-1249, doi: 10.1038/2091248a0.

Longo, D. L. (2012). **Harrison's principles of internal medicine**, McGraw-Hill, New York.

Lozanovski, V. J., Polychronidis, G., Gross, W., Gharabaghi, N., Mehrabi, A., Hackert, T., Schemmer, P. and Herr, I. (2019). **Broccoli sprout supplementation in patients with advanced pancreatic cancer is difficult despite positive effects-results from the POWDER pilot study.** *Invest New Drugs*, doi: 10.1007/s10637-019-00826-z.

Lubecka-Pietruszewska, K., Kaufman-Szymczyk, A., Stefanska, B., Cebula-Obrzut, B., Smolewski, P. and Fabianowska-Majewska, K. (2015). **Sulforaphane Alone and in Combination with Clofarabine Epigenetically Regulates the Expression of DNA Methylation-Silenced Tumour Suppressor Genes in Human Breast Cancer Cells.** *J Nutrigenet Nutrigenomics* 8, 91-101, doi: 10.1159/000439111.

Ludwig, N., Leidinger, P., Becker, K., Backes, C., Fehlmann, T., Pallasch, C., Rheinheimer, S., Meder, B., Stahler, C., Meese, E. and Keller, A. (2016). **Distribution of miRNA expression across human tissues.** *Nucleic Acids Res* 44, 3865-3877, doi: 10.1093/nar/gkw116.

- McNutt, N. S. and Weinstein, R. S. (1969). **Carcinoma of the cervix: deficiency of nexus intercellular junctions**. *Science* 165, 597-599, doi: 10.1126/science.165.3893.597.
- Mese, G., Richard, G. and White, T. W. (2007). **Gap junctions: basic structure and function**. *J Invest Dermatol* 127, 2516-2524, doi: 10.1038/sj.jid.5700770.
- Mohammed, S., Van Buren, G., 2nd and Fisher, W. E. (2014). **Pancreatic cancer: advances in treatment**. *World J Gastroenterol* 20, 9354-9360, doi: 10.3748/wjg.v20.i28.9354.
- Musil, L. S. and Goodenough, D. A. (1993). **Multisubunit assembly of an integral plasma membrane channel protein, gap junction connexin43, occurs after exit from the ER**. *Cell* 74, 1065-1077, doi: 10.1016/0092-8674(93)90728-9.
- Naus, C. C. and Laird, D. W. (2010). **Implications and challenges of connexin connections to cancer**. *Nat Rev Cancer* 10, 435-441, doi: 10.1038/nrc2841.
- Neoptolemos, J. P., Kleeff, J., Michl, P., Costello, E., Greenhalf, W. and Palmer, D. H. (2018). **Therapeutic developments in pancreatic cancer: current and future perspectives**. *Nat Rev Gastroenterol Hepatol* 15, 333-348, doi: 10.1038/s41575-018-0005-x.
- Neoptolemos, J. P., Palmer, D. H., Ghaneh, P., Psarelli, E. E., Valle, J. W., Halloran, C. M., Faluyi, O., O'Reilly, D. A., Cunningham, D., Wadsley, J., Darby, S., Meyer, T., Gillmore, R., Anthoney, A., Lind, P., Glimelius, B., Falk, S., Izbicki, J. R., Middleton, G. W., Cummins, S., Ross, P. J., Wasan, H., McDonald, A., Crosby, T., Ma, Y. T., Patel, K., Sherriff, D., Soomal, R., Borg, D., Sothi, S., Hammel, P., Hackert, T., Jackson, R., Buchler, M. W. and European Study Group for Pancreatic, C. (2017). **Comparison of adjuvant gemcitabine and capecitabine with gemcitabine monotherapy in patients with resected pancreatic cancer (ESPAC-4): a multicentre, open-label, randomised, phase 3 trial**. *Lancet* 389, 1011-1024, doi: 10.1016/S0140-6736(16)32409-6.
- Network, P. C. A. (2019). **Chemotherapy**. URL: <https://www.pancan.org/facing-pancreatic-cancer/treatment/treatment-types/chemotherapy/> [as of].
- Nielsen, M. S., Axelsen, L. N., Sorgen, P. L., Verma, V., Delmar, M. and Holstein-Rathlou, N. H. (2012). **Gap junctions**. *Compr Physiol* 2, 1981-2035, doi: 10.1002/cphy.c110051.
- Pitts, J. D. (1994). **Cancer gene therapy: a bystander effect using the gap junctional pathway**. *Mol Carcinog* 11, 127-130.

- Rausch, V., Liu, L., Kallifatidis, G., Baumann, B., Mattern, J., Gladkich, J., Wirth, T., Schemmer, P., Buchler, M. W., Zoller, M., Salnikow, A. V. and Herr, I. (2010). **Synergistic activity of sorafenib and sulforaphane abolishes pancreatic cancer stem cell characteristics**. *Cancer Res* 70, 5004-5013, doi: 0008-5472.CAN-10-0066 [pii]  
10.1158/0008-5472.CAN-10-0066.
- Reinhart, B. J., Slack, F. J., Basson, M., Pasquinelli, A. E., Bettinger, J. C., Rougvie, A. E., Horvitz, H. R. and Ruvkun, G. (2000). **The 21-nucleotide let-7 RNA regulates developmental timing in *Caenorhabditis elegans***. *Nature* 403, 901-906, doi: 10.1038/35002607.
- Ribatti, D. (2017). **The chick embryo chorioallantoic membrane (CAM) assay**. *Reprod Toxicol* 70, 97-101, doi: 10.1016/j.reprotox.2016.11.004.
- Ryan, D. P., Hong, T. S. and Bardeesy, N. (2014). **Pancreatic adenocarcinoma**. *N Engl J Med* 371, 2140-2141, doi: 10.1056/NEJMc1412266.
- Shaib, Y., Davila, J., Naumann, C. and El-Serag, H. (2007). **The impact of curative intent surgery on the survival of pancreatic cancer patients: a U.S. Population-based study**. *Am J Gastroenterol* 102, 1377-1382, doi: 10.1111/j.1572-0241.2007.01202.x.
- Shi, Y. H., Dai, D. F., Li, J., Dong, Y. W., Jiang, Y., Li, H. G., Gao, Y., Chong, C. K., Li, H. Y., Chu, X. Q., Yang, C., Zhang, Q., Tong, Z. S., Bai, C. G. and Chen, Y. (2016). **Sulforaphane Analogues with Heterocyclic Moieties: Syntheses and Inhibitory Activities against Cancer Cell Lines**. *Molecules* 21, 514, doi: 10.3390/molecules21040514.
- Siegel, R. L., Miller, K. D. and Jemal, A. (2019). **Cancer statistics, 2019**. *CA Cancer J Clin* 69, 7-34, doi: 10.3322/caac.21551.
- Singh, A. V., Xiao, D., Lew, K. L., Dhir, R. and Singh, S. V. (2004). **Sulforaphane induces caspase-mediated apoptosis in cultured PC-3 human prostate cancer cells and retards growth of PC-3 xenografts in vivo**. *Carcinogenesis* 25, 83-90, doi: 10.1093/carcin/bgg178.
- Sirnes, S., Bruun, J., Kolberg, M., Kjenseth, A., Lind, G. E., Svindland, A., Brech, A., Nesbakken, A., Lothe, R. A., Leithe, E. and Rivedal, E. (2012). **Connexin43 acts as a colorectal cancer tumor suppressor and predicts disease outcome**. *Int J Cancer* 131, 570-581, doi: 10.1002/ijc.26392.
- Slotwinski, R., Lech, G. and Slotwinska, S. M. (2018). **MicroRNAs in pancreatic cancer diagnosis and therapy**. *Cent Eur J Immunol* 43, 314-324, doi: 10.5114/ceji.2018.80051.

- Sticht, C., De La Torre, C., Parveen, A. and Gretz, N. (2018). **miRWalk: An online resource for prediction of microRNA binding sites**. PLoS One 13, e0206239, doi: 10.1371/journal.pone.0206239.
- Stiernagle, T. (2006). **Maintenance of C. elegans**. WormBook, 1-11, doi: 10.1895/wormbook.1.101.1.
- Strobel, O., Neoptolemos, J., Jager, D. and Buchler, M. W. (2019). **Optimizing the outcomes of pancreatic cancer surgery**. Nat Rev Clin Oncol 16, 11-26, doi: 10.1038/s41571-018-0112-1.
- Subramanian, A., Tamayo, P., Mootha, V. K., Mukherjee, S., Ebert, B. L., Gillette, M. A., Paulovich, A., Pomeroy, S. L., Golub, T. R., Lander, E. S. and Mesirov, J. P. (2005). **Gene set enrichment analysis: a knowledge-based approach for interpreting genome-wide expression profiles**. Proc Natl Acad Sci U S A 102, 15545-15550, doi: 10.1073/pnas.0506580102.
- Sun, L., Chua, C. Y. X., Tian, W., Zhang, Z., Chiao, P. J. and Zhang, W. (2015). **MicroRNA Signaling Pathway Network in Pancreatic Ductal Adenocarcinoma**. J Genet Genomics 42, 563-577, doi: 10.1016/j.jgg.2015.07.003.
- Suppipat, K., Park, C. S., Shen, Y., Zhu, X. and Lacorazza, H. D. (2012). **Sulforaphane induces cell cycle arrest and apoptosis in acute lymphoblastic leukemia cells**. PLoS One 7, e51251, doi: 10.1371/journal.pone.0051251.
- Takamizawa, J., Konishi, H., Yanagisawa, K., Tomida, S., Osada, H., Endoh, H., Harano, T., Yatabe, Y., Nagino, M., Nimura, Y., Mitsudomi, T. and Takahashi, T. (2004). **Reduced expression of the let-7 microRNAs in human lung cancers in association with shortened postoperative survival**. Cancer Res 64, 3753-3756, doi: 10.1158/0008-5472.CAN-04-0637.
- Teleki, I., Szasz, A. M., Maros, M. E., Gyorffy, B., Kulka, J., Meggyeshazi, N., Kiszner, G., Balla, P., Samu, A. and Krenacs, T. (2014). **Correlations of differentially expressed gap junction connexins Cx26, Cx30, Cx32, Cx43 and Cx46 with breast cancer progression and prognosis**. PLoS One 9, e112541, doi: 10.1371/journal.pone.0112541.
- Tittarelli, A., Guerrero, I., Tempio, F., Gleisner, M. A., Avalos, I., Sabanegh, S., Ortiz, C., Michea, L., Lopez, M. N., Mendoza-Naranjo, A. and Salazar-Onfray, F. (2015). **Overexpression of connexin 43 reduces melanoma proliferative and metastatic capacity**. Br J Cancer 113, 259-267, doi: 10.1038/bjc.2015.162.
- Toler, C. R., Taylor, D. D. and Gercel-Taylor, C. (2006). **Loss of communication in ovarian cancer**. Am J Obstet Gynecol 194, e27-31, doi: 10.1016/j.ajog.2006.01.024.

- Tortorella, S. M., Royce, S. G., Licciardi, P. V. and Karagiannis, T. C. (2015). **Dietary Sulforaphane in Cancer Chemoprevention: The Role of Epigenetic Regulation and HDAC Inhibition**. *Antioxid Redox Signal* 22, 1382-1424, doi: 10.1089/ars.2014.6097.
- Vincent, A., Herman, J., Schulick, R., Hruban, R. H. and Goggins, M. (2011). **Pancreatic cancer**. *Lancet* 378, 607-620, doi: 10.1016/S0140-6736(10)62307-0.
- Wang, T., Larcher, L. M., Ma, L. and Veedu, R. N. (2018). **Systematic Screening of Commonly Used Commercial Transfection Reagents towards Efficient Transfection of Single-Stranded Oligonucleotides**. *Molecules* 23, doi: 10.3390/molecules23102564.
- Wang, W., Lin, H., Zhou, L., Zhu, Q., Gao, S., Xie, H., Liu, Z., Xu, Z., Wei, J., Huang, X. and Zheng, S. (2014). **MicroRNA-30a-3p inhibits tumor proliferation, invasiveness and metastasis and is downregulated in hepatocellular carcinoma**. *Eur J Surg Oncol* 40, 1586-1594, doi: 10.1016/j.ejso.2013.11.008.
- Watanabe, S., Ueda, Y., Akaboshi, S., Hino, Y., Sekita, Y. and Nakao, M. (2009). **HMG2 maintains oncogenic RAS-induced epithelial-mesenchymal transition in human pancreatic cancer cells**. *Am J Pathol* 174, 854-868, doi: 10.2353/ajpath.2009.080523.
- Winter, J., Jung, S., Keller, S., Gregory, R. I. and Diederichs, S. (2009). **Many roads to maturity: microRNA biogenesis pathways and their regulation**. *Nat Cell Biol* 11, 228-234, doi: 10.1038/ncb0309-228.
- Wolfgang, C. L., Herman, J. M., Laheru, D. A., Klein, A. P., Erdek, M. A., Fishman, E. K. and Hruban, R. H. (2013). **Recent progress in pancreatic cancer**. *CA Cancer J Clin* 63, 318-348, doi: 10.3322/caac.21190.
- Wong, C. P., Hsu, A., Buchanan, A., Palomera-Sanchez, Z., Beaver, L. M., Houseman, E. A., Williams, D. E., Dashwood, R. H. and Ho, E. (2014). **Effects of sulforaphane and 3,3'-diindolylmethane on genome-wide promoter methylation in normal prostate epithelial cells and prostate cancer cells**. *PLoS One* 9, e86787, doi: 10.1371/journal.pone.0086787.
- Yin, L., Xiao, X., Georgikou, C., Yin, Y., Liu, L., Karakhanova, S., Luo, Y., Gladkich, J., Fellenberg, J., Sticht, C., Gretz, N., Gross, W. and Herr, I. (2019). **MicroRNA-365a-3p inhibits c-Rel-mediated NF-kappaB signaling and the progression of pancreatic cancer**. *Cancer Lett* 452, 203-212, doi: 10.1016/j.canlet.2019.03.025.
- Yu, S., Lu, Z., Liu, C., Meng, Y., Ma, Y., Zhao, W., Liu, J., Yu, J. and Chen, J. (2010). **miRNA-96 suppresses KRAS and functions as a tumor**

**suppressor gene in pancreatic cancer.** *Cancer Res* 70, 6015-6025, doi: 10.1158/0008-5472.CAN-09-4531.

Zhang, Y., Li, M., Wang, H., Fisher, W. E., Lin, P. H., Yao, Q. and Chen, C. (2009). **Profiling of 95 microRNAs in pancreatic cancer cell lines and surgical specimens by real-time PCR analysis.** *World J Surg* 33, 698-709, doi: 10.1007/s00268-008-9833-0.

Zhang, Z., Li, C., Shang, L., Zhang, Y., Zou, R., Zhan, Y. and Bi, B. (2016). **Sulforaphane induces apoptosis and inhibits invasion in U251MG glioblastoma cells.** *Springerplus* 5, 235, doi: 10.1186/s40064-016-1910-5.

Zhao, Z., Bauer, N., Aleksandrowicz, E., Yin, L., Gladkich, J., Gross, W., Kaiser, J., Hackert, T., Strobel, O. and Herr, I. (2018). **Intraductal papillary mucinous neoplasm of the pancreas rapidly xenografts in chicken eggs and predicts aggressiveness.** *Int J Cancer* 142, 1440-1452, doi: 10.1002/ijc.31160.

## 11. Publications

- [1] Yin L, Xiao X, **Georgikou C**, Luo Y, Liu L, Gladkich J, Gross W, Herr I (2019) Sulforaphane induces miR135b-5p and its target gene RASAL2, thereby inhibiting the progression of pancreatic cancer. *Molecular Therapy Oncolytics*- 14:74-81. doi: 10.1016/j.omto.2019.03.011.
- [2] Yin L, Xiao X, **Georgikou C**, Yin Y, Liu L, Karakhanova S, Luo Y, Gladkich J, Fellenberg J, Sticht S, Gretz N, Gross W, Herr I (2019) MicroRNA-365a-3p inhibits c-Rel-mediated NF- $\kappa$ B signaling and the progression of pancreatic cancer. *Cancer Letters*. 452: 203-212. doi: 10.1016/j.canlet.2019.03.025.
- [3] **Georgikou C**, Yin L, Gladkich J, Xiao X, Sticht C, Torre C, Gretz N, Gross W, Schäfer M, Karakhanova S, Herr I (2020) Inhibition of miR30a-3p by sulforaphane enhances gap junction intercellular communication in pancreatic cancer. *Cancer Letters*. 469:238-245. doi: 10.1016/j.canlet.2019.10.042.
- [4] Xiao X, Sticht C, Yin L, Liu L, Karakhanova S, Yin Y, **Georgikou C**, Gladkich J, Gross W, Gretz N, Herr I (2020) Novel plant microRNAs from broccoletti sprouts do not show cross-kingdom regulation of pancreatic cancer. *Oncotarget*. 11(14):1203-1217. doi: 10.18632/oncotarget.27527.
- [5] **Georgikou C**, Buglioni L, Bremerich M, Roubicek N, Yin L, Gross W, Sticht C, Bolm C, Herr I (2020) Novel Broccoli Sulforaphane-based Derivatives Inhibit the Progression of Pancreatic Cancer Without Side Effects. *Biomolecules*. 10(5): E769. doi: 10.3390/biom10050769



## 12. Supplement

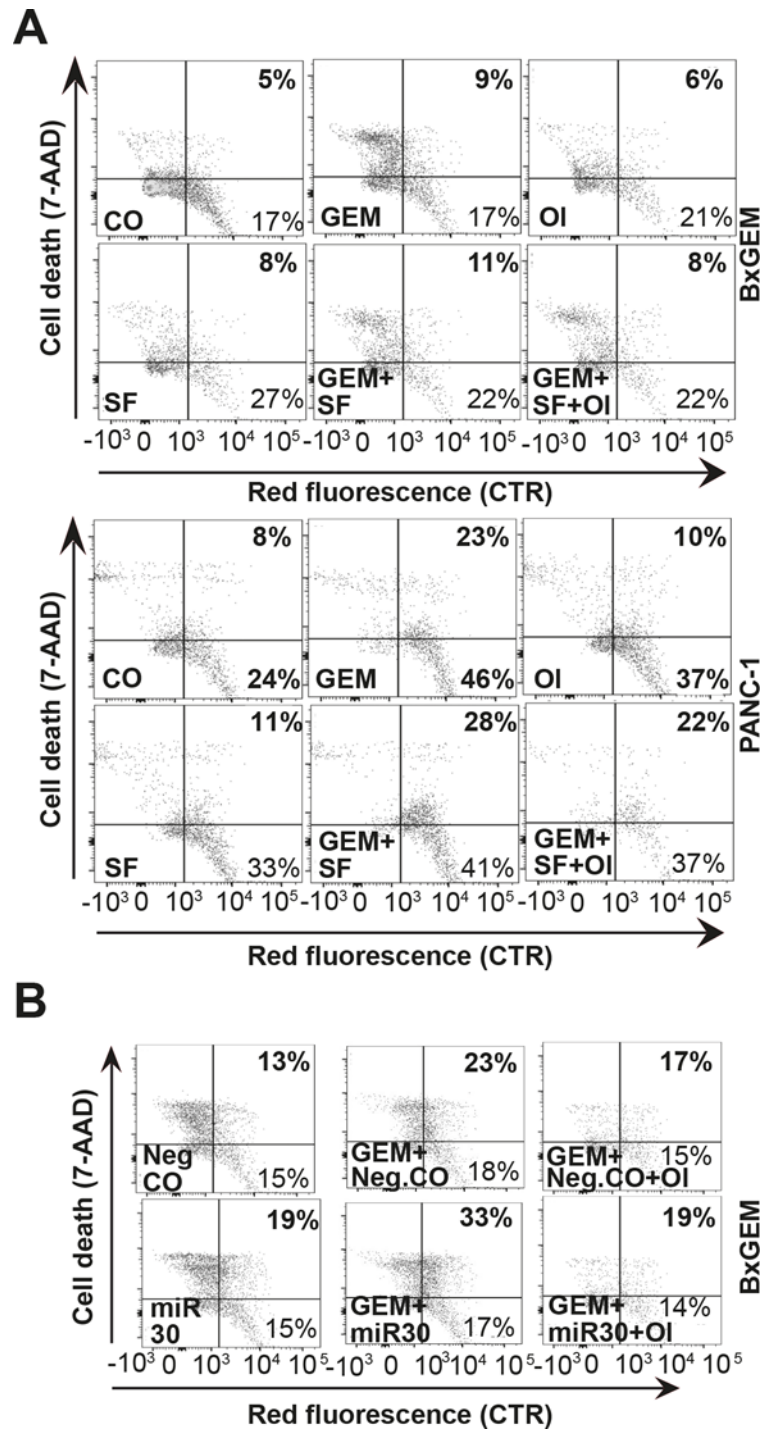


**Figure S1. Bystander effect, flow cytometry plots for PDA cells.** BxGEM and PANC-1 cells were treated as described in the methods paragraph and were co-incubated with the CTR-untreated cells. After 48h, the cells were stained with 7-AAD and then evaluated for cell death by flow cytometry. The percentage of double-positive cells (CTR<sup>+</sup>/7-AAD<sup>+</sup>) is an indicator of the bystander effect. The experiment was also conducted after transfection of the cells with negative control or miR30a-3p inhibitor.

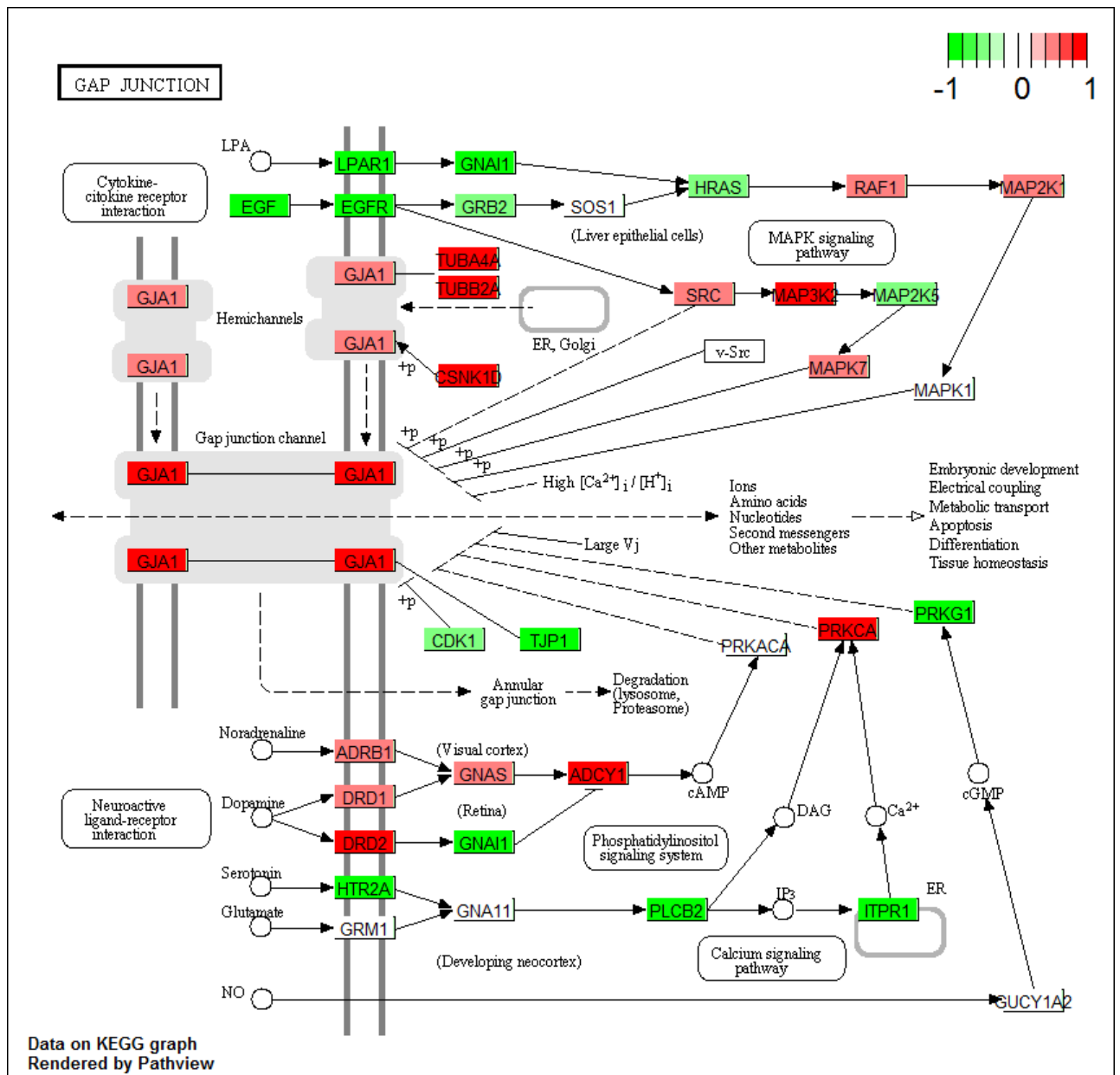


**Figure S2: Sulforaphane-regulated gap junction pathway map.** A map of the gap junction pathway from the KEGG pathway database, demonstrating the expression profile of GJA1 and other GJ genes. The red color marks upregulation, and the green color marks downregulation within a scale from 1 to -1, as indicated.

**PA961c**

**Pancreas cancer tissue array with normal pancreatic tissue, including TNM, clinical stage and pathology grade, 96 cases/96 cores, replacing PA961b**

<b>Microarray Panel:</b>	Pancreas adenocarcinoma tissue microarray with normal pancreatic tissue, containing 78 cases of pancreas adenocarcinoma, 1 each of undifferentiated carcinoma, pancreas mixed acinar-neuroendocrine carcinoma, squamous cell carcinoma, neuroendocrine carcinoma and acinic cell carcinoma, 3 each of pancreas adenosquamous carcinoma and carcinoid, 2 pancreas solid pseudo-papillary carcinoma, plus 5 normal pancreatic tissue, single core per case
<b>Cores:</b>	96
<b>Cases:</b>	96
<b>Layout:</b>	12 cols × 8 rows
<b>Core Diameter:</b>	1.5 mm
<b>Thickness:</b>	5 μm
<b>Quality Control:</b>	H&E and IHC confirmed
<b>Applications:</b>	Routine histology procedures including Immunohistochemistry (IHC) and In Situ Hybridization (ISH), protocols which can be found at our support page.
<b>Notes:</b>	<p>1. TMA slides were sectioned and stored at 4C, may not be fresh cut. Please request fresh cut if experiment involves phosphor-specific antibodies, FISH or ISH, etc., minimal 3 slides be purchased of each TMA applies to cover the cost of trimming for the fresh sectioning.</p> <p>2. Most of TMA slides were not coated with extra layer of paraffin (tissue cores can be easily seen on the glass), but it is still recommended 30 min. of baking at 60C before putting into xylene for de-paraffinization procedure.</p>

**Microarray Panel Display**

	1	2	3	4	5	6	7	8	9	10	11	12
A	Pan	Pan	Pan	Pan	Pan	Pan	Pan	Pan	Pan	Pan	Pan	Pan
B	Pan	Pan	Pan	Pan	Pan	Pan	Pan	Pan	Pan	Pan	Pan	Pan
C	Pan	Pan	Pan	Pan	Pan	Pan	Pan	Pan	Pan	Pan	Pan	Pan
D	Pan	Pan	Pan	Pan	Pan	Pan	Pan	Pan	Pan	Pan	Pan	Pan
E	Pan	Pan	Pan	Pan	Pan	Pan	Pan	Pan	Pan	Pan	Pan	Pan
F	Pan	Pan	Pan	Pan	Pan	Pan	Pan	Pan	Pan	Pan	Pan	Pan
G	Pan	Pan	Pan	Pan	Pan	Pan	Pan	Pan	Pan	Pan	Pan	Pan
H	Pan	Pan	Pan	Pan	Pan	Pan	Pan	Pan	Pan	Pan	Pan	Pan

**Legend:** Pan - Pancreas

- - Malignant tumor
- - Malignant tumor (stage I)
- - Malignant tumor (stage II)
- - Malignant tumor (stage III)
- - Malignant tumor (stage IV)
- - Normal tissue

**Specification Sheet**

Pos	No.	Sex	Age	Organ	Pathology diagnosis	Grade	Stage	TNM	Type †
A1	1	F	67	Pancreas	Duct adenocarcinoma	1	III	T3N1bM0	Malignant
A2	2	F	48	Pancreas	Duct adenocarcinoma	1	IIA	T3N0M0	Malignant
A3	3	F	47	Pancreas	Duct adenocarcinoma	1	IIA	T3N0M0	Malignant
A4	4	M	59	Pancreas	Duct adenocarcinoma	1	IIIB	T2N1M0	Malignant
A5	5	F	44	Pancreas	Adenocarcinoma (sparse)	–	IIIB	T3N1M0	Malignant
A6	6	M	34	Pancreas	Duct adenocarcinoma	1	IIA	T3N0M0	Malignant
A7	7	M	49	Pancreas	Duct adenocarcinoma	1	IB	T2N0M0	Malignant
A8	8	M	56	Pancreas	Duct adenocarcinoma	1	IB	T2N0M0	Malignant
A9	9	M	49	Pancreas	Duct adenocarcinoma	1	IB	T2N0M0	Malignant
A10	10	M	67	Pancreas	Duct adenocarcinoma	1	IB	T2N0M0	Malignant
A11	11	M	48	Pancreas	Duct adenocarcinoma	1	IB	T2N0M0	Malignant
A12	12	F	56	Pancreas	Duct adenocarcinoma	–	IB	T2N0M0	Malignant
B1	13	F	58	Pancreas	Duct adenocarcinoma	1	IIIB	T2N1M0	Malignant
B2	14	M	52	Pancreas	Duct adenocarcinoma	1	IIIB	T3N1M0	Malignant
B3	15	F	51	Pancreas	Duct adenocarcinoma	–	IIA	T3N0M0	Malignant
B4	16	M	55	Pancreas	Duct adenocarcinoma	1	IIA	T3N0M0	Malignant
B5	17	F	62	Pancreas	Duct adenocarcinoma with necrosis	2	III	T4N0M0	Malignant
B6	18	M	56	Pancreas	Duct adenocarcinoma	2	IB	T2N0M0	Malignant
B7	19	M	60	Pancreas	Duct adenocarcinoma	2	IA	T2N0M0	Malignant
B8	20	M	52	Pancreas	Duct adenocarcinoma	–	IIA	T3N0M0	Malignant
B9	21	M	42	Pancreas	Hyperplasia of duct epithelium	–	IB	T2N0M0	Malignant
B10	22	M	54	Pancreas	Duct adenocarcinoma	–	IIA	T3N0M0	Malignant
B11	23	F	51	Pancreas	Duct adenocarcinoma	1	IIA	T3N0M0	Malignant
B12	24	F	54	Pancreas	Duct adenocarcinoma	2	IB	T2N0M0	Malignant
C1	25	M	54	Pancreas	Duct adenocarcinoma	2	IIA	T3N0M0	Malignant
C2	26	M	39	Pancreas	Duct adenocarcinoma	2	IIA	T3N0M0	Malignant
C3	27	F	41	Pancreas	Duct adenocarcinoma	–	IIA	T3N0M0	Malignant
C4	28	F	68	Pancreas	Duct adenocarcinoma	2	IIA	T3N0M0	Malignant
C5	29	F	44	Pancreas	Duct adenocarcinoma	2	IIIB	T3N1M0	Malignant
C6	30	M	42	Pancreas	Duct adenocarcinoma	1	IIA	T3N0M0	Malignant
C7	31	M	53	Pancreas	Duct adenocarcinoma	2	IB	T2N0M0	Malignant
C8	32	M	51	Pancreas	Duct adenocarcinoma	1	IIA	T3N0M0	Malignant
C9	33	M	48	Pancreas	Duct adenocarcinoma	1	IIA	T3N0M0	Malignant
C10	34	M	57	Pancreas	Duct adenocarcinoma	–	IIA	T3N0M0	Malignant
C11	35	F	64	Pancreas	Duct adenocarcinoma	1	IIA	T3N0M0	Malignant
C12	36	M	49	Pancreas	Duct adenocarcinoma	2	IIA	T3N0M0	Malignant
D1	37	M	72	Pancreas	Duct adenocarcinoma	1	IIA	T3N0M0	Malignant
D2	38	F	72	Pancreas	Duct adenocarcinoma	2	IIA	T3N0M0	Malignant
D3	39	M	59	Pancreas	Duct adenocarcinoma	2	IIA	T3N0M0	Malignant
D4	40	F	45	Pancreas	Duct adenocarcinoma	2	III	T3N2M0	Malignant
D5	41	F	60	Pancreas	Duct adenocarcinoma	2	IV	T2N1M1	Malignant
D6	42	M	52	Pancreas	Chronic inflammation of pancreas tissue	–	IA	T1N0M0	Malignant
D7	43	F	44	Pancreas	Duct adenocarcinoma with necrosis	2	IB	T2N0M0	Malignant
D8	44	F	46	Pancreas	Duct adenocarcinoma	2	IB	T2N0M0	Malignant
D9	45	M	52	Pancreas	Duct adenocarcinoma	2	IB	T2N0M0	Malignant
D10	46	M	52	Pancreas	Duct adenocarcinoma	2	IB	T2N0M0	Malignant
D11	47	F	53	Pancreas	Duct adenocarcinoma	2	IIIB	T2N1M0	Malignant
D12	48	M	40	Pancreas	Duct adenocarcinoma	1	IIIB	T3N1bM0	Malignant
E1	49	M	57	Pancreas	Duct adenocarcinoma	1	IIA	T3N0M0	Malignant
E2	50	M	31	Pancreas	Duct adenocarcinoma	1	IIA	T3N0M0	Malignant
E3	51	M	44	Pancreas	Duct adenocarcinoma	2	IIA	T3N0M0	Malignant
E4	52	M	61	Pancreas	Adenocarcinoma	3	IV	T3N0M1	Malignant
E5	53	M	51	Pancreas	Duct adenocarcinoma	2	IIA	T3N0M0	Malignant
E6	54	M	59	Pancreas	Duct adenocarcinoma	2	IA	T1N0M0	Malignant
E7	55	M	44	Pancreas	Adenocarcinoma	3	IIA	T3N0M0	Malignant
E8	56	M	45	Pancreas	Adenocarcinoma	3	IIIB	T2N1M0	Malignant

Pos	No.	Sex	Age	Organ	Pathology diagnosis	Grade	Stage	TNM	Type †
E9	57	M	41	Pancreas	Duct adenocarcinoma	2	IB	T2N0M0	Malignant
E10	58	F	72	Pancreas	Duct adenocarcinoma	2	IIA	T3N0M0	Malignant
E11	59	F	51	Pancreas	Duct adenocarcinoma	–	IIA	T3N0M0	Malignant
E12	60	F	42	Pancreas	Duct adenocarcinoma	2	IB	T2N0M0	Malignant
F1	61	F	39	Pancreas	Duct adenocarcinoma	2	IIA	T3N0M0	Malignant
F2	62	F	51	Pancreas	Duct adenocarcinoma with necrosis	2	IIA	T3N0M0	Malignant
F3	63	M	62	Pancreas	Duct adenocarcinoma	1	IIA	T3N0M0	Malignant
F4	64	M	60	Pancreas	Duct adenocarcinoma	2	IB	T2N0M0	Malignant
F5	65	F	53	Pancreas	Duct adenocarcinoma	2	IIA	T3N0M0	Malignant
F6	66	M	77	Pancreas	Duct adenocarcinoma	2	IA	T1N0M0	Malignant
F7	67	M	47	Pancreas	Adenocarcinoma	3	IIA	T3N0M0	Malignant
F8	68	M	67	Pancreas	Adenocarcinoma	3	IIA	T3N0M0	Malignant
F9	69	M	78	Pancreas	Adenocarcinoma	3	IB	T2N0M0	Malignant
F10	70	M	62	Pancreas	Adenocarcinoma	3	IIA	T3N0M0	Malignant
F11	71	M	50	Pancreas	Adenocarcinoma	3	IB	T2N0M0	Malignant
F12	72	M	55	Pancreas	Adenocarcinoma	3	IIB	T3N1M0	Malignant
G1	73	F	48	Pancreas	Adenocarcinoma	3	IIA	T3N0M0	Malignant
G2	74	M	50	Pancreas	Adenocarcinoma	3	IIB	T3N1M0	Malignant
G3	75	F	53	Pancreas	Adenocarcinoma with necrosis	3	IB	T2N0M0	Malignant
G4	76	M	50	Pancreas	Adenocarcinoma	3	IB	T2N0M0	Malignant
G5	77	F	23	Pancreas	Adenocarcinoma	3	IB	T2N0M0	Malignant
G6	78	M	56	Pancreas	Adenocarcinoma	–	IIB	T2N1bM0	Malignant
G7	79	F	56	Pancreas	Undifferentiated carcinoma	–	IIA	T3N0M0	Malignant
G8	80	F	54	Pancreas	Mixed acinar-neuroendocrine carcinoma	–	IB	T2N0M0	Malignant
G9	81	M	52	Pancreas	Adenosquamous carcinoma	–	IIA	T3N0M0	Malignant
G10	82	F	49	Pancreas	Adenosquamous carcinoma	–	IIB	T3N1M0	Malignant
G11	83	M	50	Pancreas	Adenosquamous carcinoma	–	IIA	T3N0M0	Malignant
G12	84	M	62	Pancreas	Squamous cell carcinoma	2	IIA	T3N0M0	Malignant
H1	85	F	52	Pancreas	Carcinoid	–	IIA	T3N0M0	Malignant
H2	86	F	50	Pancreas	Carcinoid	–	IIA	T3N0M0	Malignant
H3	87	M	51	Pancreas	Atypical carcinoid	–	III	T4N0M0	Malignant
H4	88	M	42	Pancreas	Neuroendocrine carcinoma	–	IIA	T3N0M0	Malignant
H5	89	M	53	Pancreas	Acinic cell carcinoma	–	IB	T2N0M0	Malignant
H6	90	F	33	Pancreas	Solid pseudo-papillary carcinoma (chronic inflammation of pancreas tissue)	–	IIA	T3N0M0	Malignant
H7	91	M	42	Pancreas	Solid pseudo-papillary carcinoma	–	IB	T2N0M0	Malignant
H8	92	F	21	Pancreas	Pancreatic tissue	–	–	–	Normal
H9	93	M	47	Pancreas	Pancreatic tissue	–	–	–	Normal
H10	94	M	38	Pancreas	Pancreatic tissue	–	–	–	Normal
H11	95	M	40	Pancreas	Pancreatic tissue	–	–	–	Normal
H12	96	F	38	Pancreas	Pancreatic tissue	–	–	–	Normal
–	–	M	42	Adrenal gland	Pheochromocytoma (tissue marker)	–			Malignant

† For precise diagnosis, refer to pathology description.

\*\*The grade 1-3 (or I-III) in Pathology Diagnosis is equivalent to well-differentiated, moderately-differentiated or poorly differentiated, respectively, under microscope.

**Grade 1 or well-differentiated:** Cells appear normal and are not growing rapidly.

**Grade 2 or moderately-differentiated:** Cells appear slightly different than normal.

**Grade 3 or poorly differentiated:** Cells appear abnormal and tend to grow and spread more aggressively.

**Grade 4 or undifferentiated:** \*(for certain tumors), features are not significantly distinguishing to make it look any different from undifferentiated cancers which occur in other organs.

#### TNM grading:

##### T - Primary tumor

Tx - Primary tumor cannot be assessed

T0 - No evidence of primary tumor

Tis - Carcinoma in situ; intraepithelial or invasion of lamina propria

T1 - Tumor invades submucosa  
T2 - Tumor invades muscularis propria  
T3 - Tumor invades through muscularis propria into subserosa or into non-peritonealized pericolic or perirectal tissues.  
T4 - Tumor directly invades other organs or structures and/or perforate visceral peritoneum

**N - Regional lymph nodes**

Nx - Regional lymph nodes cannot be assessed  
N0 - No regional lymph node metastasis  
N1 - Metastasis in 1 to 3 regional lymph nodes  
N2 - Metastasis in 4 or more regional lymph nodes

**M - Distant metastasis**

Mx - Distant metastasis cannot be assessed  
M0 - No distant metastasis  
M1 - Distant metastasis

**Figure S3. Description of the pancreas tissue array.** For each patient tissue section, the TNM, clinical stage and pathology grade were provided. 96 cases/96 cores.

Table S1: List of the 36 most significantly SF-regulated miRNAs.

Transcript ID(Array Design)	Estimate of BxG SF vs BxG CO	-log <sub>10</sub> (p-Value) for Estimate of BxG SF vs BxG CO
hsa-miR-30a-3p	-0,515691759	2,307500498
hsa-miR-103a-3p	0,282360185	2,099375036
hsa-miR-192-5p	0,243035685	2,651196084
hsa-miR-196a-5p	-1,719896056	4,54498928
hsa-miR-10a-5p	-0,683088296	3,418595976
hsa-miR-205-3p	-1,302094185	2,372354101
hsa-miR-181a-3p	-1,814912926	2,789621402
hsa-miR-210-3p	-0,77576313	2,220046044
hsa-miR-221-3p	-0,247226296	2,317880426
hsa-miR-23b-5p	-1,223345481	3,364836848
hsa-miR-27b-5p	-1,481377278	6,677552014
hsa-miR-27b-3p	-0,655353333	3,723717471
hsa-miR-125b-5p	-0,352389259	2,79827584
hsa-miR-132-5p	-0,739552556	2,335439443
hsa-miR-135a-3p	1,50770742	3,433865762
hsa-miR-194-5p	0,21495963	3,884431449
hsa-miR-365a-3p	-0,778674946	2,370976267
hsa-miR-365b-3p	-0,779343781	2,369460275
hsa-miR-151a-5p	-0,136245556	2,313935953
hsa-miR-335-5p	-1,798210204	2,243135485
hsa-miR-431-5p	-0,432510994	2,867277056
hsa-miR-486-5p	-0,568198537	2,992447158
hsa-miR-486-3p	-1,021382648	2,450515817
hsa-miR-193b-5p	1,060048981	3,243830342
hsa-miR-499a-3p	-0,522496961	2,523593988
hsa-miR-508-5p	0,522536409	2,911859612
hsa-miR-568	-0,451092843	2,90932264
hsa-miR-574-5p	-0,974587463	2,799837442
hsa-miR-550a-5p	0,521688204	2,334550241
hsa-miR-605-3p	-0,427579811	3,111549879
hsa-miR-663a	0,547952	2,468853453
hsa-miR-1301-3p	0,942618352	2,482661487
hsa-miR-378d	-1,265947296	3,091790789
hsa-miR-675-5p	-1,639689111	4,213668454
hsa-miR-298	-0,840100639	3,036088093
hsa-miR-1469	0,618989611	3,272190322
hsa-miR-30a-5p	-0,223904815	1,701604939

Table S2. List of miRNA candidates shown in the heatmaps of Figure 27B.

Transcript ID(Array Design)	Fold change As SF vs As CO	-log <sub>10</sub> (p-Value) for Fold change As SF vs As CO
hsa-miR-92a-1-5p	-1,372521778	3,75505874
hsa-miR-139-5p	1,643831167	2,171386888
hsa-miR-181a-3p	-1,517916889	2,264995123
hsa-miR-23b-5p	-1,320086537	3,641174453
hsa-miR-27b-5p	-1,481057778	6,676530399
hsa-miR-200a-5p	-1,008850574	4,535356109
hsa-miR-933	1,004593711	2,82838023
hsa-miR-2278	-1,454670037	4,497590006
hsa-miR-3617-5p	1,375816648	4,164613745
hsa-miR-29b-1-5p	-0,836535981	5,822817777

Transcript ID(Array Design)	Fold change As 102 vs As CO	-log <sub>10</sub> (p-Value) for Fold change As 102 vs As CO
hsa-miR-222-5p	-1,619505926	2,46987786
hsa-miR-608	-0,813965009	2,51964538
hsa-miR-885-3p	-1,1512765	2,14622962
hsa-miR-2278	-1,953776504	5,779851604
hsa-mir-3130-1	0,544790541	2,550401342
hsa-miR-514b-5p	0,961224581	2,110771925
hsa-miR-4784	-0,617792344	4,283023847
hsa-miR-4701-3p	-1,645821574	2,327247792
hsa-miR-4740-5p	1,454254422	2,273906768
hsa-miR-6823-3p	0,841931665	2,209963967

Transcript ID(Array Design)	Fold change As 134 vs As CO	-log <sub>10</sub> (p-Value) for Fold change As 134 vs As CO
hsa-miR-509-5p	0,990048778	3,475932331
hsa-miR-550b-2-5p	0,984038667	3,368279238
hsa-miR-885-3p	-1,132580519	2,103883581
hsa-miR-2278	-1,576873574	4,835629473
hsa-miR-4444	1,660302852	2,810881792
hsa-miR-4517	1,279263833	2,004627051
hsa-miR-4640-5p	-1,574678796	2,376120891
hsa-miR-4776-5p	1,217612185	2,226594385
hsa-miR-6729-3p	1,002040461	2,669521405
hsa-miR-525-5p	0,557206904	3,909007438



**Table S3. List of the differently expressed miRNAs for Venn diagram of Figure 27D.**

<b>Transcript ID</b>	<b>SF-CO</b>	<b>SF102-SF</b>	<b>SF134-SF</b>
hsa-miR-22-3p	1	0	0
hsa-miR-25-5p	0	1	1
hsa-miR-92a-1-5p	1	0	0
hsa-miR-29b-1-5p	1	1	1
hsa-miR-105-5p	0	0	1
hsa-miR-200b-5p	1	0	0
hsa-miR-23b-5p	1	0	0
hsa-miR-27b-5p	1	1	1
hsa-miR-200a-5p	1	0	0
hsa-miR-525-5p	1	0	0
hsa-miR-2278	1	0	0
hsa-miR-3617-5p	1	0	0
hsa-miR-4521	1	0	1
hsa-miR-4737	1	0	1
hsa-miR-4774-5p	1	0	0
hsa-miR-4784	1	0	0
hsa-miR-5089-5p	0	1	0
hsa-miR-6779-5p	1	0	0
hsa-miR-6892-3p	0	0	1
ENSG00000212377	0	1	0
ENSG00000238791	1	0	0
ENSG00000252543	1	0	0
HBII-240	1	1	0
HBII-52-15	0	1	0
hsa-mir-548g	1	1	0
hsa-mir-4257	0	1	1
hsa-mir-3656	0	0	1
hsa-mir-3689e	0	1	1
hsa-mir-4718	1	0	0
hsa-mir-6828	0	0	1
<b>Sum</b>	<b>20</b>	<b>10</b>	<b>11</b>
SF+102+134	2	2	2
SF+102	2	2	0
SF+134	2	0	2
102+134	0	3	3
<b>Sum - No. of joined miRs</b>	<b>14</b>	<b>3</b>	<b>4</b>

**Table S4. Bioinformatics analysis of target genes of the identified miRNA candidates miR2278, miR27b-5p and miR29b-1-5p regarding their involvement in the NF-κB signaling pathway.**

<b>hsa-miR</b>	<b>Source</b>	<b>Gene Symbol (NF-κB signaling )</b>
hsa-miR-2278	TargetScan Human and mirDB	<b>CCL21</b>
	TargetScan Human and mirDB	<b>TLR4</b>
	TargetScan Human and mirDB	<b>TRAF1</b>
	TargetScan Human and mirDB	<b>LTA</b>
	TargetScan Human and mirDB	<b>CFLAR</b>
	TargetScan Human and mirDB	<b>BCL2</b>
	TargetScan Human and mirDB	<b>TRAF3</b>
	TargetScan Human and mirDB	<b>TIRAP</b>
	TargetScan Human and mirDB	<b>ERC1</b>
	TargetScan Human and mirDB	<b>PRKCB</b>
	TargetScan Human and mirDB	<b>IL1R1</b>
	TargetScan Human and mirDB	<b>PLCG2</b>
	TargetScan Human and mirDB	<b>XIAP</b>
	TargetScan Human and mirDB	<b>IKBKG</b>
	TargetScan Human and mirDB	<b>TAB1</b>
	TargetScan Human and mirDB	<b>TAB3</b>
	TargetScan Human and mirDB	<b>CSNK2A1</b>
	TargetScan Human and mirDB	<b>CARD10</b>
	TargetScan Human and mirDB	<b>MAR3K7</b>
	TargetScan Human and mirDB	<b>RELA</b>
	TargetScan Human and mirDB	<b>MYD88</b>
	TargetScan Human and mirDB	<b>TRAF6</b>
	TargetScan Human and mirDB	<b>DDX58</b>
hsa-miR-27b-5p	TargetScan Human and mirDB	<b>PLCG1</b>
	TargetScan Human and mirDB	<b>CFLAR</b>
	TargetScan Human and mirDB	<b>TRAF3</b>
	TargetScan Human and mirDB	<b>TRIM25</b>
	TargetScan Human and mirDB	<b>ERC1</b>
	TargetScan Human and mirDB	<b>PRKCB</b>
	TargetScan Human and mirDB	<b>XIAP</b>
	TargetScan Human and mirDB	<b>UBE2I</b>
	TargetScan Human and mirDB	<b>TNFSF14</b>
hsa-miR-29b-1-5p	TargetScan Human and mirDB	<b>PLCG1</b>
	TargetScan Human and mirDB	<b>TRAF3</b>
	TargetScan Human and mirDB	<b>BCL2A1</b>
	TargetScan Human and mirDB	<b>TRIM25</b>
	TargetScan Human and mirDB	<b>TIRAP</b>
	TargetScan Human and mirDB	<b>XIAP</b>
	TargetScan Human and mirDB	<b>DDX58</b>
	TargetScan Human and mirDB	<b>CXCL12</b>
	TargetScan Human and mirDB	<b>MAP3K7</b>
	TargetScan Human and mirDB	<b>TAB2</b>
	TargetScan Human and mirDB	<b>RIPK1</b>
	TargetScan Human and mirDB	<b>ICAM1</b>

## 13. Curriculum Vitae

### Personal data

First name: Christina  
Surname: Georgikou  
Address: Lange Rötterstraße 26, 68167 Mannheim Germany  
Date of Birth: 2<sup>nd</sup> August 1991  
Place of birth: Athens, Greece  
Citizenship: Greek  
E-mail: [christine.georgikou@outlook.com](mailto:christine.georgikou@outlook.com)

### Education

Jan 2016 – Nov 2019: Molecular OncoSurgery, Heidelberg University Hospital, Germany, PhD candidate  
Sep 2014 - Nov 2015: Translational Medical Research, Heidelberg University, Germany, Master of Science  
Sep 2009 - July 2014: Biology, University of Crete, Greece, Bachelor of Science

### Languages

Greek: Mother tongue

German: Fluent

English: Fluent

Spanish: Basic

## 14. Acknowledgments

Conducting a PhD thesis was a unique life experience for me and it would not have been possible without the kind help and support of many individuals.

First and foremost, I would like to express my deepest and most earnest gratitude to my doctoral supervisor Prof. Dr. rer. nat. Ingrid Herr for her effective and invaluable supervision and providing me with the funding sources in order to accomplish my doctoral studies. Within these years, Prof. Ingrid Herr's unrivaled scientific attitude and meticulous academic spirit inspired me deeply. I appreciate her guidance and critique in scientific writing and data preparation.

Secondly, I am very grateful to express my sincere appreciation to PD Dr. rer. nat. Svetlana Karakhanova for her continuous help and support. Her passionate spirit and her valuable guidance will be unforgettable to me. I also would like to thank my dear colleagues Dr. Libo Yin, Dr. Xiao Xi, Jury Gladkich and Yangyi Wang for their constant assistance and immense contribution not only in every stage of my work but also in my daily life.

Then, I would like to express my sincere thanks to Mrs. Ellen Watson for her constant help, to Dr. sc. hum. Wolfgang Groß for performing statistical analysis for my experiments and to Dr. rer. nat. Michael Schäfer for his technical assistance and fruitful discussions. To all my current and former group members: Dr. Li Liu, Dr. Yefeng Yin, Dr. Nathalie Bauer, Dr. Zhefu Zhao, Dr. Alia Abukiwan, Dr. Clifford Nwaeburu, Dr. Giulia Occhipinti, Yiqiao Luo, Huihui Ji, Monika Le, Liping Bai, Zhimin Qi, Angela Wieland, Lena Bauer, Rene Wouters, Sonja Bauer, Sebastian Faus, Katharina Piwowarczyk and Jale Ottinger for the constant help and advice. They contributed in many ways to my work and life. It was a pleasure for me working with all of you.

Next, I would like to express my sincere gratitude to Prof. Dr. med. Norbert Gretz and his co-workers, Dr. Carsten Sticht and Dr. Carolina De La Torre for the help on miRNA and mRNA microarray analysis.

I am also very grateful to Prof. Dr. Carsten Bolm and his laboratory members, Laura Buglioni and Max Bremerich, for kindly providing us with the sulforaphane derivatives they developed.

Special thanks to my beloved parents, Charilaos Georgikos and Dionysia Kokkini, my brother Kwnstantinos Georgikos, my partner Dr. Vysakh Pushpa Prasad and all my friends around the globe. Your love and support make me a better person every day and I wouldn't be able to achieve this goal without you.

## 15. Eidesstattliche Versicherung

Bei der eingereichten Dissertation zu dem Thema

### **Inhibition of pancreatic cancer progression by sulforaphane-mediated downregulation of miR30a-3p and sulforaphane derivatives**

handelt es sich um meine eigenständig erbrachte Leistung.

1. Ich habe nur die angegebenen Quellen und Hilfsmittel benutzt und mich keiner unzulässigen Hilfe Dritter bedient. Insbesondere habe ich wörtlich oder sinngemäß aus anderen Werken übernommene Inhalte als solche kenntlich gemacht.
2. Die Arbeit oder Teile davon habe ich bislang nicht an einer Hochschule des In- oder Auslands als Bestandteil einer Prüfungs- oder Qualifikationsleistung vorgelegt.
3. Die Richtigkeit der vorstehenden Erklärungen bestätige ich.
4. Die Bedeutung der eidesstattlichen Versicherung und die strafrechtlichen Folgen einer unrichtigen oder unvollständigen eidesstattlichen Versicherung sind mir bekannt. Ich versichere an Eides statt, dass ich nach bestem Wissen die reine Wahrheit erklärt und nichts verschwiegen habe.

Ort und Datum

Unterschrift